# Engineering Decellularized Matrices to Support Adherent Cell Therapy

by

Bredon Crawford

A thesis

presented to the University of Waterloo

in fulfillment of the

thesis requirement for the degree of

Master of Applied Science

in

Chemical Engineering

Waterloo, Ontario, Canada, 2011

## Author's Declaration

I hereby declare that I am the sole author of this thesis. This is a true copy of the thesis, including any required final revisions, as accepted by my examiners.

I understand that my thesis may be made electronically available to the public.

## Abstract

Whole-organ perfusion decellularization was performed with rat hearts on a modified chromatography apparatus. Analysis of the flow properties and effluent material over time provided insights into the decellularization process, and allowed non-destructive testing of perfused cardiac tissue. Decellularized matrices were stored for up to 1 year at -80°C and then conditioned to remove residual detergent and cryoprotectant. Tissue was reseeded with canine blood outgrowth endothelial cells (BOECs) and cultured in an autoclavable closed-circuit bubble-free reactor. The entire process was considered in the context of eventual scale-up in equipment design, the use of disposable components, and extracellular matrix (ECM) product storage.

Tissue patch substrates for cell growth were studied for cytotoxic effects towards process development. Decellularization protocols were compared. Extracellular matrix derived coatings and gels were investigated as process assays and potential cell delivery vehicles. Peracetic acid and UV disinfection were tested. Micronized ECM carriers were developed for scalable culture, with considerations to carrier morphology, cell attachment, and egress. Micronized ECM carriers were tested with a novel *in vitro* assay to simulate the support of adherent cells for gene-modified cell therapy.

**Acknowledgements**

I would like to acknowledge the supervision of Professor Eric Jervis, whose genuine enthusiasm and wealth of experience were a great encouragement and a lot of fun. I would like to also acknowledge Professors Guy Guillemette and Heidi Engelhardt for providing me with advice and resources for no good reason.

The whole-organ decellularization work was completed with Curtis Woodford and Christine Thompson; the subsequent seeding and culture was done with Sandeep Koshy and Gheeta Jhamb; and early tissue piece decellularization was performed with Kathryn Futrega.

Blood outgrowth endothelial cell isolation and gene modification was completed by the lab of Dr. David Lillicrap and generously provided.

I could not have completed this work without the technical expertise and advice of my colleagues Julien Verneau, Erika Murray, Sasha Avreline, Andrew Levy, and Alyssa Shepherd.

## Dedication

*To my Parents.*

*They know why.*

## Table of Contents

## List of Figures

## List of Tables

## List of Abbreviations

| | |
|---|---|
| APTS | (3-aminopropyl)trimethoxysilane. |
| bFGF | basic fibroblast growth factor |
| CFDA-SE | 6-carboxyfluorescein diacetate succinimidyl ester |
| CMC | critical micelle concentration |
| cBOEC | canine blood outgrowth endothelial cell |
| CTAB | cetyltrimethylammonium bromide |
| DAPI | 4',6-diamidino-2-phenylindole |
| DMEM | dulbecco's modified eagle medium |
| ECM | extracellular matrix |
| EDTA | ethylenediaminetetraacetic acid |
| EGF | epidermal growth factor |
| GFP | green fluorescent protein |
| GAG | glycosaminoglycan |
| H&E | Hematoxylin and eosin |
| HEPES | 4-(2-hydroxyethyl)-1-piperazineethanesulfonic acid |
| HLB | hydrophilic-lipophilic balance |
| HUVEC | human umbilical vein endothelial cell |
| mBOEC | murine blood outgrowth endothelial cell |
| MWC | molecular weight cutoff |
| NS | neurostem |
| PEEK | poly-ether-ether-ketone |

# Chapter 1 – Introduction

Hemophilia A is a hereditary clotting disorder caused by a deficiency of the clotting factor VIII (FVIII) protein. Symptoms of the disease include painful and recurrent bleeding of the joints, while treatment includes costly (~$140 000 US per year) replacement of FVIII (Feldman, Pai et al. 2006). Hemophilia A is one of the most extensively studied disease in gene therapy, owing in part to the quantitative clotting assays, and estimated clinical significance at even low (2-3% wild type) protein expression (Murphy and High 2008).

Promising results have been achieved by delivery of viral vectors designed to deliver functional copies of the FVIII-coding gene to patient liver cells. However, safety concerns including adverse immunological reactions, vector-mediated cytotoxicity, germ-line transmission, and oncogenesis remain. An *ex vivo* approach may reduce these risks by delivering patient cells that have been transfected, expanded, and tested outside of the body prior to re-implantation (Lin, Chang et al. 2002; Matsui, Shibata et al. 2007).

Blood outgrowth endothelial cells (BOECs) have been employed as a target cell for *ex vivo* gene therapy of the FVIII-coding gene (Lin, Chang et al. 2002). BOECs can be reproducibly produced from human peripheral blood, tolerate growth from low density following selection, and have high proliferative potential (Lin, Weisdorf et al. 2000). These advantages have facilitated the production of transfected therapeutic BOECs, however when injected back into circulation, the majority of cells die within 24 hr (Milbauer, Enenstein et al. 2009).

One cause of early losses in transplanted cells may be *anoikis*, a programmed cell death associated with lack of attachment in adherent cells (Frisch and Screaton 2001). Delivering cells with a surface carrier has improved survival of transplanted chromaffin cells in the rat striatum (Saporta, Borlongan et al. 1997), hepatocytes in the rat peritoneum (Demetriou, Reisner et al. 1988), and bone mesenchymal stromal cells in subcutaneous implantation (Yang, Rossi et al. 2007). Developing a tissue engineering approach including a biocompatible scaffold or carrier may promote long-term survival of delivered cells and extend *in vivo* production of FVIII.

Decellularization is the process of removing cells and cellular debris from a tissue to isolate the extracellular matrix (ECM) of the tissue (Badylak, Taylor et al.). *In vivo*, the ECM supports cells through structural support and complex signaling integration (Hynes 2009). Transplant applications of decellularized tissue include recellularization of ECM towards the production of patient-specific functional adult tissue (Ott, Matthiesen et al. 2008; Uygun, Soto-Gutierrez et al. 2009; Ott, Clippinger et al. 2010). The cell-supportive properties of tissue-derived ECM may facilitate gene-modified cell therapy, and are discussed in more detail in Chapter 2. The development and processing of ECM-based constructs for gene-modified cell therapy is the focus of the work presented in this thesis.

The support of implanted endothelial cells may not require the complex co-cultures and large-scale architecture of the replacement tissues. Consequently, a variety of source tissues and configurations of ECM products may be suitable for improving adherent cell delivery and survival and are explored in this work. In addition to whole-organ ECM scaffolds, micronized

ECM developed for wound repair and surgical augmentation (Sclafani, Romo et al. 2000; Zhang, Deng et al. 2009) were investigated. Tissue-specific ECM gels used to promote cell phenotype in culture (Zhang, He et al. 2009) were also studied. In this work, source tissue was collected from multiple rat strains as it became available to reduce animal sacrifice.

# Chapter 2 – Literature Review

## 2.1 Properties of Extracellular Matrix

Tissue-derived extracellular matrix (ECM) is a model material for the development of near-native tissue constructs; it resembles native tissue in composition (Akhyari, Kamiya et al. 2008), mechanical properties (Gratzer, Harrison et al. 2006), and vasculature structure (Ott, Matthiesen et al. 2008). *In vivo*, native ECM helps regulate cellular differentiation, proliferation, and migration. Mesenchymal stem cell differentiation is sensitive to the mechanical stiffness of the collagen matrix used for culture (Engler, Sen et al. 2006). Growth factors such as epidermal growth factor and insulin-like growth factor-1 are immobilized in the ECM by glycosaminoglycans (GAGs), and impact cellular migration (Stefonek-Puccinelli and Masters 2008). Cryptic sites within ECM facilitate angiogenesis (Xu, Rodriguez et al. 2001), and ECM degradation products attract progenitor cells (Beattie, Gilbert et al. 2009).

The goal of decellularization is to produce an ECM isolate free of cells and cellular remnants such as DNA, membrane fragments, and cytosolic materials. Protocols to extract morphologically preserved and chemically pure extracellular matrix have been available for more than thirty years (Meezan, Hjelle et al. 1975) and vary extensively. Basic methods of decellularization include mechanical, freeze/thaw, alkaline or acid, enzymatic, detergent, and solvent treatments, and have been extensively reviewed (Gilbert, Sellaro et al. 2006). The isolation of ECM is both a chemical and a transport problem: the cellular components must be brought into solution in a manner that is minimally disruptive to the surrounding matrix; and

these components must pass through any interstitial matrix, compartments, and membranes to the exterior of the tissue. In practice, convective decellularization by perfusion is more effective in removing cellular materials such as phospholipids than batch decellularization with agitation, regardless of the specific solubilization treatment (Montoya and McFetridge 2009). In these systems, increased pressure also significantly increases lipid removal, highlighting the importance of physicochemical processes underlying decellularization.

## 2.2 Detergents

### *2.2.1 Phospholipid Removal*

The process of phospholipid bilayer solubilization can be described by the three-stage hypothesis (Helenius and Simons 1975): First, detergent monomers are incorporated into the lipid bilayer. The bilayer then becomes saturated with detergent, reaching equilibrium with newly-formed mixed micelles that are saturated with phospholipid. In the final stage, membrane components are fully solubilized within mixed-micelles that decrease in size as detergent concentration rises, approaching the behaviour of pure detergent micelles. For decellularization, the soluble, phospholipid-bearing mixed-micelles must then be removed from the system.

A geometric interpretation of the three-stage hypothesis can be provided by wedge theory (Haydon and Taylor 1963). This theory proposes that the two hydrocarbon chains of a phospholipid are similar enough in size to the polar head to prevent the formation of soluble micelles, leaving a continuous bilayer as the most favoured structure. However, molecules with

relatively large polar groups and narrow hydrocarbon structures, such as detergents, are sufficiently wedge-shaped to form micelles and can cause the disruption of the lipid bilayer upon their insertion.

The three-stage hypothesis only describes the solubilization of a chemically pure phospholipid bilayer. The behaviour of cell membranes can be more closely modeled by considering a membrane composed of two distinct phospholipids interacting with a detergent in aqueous solution and forming four phases: liquid-ordered membranes, liquid-disordered membranes, micelles, and dissolved detergent monomers (Keller, Tsamaloukas et al. 2005). An advantage of this model is its consistency with the presence or formation of detergent-resistant membrane fragments (Yu, Fischman et al. 1973), that survive mild detergent treatments.

### *2.2.2 Protein Solubilization*

Detergent solubilization of proteins also begins with detergent monomers in solution (Helenius and Simons 1975). These molecules bind to discrete sites on the protein, which can vary in their affinity for detergent molecules. Binding can be cooperative and accompanied with a conformational change of the protein that exposes previously buried lipophilic groups, especially for strong detergents. For mild detergents, it may be possible that not all detergent molecules bind directly with the protein, with some molecules binding cooperatively to form a micelle-like region on the surface of the protein. At higher detergent concentrations, proteins may associate directly with detergent micelles.

### *2.2.3 Detergent Strength*

Detergents vary in their strength to bind and denature proteins. Detergents are commonly classified by their hydrophilic character as non-ionic, zwitterionic, anionic, or cationic. Another important distinction can be made between the hydrophobic groups composed of flexible alkyl chains or the rigid and bulky steroid moiety of bile salts. The relative size and strength of the hydrophilic and lipophilic groups can be used to calculate a hydrophilic-lipophilic balance (HLB) and roughly characterize the strength of a detergent. Assigned values have ranged from 1 to 40, with higher numbers corresponding to increasing hydrophilic character (Griffin 1949). Detergents with HLBs between 12 and 16 are considered relatively non-denaturing, and values above 20 are more likely to denature protein. (Rosenberg 2004). Sodium dodeceyl sulfate, for instance, has an HLB of 40 and increases the crimp amplitude and periodicity of collagen, and increase the susceptibility of collagen to trypsin in porcine ligament, suggesting matrix denaturation during decellularization (Gratzer, Harrison et al. 2006).

However, HLB values alone cannot predict the denaturing behaviour of a decellularization solution. Detergent free monomer concentration and negative synergism between detergents also determine binding and extent of denaturation (Miyazawa, Ogawa et al. 1984). Detergent-protein binding is also influenced by temperature, pH, ionic strength, and other environmental effects (Otzen 2002). Additionally, not all proteins are equally susceptible to denaturation by a given detergent at given conditions (Helenius and Simons 1975).

An ideal decellularization process is optimized for maximum solubilization of cellular components with minimum denaturation of native ECM proteins. This also requires a prioritization of ECM components for a given application. To improve the quality of ECM, additional processing may required. Examples could include the replacement of any desirable ECM proteins lost in extraction, repair by fibroblast culture, or partial refolding with chaperone proteins.

### *2.2.4 Detergent Properties*

Physical parameters of candidate detergents are presented in Table 1. SDS and Triton X-100 occur frequently in literature and are some of the best characterized detergents. Triton X-100 has been found insufficient for cardiac decellularization (Ott, Matthiesen et al. 2008). N-Lauroyl Sarcosinate has been used as a less-denaturing alternative to SDS in cardiovascular applications (Ketchedjian, Jones et al. 2005). Bile salts are also commonly employed, often used in combination with Triton X-100 (Samouillan, Lamure et al. 2000; Spina, Ortolani et al. 2003). Centrimonium bromide (CTAB) is less often employed in decellularization, but is often used in DNA extraction(Gani, Chattoraj et al. 1999).

| Detergent | Type | HLB | CMC (mM) | Micellar Mass (u) |
|---|---|---|---|---|
| Triton X-100™ | Non-ionic | 13.4[1] | 0.25[2] | 47,000 – 103,000[2] |
| Sodium Deoxycholate[(40)3] | Anionic (Bile salt) | 16.0 | 2 – 6 | 1,200 – 5,000 |
| Centrimonium Bromide (CTAB) | Cationic[4] | 21.4[4] | 1[(40)5] | 62,000[(40)5] |
| N-Lauroyl Sarcosinate | Anionic[5] | 29.8[5] | 14.6[(40)3] | 600[(40)3] |
| Sodium Dodecyl Sulfate (SDS) | Anionic[1] | 40.0[1] | 1.2 – 7.1[2] | 17,800 – 29,100[2] |

**Table 2.1 Properties of Detergents Tested for Decellularization.**

**Hydrophilic-lipophilic balance values indicate the relative strength of the detergent. The critical micellar concentrations are the concentration at which given detergent molecules form micellar structures. CMC values correspond to 20-25°C. Triton X-100™ is a weak detergent that forms large micelles at low concentration, compared to SDS, which is stronger, and forms smaller micelles at higher concentrations. ([1]McCutcheon's Detergents & Emulsifiers, 2009; [2]le Maire, Champeil, et al. 2000; [3]Sigma Aldrich, 2009; [4]Retter, Koch, et al. 1999; [5]DeWolf Chemical, 2000)**

### *2.2.5 Detergent Removal*

Following decellularization, significant amounts of detergent may remain in the matrix. Reduced peptides in the presence of SDS at 0.8mM or greater will form complexes of about 1.4g SDS per gram protein (Reynolds and Tanford 1970). SDS can also form complexes with membrane glycoproteins containing as much as 5-7g SDS per gram protein, likely due to detergent interaction with sugar residues in addition to protein (Grefrath and Reynolds 1974).

The critical micelle concentration (CMC), where monomers in solution begin to form micelles is low for the most commonly used detergents in decellularization, typically only a few millimolar. Detergent-protein binding also occurs at free monomer concentrations well below the CMC (Miyazawa, Ogawa et al. 1984), permitting a limited concentration gradient for detergent removal during tissue rinsing.

Radiolabelled detergent molecules have been used to validate the removal of N-lauroyl sarcosinate from a $1cm^2$ section of sheep heart using a 24-36 hour rinse of sterile water, recirculating through hydrophobic adsorbent resin and anion exchange resin beads (Ketchedjian, Jones et al. 2005). A half-hour Triton X-100 wash, followed by a 124 hour PBS wash has been used to remove residual SDS from a perfusion-decellularized rat heart (Ott, Matthiesen et al. 2008). This procedure presumably took advantage of the negative synergism between detergents resulting from competing formation of mixed detergent micelles (Miyazawa, Ogawa et al. 1984). SDS removal has also been performed with a pH 9 buffer and, alternatively, a 75% ethanol solution in porcine ACL tissue, with residual detergent quantified with methylene blue dye-binding assay (Gratzer, Harrison et al. 2006).

### *2.2.6 Detergent Transport*

Detergent, nuclear material, soluble cellular protein, and detergent-protein complexes must all travel through tissue interstitial matrix and endothelial basement membranes during the decellularization of whole organs or tissue sections large enough to support a cell therapy implant. A better understanding of these transport phenomena will aid in the preparation of

extracellular matrix for a target application. For example, convective flow decellularization was found to be more efficient than rotary agitation decellularization, with low pressures associated with most efficient protein removal, and high pressures corresponding to more efficient phospholipid extraction in a solvent mixture (Montoya and McFetridge 2009).

Flow through the intersitium has been previously reviewed by other groups (Levick 1987), and some useful introductory information will be repeated here. The intersitium fills the intercellular spaces of an adult and allows 2-4 L of plasma ultrafiltrate to flow into the lymphatic system per day. It is composed of coarse fixed elements, such as collagen fibrils and a fine meshwork of glycosaminoglycans (GAGs) surrounding a core proteoglycan protein immobilized onto the larger network. These substances are hydrated, expanding their effective size. Observed hydraulic conductivities for tissues of low and high cell density have shown the matrix to dominate flow resistance in whole tissues. Mean hydraulic radii have been calculated for the interstitium considering collagen fibrils, proteoglycans, and GAGs as randomly oriented cylinders. Several mean hydraulic radii have been calculated, ranging from 3 to 31nm, depending on tissue. It was found that GAGs, collagen, and proteoglycans together provide resistance greater than that of their individual contributions. This is consistent with experiments in tumour models that suggest proteoglycans and GAGs must be fixed to the collagen network to exhibit their full transport-limiting effect (Netti, Berk et al. 2000). Conductivity experiments on a basement membrane formed from Matrigel™ have yielded a mean hydraulic radius of 0.6 to 0.7nm (Katz, Barrette et al. 1992).

Experiments with dynamic light scattering have been performed to study the interaction of Triton X-100™ with phosphatidylcholine liposomes (Lopez, de la Maza et al. 1998). The detergent monomers were found to have a hydraulic radius of 5.0nm in a system of TRIS buffer with liposomes of 100nm radius. Mixed micelles, saturated with detergent were found to have a hydraulic radius of 5.9nm. As the detergent concentration increased, larger mixed vesicles and mixed micelles appeared, while pure liposomes decreased in size. Eventually, only mixed micelles of 8.5nm radius persisted, decreasing to 5.0nm with even higher detergent concentration.

A similar experiment was subsequently performed with SDS (Lopez, Cocera et al. 1999). The liposomes initially decreased from a radius of 95 to 85nm as SDS monomers inserted themselves. With increasing detergent, mixed micelles began to form with a radius of roughly 3nm, coupled with a relaxation of vesicles up to a radius of 110nm. As SDS concentration increased further, only mixed micelles persisted with a radius of 2.6nm.

When bile salts insert themselves into vesicle membranes, transient holes lined with the detergent appear, through which some vesicle contents escape (Schubert and Schmidt 1988). As bile salt concentration increases to approximately a third that of the lipid, the membrane holes begin to connect, creating islands that leave the membrane. Experiments with cholate and phospholipid have shown that after the detachment of small membrane patches, cylindrical vesicles form from the cholate-lined edges of the bilayer sheet (Walter, Vinson et al. 1991). These rods have a radius of 2.7nm and a length that decreases with increasing bile salt to 16nm.

As cholate concentration increases further, the rods are reduced to spheroidal mixed micelles with a hydrodynamic radius of 2-3 nm.

The relative sizes of soluble and detergent-solubilized protein complexes should be considered when determining source tissue and protocols to isolate ECM for a target application. Muscle tissue contains large contractile proteins and protein subunits, such as titin and heavy-chain myosin, which may be difficult to remove without damage to the basement membrane and interstitial matrix. Mild detergents, such as Triton X-100 and deoxycholate, are unable to dissociate most protein complexes into their subunits, instead solubilizing complete quaternary structures (Helenius and Simons 1975). Proteins solubilized in non-ionic detergent can also form larger aggregates (Aivaliotis, Samolis et al. 2003), which may leave the matrix more slowly.

# Chapter 3 – Whole Organ Processing

## 3.1 Methods

### *3.1.1 Tissue Preparation*

All animal-related procedures were approved by the University of Waterloo Animal Care Committee. Adult Sprague Dawley rats (480-580g; $n$ = 8) were group housed 4 per cage at constant air temperature (20-21°C) and humidity (approx. 50%) in a 12:12-hr reverse light:dark cycle facility. Rats had free access to water and standard 22/5 Rodent Diet (W) lab chow (Harlan, Indianapolis IN). On the day of the experiment, body mass was recorded and rats were anesthetized with sodium pentobarbital injection (60 mg/kg intraperitoneally; Vetoquinol N-A, Lavaltrie, QC, Canada). The heart was removed, cannulated with a 10 cm section of polyether ether ketone (PEEK) tubing (Supelco Analytical, Bellefonte, PA) and tied with 4.0 silk suture. The heart was flushed with 2500 U of heparin (Bioshop, Burlington ON, Canada) in phosphate buffered saline (PBS) via cannula until the effluent was clear, and then placed in chilled PBS prior to decellularization.

### *3.1.2 Perfusion Decellularization*

Cannulated hearts were connected to a modified chromatography system (Figure 3.1A) including a peristaltic pump, injection loop, and fraction collector (Amersham Bioscience AB, Uppsala, Sweden). The tissue was placed in a glass enclosure and then perfused at a flow rate of 2

mL/min with PBS containing 1% (w/v) sodium dodecyl sulfate (Bio-Rad Laboratories, Hercules, CA). The effluent material was collected in 15 mL fractions that were analyzed with a detergent-compatible modified Lowry protein assay (Bio-Rad Laboratories) in a plate colorimeter (Molecular Devices, Sunnyvale, CA). For tracer pulse experiments, a 200 µL injection loop was loaded with 10 µM fluorescein isothiocyanate (FITC). Flow was reduced to 1 ml/min during pulse injections and effluent was collected dropwise over 2 min. Effluent was assayed in a plate fluorometer (Molecular Devices, Sunnyvale, CA) against a standard curve and normalized to total tracer. Decellularization was considered complete when the heart had a uniform translucent appearance, typically after 24 hr perfusion.

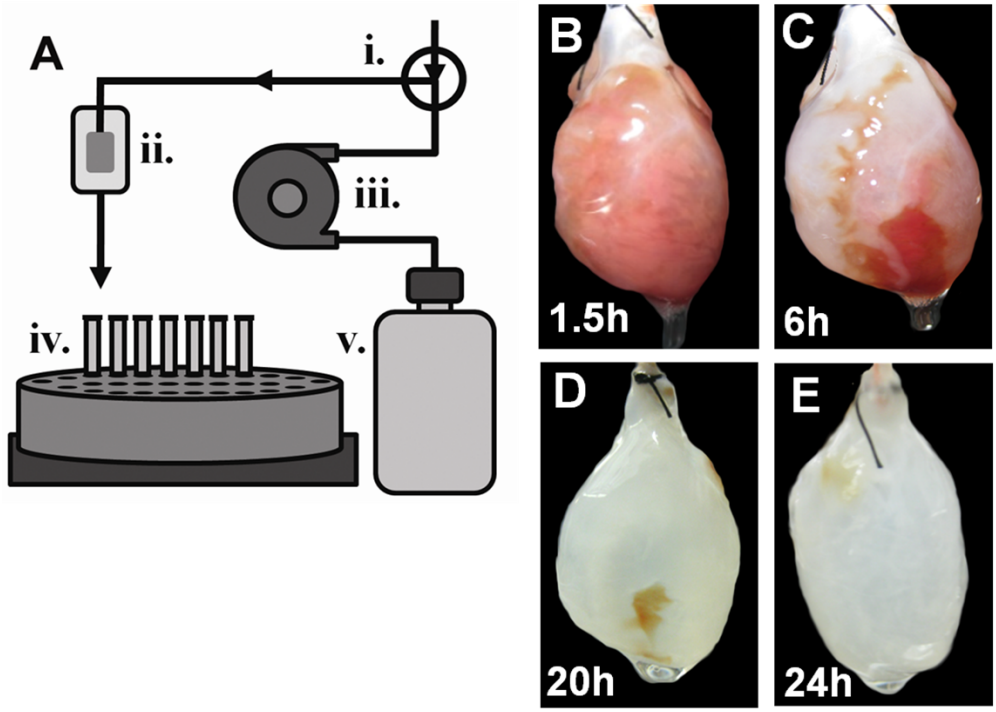


**Figure 3.1 – Decellularization Apparatus and Physical Observations**

**The decellularization apparatus (A) comprises an injection loop (i), glass enclosure (ii), peristaltic pump (iii), fraction collector (iv), and detergent solution (v). Decellularization occurs early in the aortic arch and carotid arteries. The dense ventricular mass decellularized more slowly. This may be due to mass transport limitations.**

### *3.1.3 Cryostorage and Reconditioning*

After decellularization, the cannulated hearts were removed from the perfusion system and stored in 10% DMSO in PBS at -80°C for up to 1 yr. Cannulated tissue was thawed in a polypropylene container in a water bath at 37°C, and rinsed thoroughly with deionized (DI) water. The PEEK tubing was connected to the reconditioning system and perfused with 1% (v/v) Triton® X-100 (Sigma-Aldrich Canada Ltd., Oakville, ON, Canada) in deionized water for 3.5 hr at a flowrate of 2 mL/min at room temperature. The cannulated tissue was then perfused with DI water for 1 hr, removed from the apparatus, and then incubated with 6.7 U/mL Benzonase™ nuclease (EMD Biosciences, San Diego, CA) in buffer (50 mM Tris-HCL pH 8, 20 mM NaCl, 2 mM $MgCl_2$) for 3.5 hr at 37°C. The tissue was then re-mounted on the reconditioning apparatus (Figure 3.2) and perfused with a 1.8% (w/v) skim milk powder solution for 1.5 hr followed with 1 hr rinse of DI water. The tissue was removed from the pumping system and flushed via the cannula and soaked with a disinfecting solution (Remlinger, Czajka et al.) of 0.1% (v/v) peracetic acid and 4% (v/v) ethanol in DI water for 20 min. The tissue was then flushed and soaked in DI water, media, and fetal bovine serum for 1 hr each, with aseptic handling performed in a biological safety cabinet.

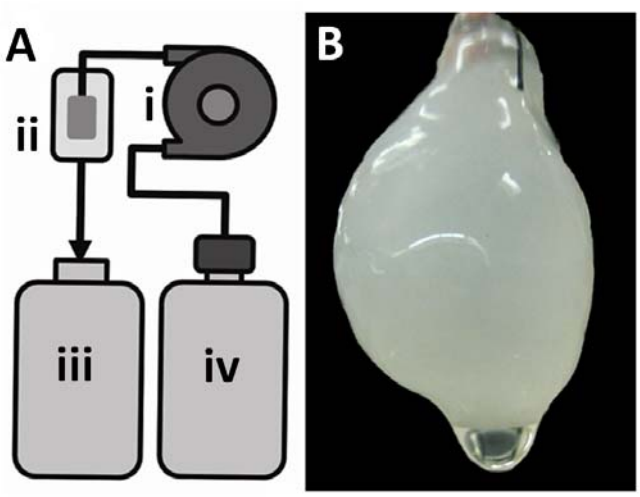


**Figure 3.2 – Tissue Reconditioning**

**Tissue was loaded in a second apparatus (A) comprising a peristaltic pump (i), glass enclosure (ii), and waste resevoir (iii) to be perfused with protein solution and water rinses (iv) to remove residual cryoprotectant, and replace adsorbed detergent. Tissue is shown following perfusion (B). Nuclease incubation and FBS rinses were also applied to reduce cytotoxicity of the culture surface.**

### *3.1.4 Cell Maintenance*

Canine blood outgrowth endothelial cells (cBOECs) were a generous gift from Dr. David Lillicrap, Queen's University. Cells were cultured in MCDB-131 (Invitrogen Canada Inc., Burlington, ON, Canada) supplemented with an endothelial growth medium-2 Sinqlequot™ (Lonza, Walkersville, MD), 2 mM L-Glutamine, and 10% (v/v) fetal bovine serum (Invitrogen Canada Inc., Burlington, ON, Canada) . Cells were cultured in tissue-treated 75 $cm^2$ polystyrene flasks (BD, Mississauga, ON, Canada) coated with gelatin from bovine skin, type B (Sigma-Aldrich Canada Ltd., Oakville, ON, Canada) in a controlled atmosphere at 37°C and 5% $CO_2$. Cells were passaged at 90% confluency with 2.5 g/L trypsin with 0.38 g/L EDTA (Invitrogen Canada Inc., Burlington, ON, Canada) every 3-4 days.

### *3.1.5 Seeding and Recellularization Culture*

Trypsinized cells ($2x10^7$) were concentrated and resuspended in 2mL of medium and injected via the cannula and directly through the walls of the heart at regular spacing (~5mm) with an 18 gauge needle. The tissue was placed in static culture at 37°C with medium for 45 min before being loaded into the sterile recellularization culture reactor in a biological safety cabinet (Figure 3.3). The reactor included a modified spinner flask in which the tissue was partially submerged in 500mL of recirculating media that had been equilibrated at 37°C and 5% $CO_2$. The closed tubing circuit, including vessels, was attached to the peristaltic pump (Cole-Parmer, Vernon Hills, IL), placed in an incubator, and connected to a gas line of 5% $CO_2$, with balance oxygen (Praxair Canada Inc., Mississauga, ON, Canada). The media was drawn into the peristaltic pump at a rate of 3 mL/min and sent to a gas-exchange vessel containing 25 ft of silicone rubber laboratory tubing with 1/8" inner diameter and 1/32" wall thickness (Sigma-Aldrich Canada Ltd., Oakville, ON, Canada). The media was passed through a glass settling chamber before entering the heart cannula. The tissue was cultured for 9 d.

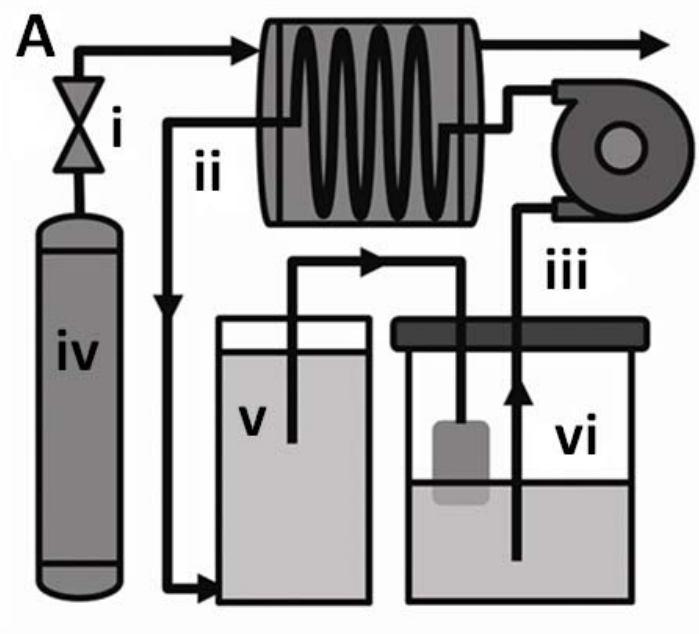


**Figure 3.3 – Recellularization Culture**

**Conditioned tissue was loaded into a culture apparatus (A) comprising a 95% oxygen, 5% carbon dioxide atmosphere (iv) controlled with a needle valve (i) and delivered in a bubble-free aerator (ii). Media was circulated with a peristaltic pump (iii) and passed through a settling chamber to collect debris and bubbles before entering the semi-submerged culture chamber (vi), (B). The entire apparatus was maintained at 37°C.**

### *3.1.6 Staining and Imaging*

After culture, the tubing circuit and vessels were brought into a biological safety cabinet, and the tissue was removed for dissection. A randomly selected portion of the ventricular mass was excised and incubated at 37°C in media containing 10 μM CFDA-SE (Invitrogen Canada Inc., Burlington, ON, Canada) and 2 μg/mL Hoescht 33342 (ABD Bioquest, Sunnyvale, CA) for 30 min to stain metabolically active cells, and nucleic acids, respectively. The tissue section was rinsed 3 times with media, then once with PBS. The sample was fixed in 4% paraformaldehyde for 15 min, permeabilized in 0.5% (v/v) Triton-X100™ (Sigma-Aldrich Canada Ltd., Oakville, ON, Canada) solution for 20 min, blocked with 5% BSA for 20 min, then rinsed 3 times in PBS for 5 min each, stained with AlexaFluor® 546 phalloidin (Invitrogen Canada Inc., Burlington, ON, Canada), to stain the cytoskeletal protein F-acticn, washed 3 times for 5 min each in PBS, and placed on a coverslip. Epifluorescent imaging was performed on an inverted fluorescent microscope (Axiovert 200; Carl Zeiss MicroImaging GmbH, Berlin, Germany) with a monochrome high resolution CCD camera (XCD-SX910/X710; Sony Corporation, Tokyo, Japan), followed by sequential fluorescent imaging on a confocal microscope (FV1000; Olympus Canada Inc., Markham, ON, Canada).

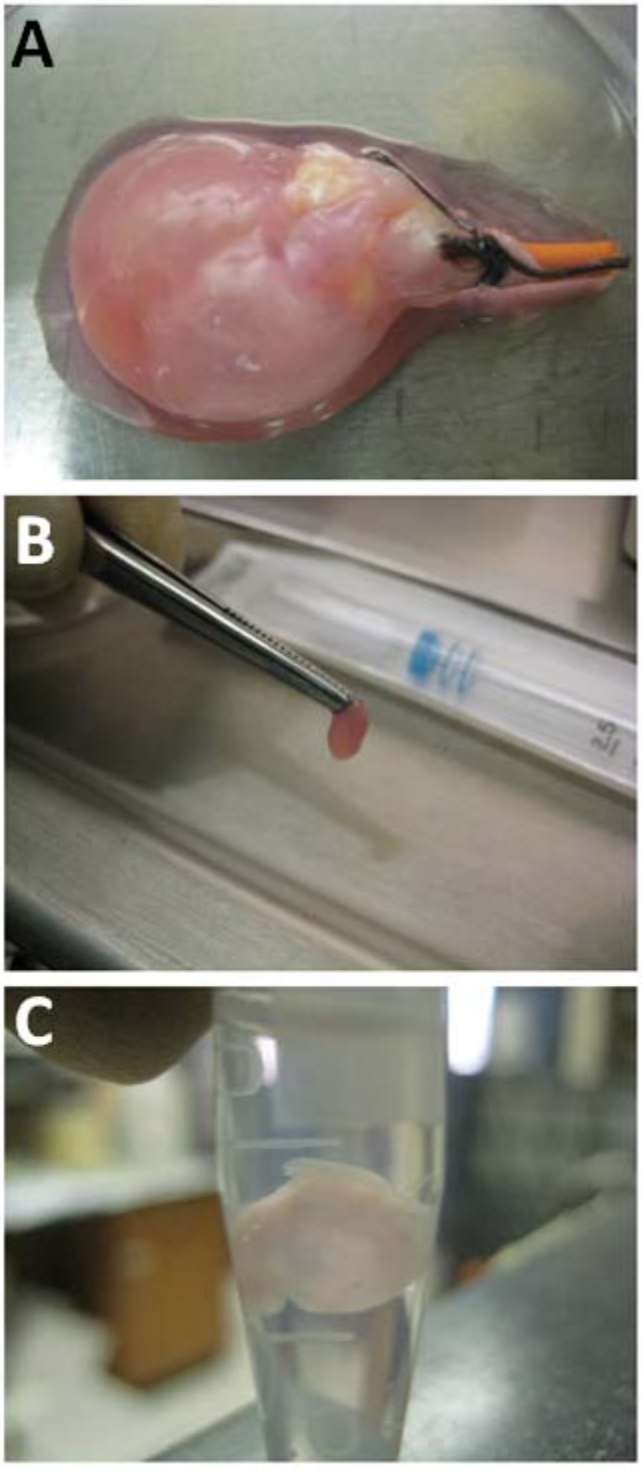


**Figure 3.4 – Tissue Sample for Imaging**

**After 9 days of recellularization culture, tissue was removed from the reactor (A) and handled in a biological safety cabinet. Random tissue was removed (B) and stained in a microcentrifuge tube (C). Tissue was then mounted and the lumen was imaged on an inverted fluorescent microscope.**

### *3.1.7 Analysis*

Flow models for the decellularizing heart were fitted to reproduce the observed outlet tracer pattern using a square pulse of fluorescent tracer at the inlet. These studies were performed to gain a better qualitative understanding of the transport processes of the decellularizing heart. Candidate flow models included combinations of ideally mixed tanks and plug-flow tubular reactors; tanks in series; and axial dispersion tubular flow. The models are commonly used to diagnose flow behavior in industrial mixing (Blanch and Clark 1996; Fogler 2006) and to study material residence in pharmacokinetic models of perfused organs (Roberts, Donaldson et al. 1988). Bypassing and dead zones were considered to study leaking and blockage before and after decellularization. These deviations from ideal mixing always lower performance in industrial process units (Levenspiel 1999) and may similarly reduce efficiency in decellularization processes by allowing solubilized cellular materials to remain in the system, and causing detergent to exit the system without contacting tissue or removing debris. Models were fitted to data at 45 minutes and 15 hours of detergent perfusion from a representative decellularization.

Flow models were produced and analyzed using MatLab™ (The MathWorks, Inc., Natick, MA) and COMSOL Multiphysics (COMSOL Inc., Burlington, MA).

## 3.2 Results

### *3.2.1 Effluent Protein*

To characterize the kinetics of protein removal during decellularization, the protein concentration in the effluent from the tissue was measured. Within six hours of a typical run, protein concentration in the effluent was observed to decrease sharply and approach zero in a manner that reflected the rate of color loss in the tissue (Figure 3.5). Total removed material typically comprised 130 to 200 mg protein per gram of fresh heart wet weight. Required decellularization time to achieve uniform translucency varied from 6 to 24 hr.

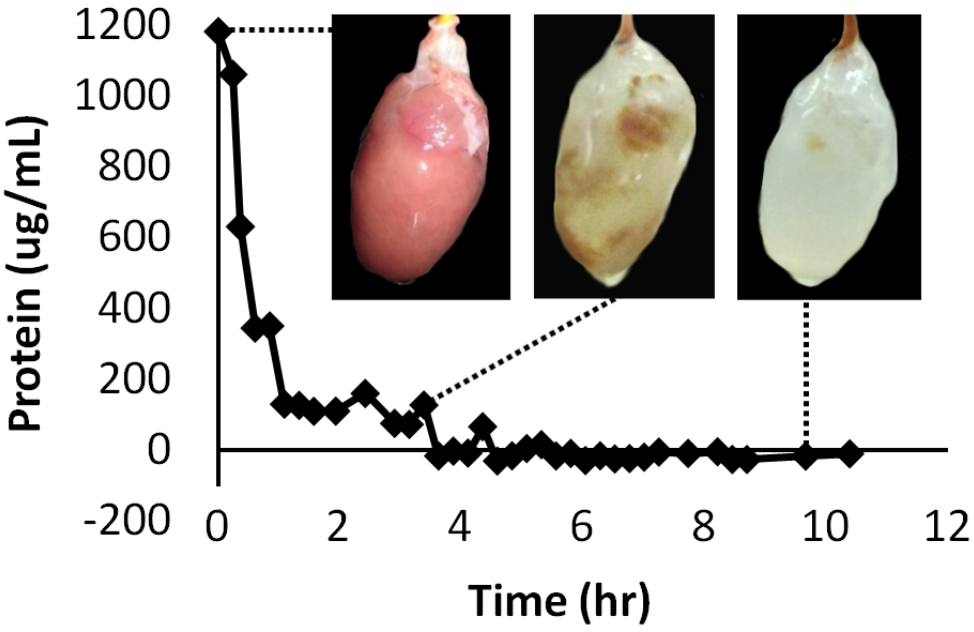


**Figure 3.5 – Effluent Protein Concentration**

**The protein concentration of effluent detergent was assayed for protein content using a detergent-compatible modified Lowry assay. Rate of protein loss was consistent with observed rate of colour loss. Most protein removal occurs in the first hours of perfusion decellularization. Data shown for a typical process run.**

### *3.2.2 Perfusion Flow*

Non-zero bypass flow was found to reduce goodness-of-fit in all initial models, suggesting the absence of leaks. Bypassing was then excluded from models for model simplification. Models with a maximum of two parameters were evaluated to facilitate physical interpretation and improve convergence. The chosen model comprised two tanks in series with recirculation with total perfused volume and recirculation fitted as parameters (Figure 3.6A). Perfused volume in the heart was found to reduce from 0.37 to 0.30 mL, with a reduction in recirculation ratio from 5.3 to 1.3 between decellularization of 45 min (Figure 3.6B) and 15 hr (Figure 3.6C). These results imply accumulation of cellular debris in the lumen even at late decellularization and are consistent with physical observations of persistent muculent effluent. This material build-up may act as a barrier to transport during decellularization and impede subsequent recellularization and proliferation if not effectively removed.

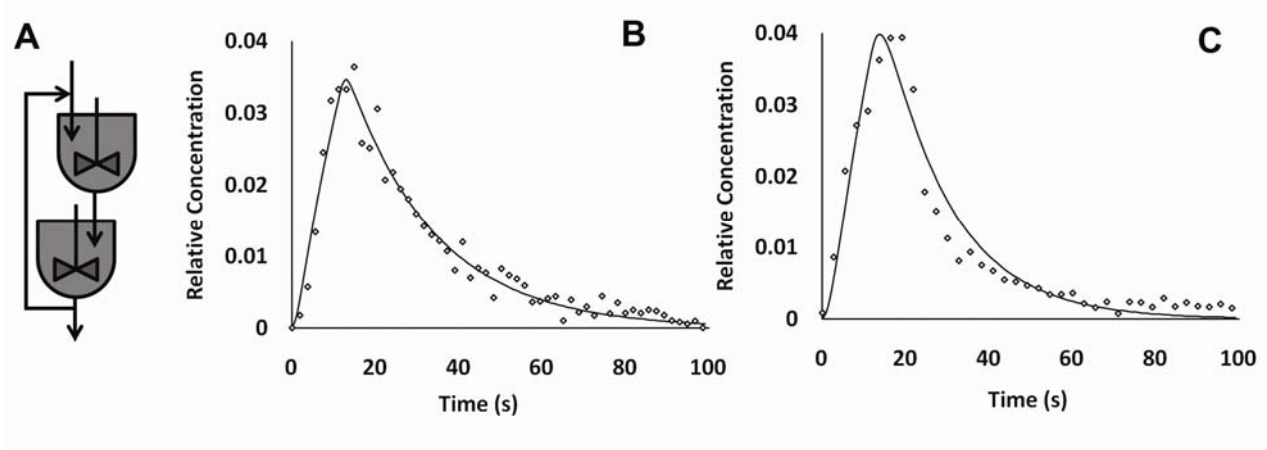


**Figure 3.6 – Residence Time Distributions**

**Modeling of tracer pulse experiments using MatLab™ and COMSOL™ with two-parameter flow models showed best fit with two ideal continuously stirred tank reactors in series with recycle (A). The flow properties of the entire organ before (B) and after decellularization (C) were considered from a mass transport perspective. Ideally mixed volume and recirculation parameters were both reduced after decellularization, suggesting accumulation of debris in the tissue lumen. This agrees with observed persistence of muculent effluent.**

### *3.2.3 Tissue Conditioning and Culture*

Cryopreservation was observed to reduce the overall size of the cannulated whole-organ ECM. This compression may have been caused by uniform freezing and the expansion of the surrounding cryoprotectant medium or by dehydration of matrix proteins during freezing. The tissue was found to expand to typical volume following perfusion reconditioning (Figure 3.2). Disinfection with an aqueous solution of 0.1% (v/v) peracetic acid and 4% (v/v) ethanol slightly increased the opacity of the ECM.

Phase contrast images of the ventricular lumen (Figure 3.7A,C) suggest preserved tissue microstructure as previously demonstrated with similar decellularization protocols (Ott, Matthiesen et al. 2008). Corresponding fluorescent images showed widespread adhesion of seeded cells following 9 days of culture. The clusters of observed cells suggest proliferation during culture. High magnification images showed substantial cell spreading and multiple focal adhesions (Figure 3.7B,D). Collocation of CFDA-SE signal with Hoescht and phalloidin demonstrated cell viability (Figure 3.7E-H).

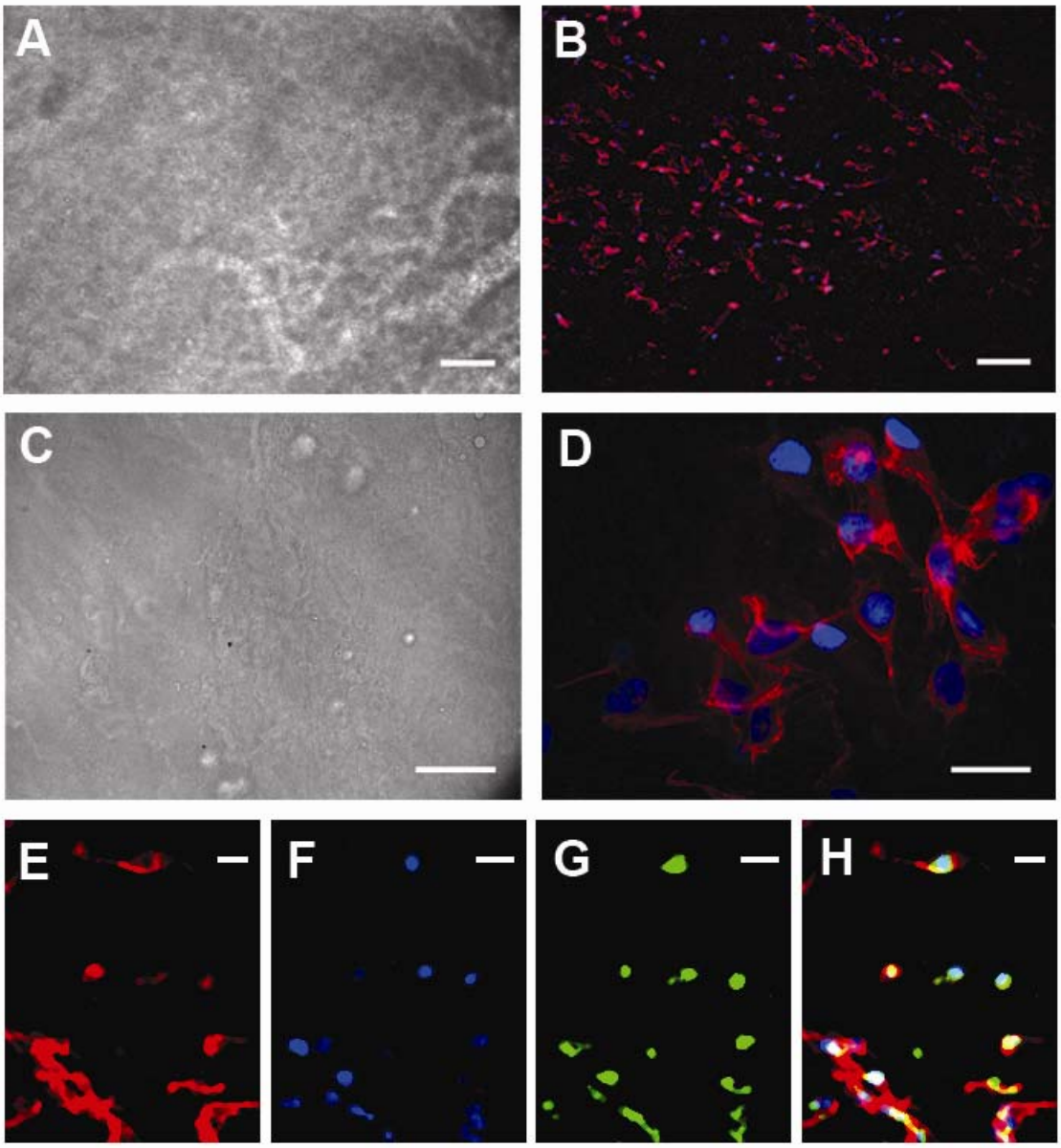


**Figure 3.7 – Staining and Imaging of Tissue Lumen**

**Phase contrast images of the tissue microstructure are shown following decellularization, reconditioning and culture (A,C). Corresponding fluorescent imaging (B,D) shows extensive cell attachment with DAPI (blue) and phalloidin (red) staining. Cell morphology including focal adhesions indicates cell health and viability (D). Colocalization (H, merge) of phalloidin (E, red), Hoescht (F, blue), and CFDA (G, green) with confocal imaging confirmed viability after 9 days of culture. Scale bars correspond to 100µm (A,B) and 25µm (C-H).**

## 3.3 Discussion

This work examined practical aspects of the production of tissue-engineered constructs from animal tissue. These included the study of transport phenomena central to perfusion decellularization protocols. Specifically, we investigated the dynamics of protein loss in decellularizing tissue and flow properties in perfusion decellularization.

The importance of flow considerations in perfusion decellularization was highlighted in preliminary work by induced mechanical modifications such as perforation and clotting by heparin omission. These conditions increased the decellularization time by a factor of 3 or more (data not shown). Mechanical modification and processing is common in the isolation and decellularization of tissue (Lin, Chan et al. 2004; Mertsching, Walles et al. 2005; Brown, Lindberg et al. 2006) and resultant flow effects may be significant to process efficiency and completeness.

In perfusion decellularization, model fitting suggests an increase in stagnant volume at 15 hours of SDS treatment. This is believed to be caused by the accumulation of muculent cellular debris, such as chromatin and glycosylated proteins. Stagnant regions have little exchange of material with well-mixed volumes (Nauman 2004), and decrease the efficiency of transport processes as both a physical barrier and by reducing the magnitude of concentration gradients that drive perfusion decellularization process.

Flow properties are not only important to the efficiency and completeness of a decellularization process, but also influence the detergent denaturation processes on extracellular matrix. For example, the denaturing power of detergents such as SDS increases with concentration (Reynolds and Tanford 1970). High local concentrations of SDS may result in increased denaturation of extracellular matrix proteins which have been shown vulnerable to detergents (Gratzer, Harrison et al. 2006). Flow patterns determine the distribution and severity of hotspots in the tissue with respect to detergent damage.

Variation in total removed protein from 130 to 200 mg protein per gram of heart wet weight, and required decellularization time from 6 to 24 hr may reflect variations in residual clotted blood, particularly microclots following heparin flushing. The presence of microclots enhanced by the absence of systemic heparinization, may present transport challenges that would be encountered in the development of bioartificial hearts from human donors.

Bulk protein effluent curves (Figure 3.5) indicated that the protein loss occurred primarily in the initial hours of decellularization before approaching zero. This profile agrees with the hypothesis that the organ comprises solubilizable and nonsolubilizable pools of protein with respect to decellularization. In an ideal protocol, the former would comprise all of the tissue's cellular material, while the latter would comprise all of the desirable matrix materials to remain after decellularization.

In this work decellularized ECM was preserved for up to 1 yr before being used successfully for cell attachment and culture. Such "stops" are advantageous for tissue engineering processes

which operate on a commercial scale to help match output to need (Kemp 2006). A strategy of modular processing was adopted to decrease the potential of cross-contamination of surfactant or pathogens and increase equipment specialization with the long-term goal of increasing throughput, and lowering cost.

Reconditioning was considered a distinct and important process step. It has been shown that residual detergent can persist in tissue even after extensive washing (Cebotari, Tudorache et al.). The goal of the mild detergent treatment is to remove SDS from tissue (Ott, Matthiesen et al. 2008) via the formation of mixed detergent micelles that serve as an SDS carrier with a higher affinity than water alone (Ossipow, Laemmli et al. 1993). However, this treatment may deposit secondary detergent on the tissue proteins. In this way, the reconditioning steps are considered as substitutions of progressively less harmful surfactants. Following the secondary detergent wash, a protein solution was passed through the tissue. Surfactants can then partition onto the proteins in solution, combining the transport efficiencies of perfusion with the detergent binding sites of proteins for surfactant removal. The protein wash could also comprise autologous plasma or recombinant proteins. Media protein components (FBS) were used to displace adsorbed proteins from the previous wash, and the tissue was finally equilibrated against media. Together, this treatment was designed to help ensure the removal of residual detergent, DNA, and cryoprotectant; balance the ECM with respect to pH and osmolarity; and deposit media growth factors and nutrients prior to cell seeding

Sterility and throughput are critical for decellularization processes for routine application. Towards this goal, disposable/autoclavable cannulae and culture environments were designed.

The disposable tubing cannulae may be cut as desired, interfaced with standard chromatography fittings, and kept with the tissue during storage. The entire liquid circuit is autoclavable prior to use, comprising the glassware (settling vessel, and reactor) and optionally disposable tubing. The bubble-free aeration used prevents bubble-associated cell death (Handa-Corrigan and Emery 1989; Chisti 2000) and the production of foam that could block the material flow in the bioreactor or tissue lumen.

The properties of decellularized tissue have made it a material of choice for engineering complex tissues including heart (Ott, Matthiesen et al. 2008) and liver (Uygun, Soto-Gutierrez et al. 2009). Although tissue-derived ECM is a popular material for tissue engineering applications, processing is poorly understood and often requires empirical optimization for a given application (Hudson, Liu et al. 2004; Woods and Gratzer 2005; Ott, Matthiesen et al. 2008; Liu, Bharadwaj et al. 2009). An improved understanding of decellularization in the context of cell seeding and culture can aid in the development of protocols for a given application and interpretation of the results. This was facilitated by the separation of process steps, including storage.

# Chapter 4 – Derivative Materials

## 4.1 Semi-Batch Tissue Decellularization

### *4.1.1 Introduction*

Decellularization of subsections of tissues using washes was investigated as an alternative to whole-organ perfusion to facilitate parallel production and throughput while simultaneously reducing tissue use and animal sacrifice in screening experiments. Decellularization in a rack of centrifuge tubes to produce ECM for study eliminates the need for cannulation and the perfusion decellularization apparatus. Removing the requirement of cannulation also simplifies the study of decellularization of a broader range of tissues.

Decellularization of tissue sections without whole-organ perfusion may have clinical potential in additional to experimental utility. Applications may include decellularization of damaged tissues and the production of tissue patches or other surgical materials. It is conceivable that the decellularization of diffuse tissues, partial tissues, or tissue sections will be more clinically relevant than the decellularization of whole organs, which may require whole-organ tissue engineering or replacement.

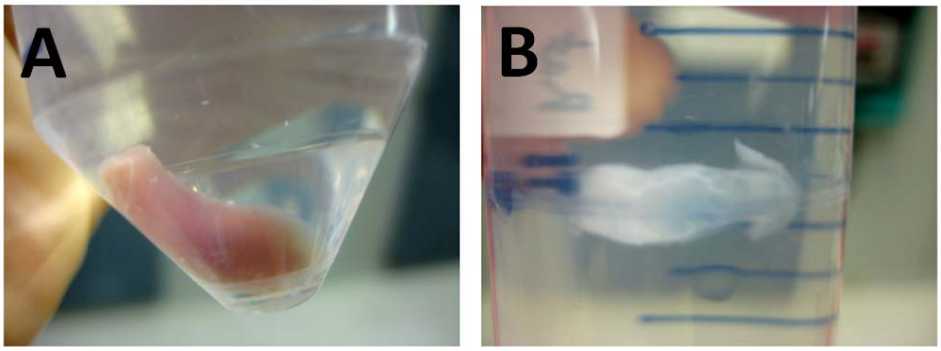


**Figure 4.1 – Cardiac Tissue Decellularized in a Semi-Batch Process**

**The feasibility of semi-batch tissue decellularization was also investigated. In this scheme, sequential washes are used to remove cellular debris without perfusion through the vasculature. This allows more tissue sections to be processed and eliminates the need for surgical cannulation. However, transport efficiency may be decreased. A preliminary experiment with heart tissue (A) is shown after 48 hrs of decellularization with 1% SDS.**

### *4.1.2 Materials and Methods*

All animal-related procedures were approved by the University of Waterloo Animal Care Committee. Adult Sprague Dawley rats (475-585g; $n$ = 3) were group housed 4 per cage at constant air temperature (20-21°C) and humidity (approx. 50%) in a 12:12-hr reverse light:dark cycle facility. Rats had free access to water and standard 22/5 Rodent Diet (W) lab chow (Harlan, Indianapolis IN). On the day of the experiment, body mass was recorded and rats were anesthetized with sodium pentobarbital injection (60 mg/kg intraperitoneally; Vetoquinol N-A, Lavaltrie, QC, Canada). The animals were systemically injected with 2500 U of heparin (Bioshop, Burlington ON, Canada) in phosphate buffered saline (PBS) as an anticoagulant. Tissues were removed, and placed in chilled PBS with 100 μg/mL ampicillin and 50 μg/mL kanamycin.

Tissues were rinsed thoroughly in PBS with ampicillin and kanamycin, and divided into sections of tissue. Hearts were divided into left and right atria, and dorsal / ventral left and right ventricular masses. Kidney, Liver and Lung were left intact at this stage.

Tissues were treated with combinations of decellularization approaches to broadly screen for effective techniques. Elements included 1 hr treatment in a sonication bath, a freeze-thaw cycle to -38°C, 4% (v/v) Triton X-100™ detergent (octyl phenol ethoxylate), 1% (w/v) sodium dodecyl sulfate, and 0.1% (w/v) EDTA. Detergents were dissolved in PBS with ampicillin and kanamycin. Tissue samples were placed in centrifuge tubes with detergent solutions, and solutions were changed every 2 hr during the day in a laminar flow hood. Decellularizing tissues

were kept under agitation at 4°C. The assignment of tissues and protocols is outlined in Table 4.1. After 24 hr, tissue sections that were large enough to cause gross decellularization gradients were dissected into smaller pieces and the decellularization protocol was repeated.

Tissues were rinsed twice for 12 hr with deionized water with ampicillin, kanamycin and 100 µg/mL streptomycin then rinsed with DMEM. Tissues were then rinsed in NeuroCult® NS-A medium supplemented with 20 ng/mL recombinant human EGF, 10 ng/mL recombinant human bFGF, and 2 µg/mL heparin. NS medium was conditioned with equal parts medium that had been exposed to NS cell culture for two days and contained cell-secreted cytokines.

Tissue samples were placed in a six-well plate with additional conditioned media and each well was seeded with $2x10^5$ neural stem (NS) cells, chosen for their sensitivity and availability, to determine the cytotoxicity of the tissue samples.

| Sample | Anatomy | Protocol Summary |
|---|---|---|
| A | Left Atrium | Sonication, then 4% Triton |
| B | Right Atrium | Freeze, then 4% Triton |
| C | Left Atrium | 4% Triton |
| D | Right Atrium | 4% Triton, 0.1% EDTA |
| E | Dorsal Right Ventricle | 1% SDS, then 1%Triton |
| F | Ventral Right Ventricle | 1% SDS, 1% Triton |
| G | Dorsal Left Ventricle | Freeze, Sonication, then 1% SDS, 1% Triton |
| H | Ventral Left Ventricle | 0.5% SDS |
| I-1 | Left Atrium | 1% SDS |
| I-2 | Right Atrium | 1% SDS |
| I-3 | Dorsal Left Ventricle | 1% SDS |
| I-4 | Ventral Left Ventricle | 1% SDS |
| I-5 | Dorsal Right Ventricle | 1% SDS |
| I-6 | Ventral Right Ventricle | 1% SDS |
| J | Dorsal Left Ventricle | Sonication, then 1% SDS |
| K | Ventral Left Ventricle | Freeze, then 1% SDS |
| L | Dorsal Right Ventricle | 1.5% SDS |
| M | Ventral Right Ventricle | 1% SDS, 0.1% EDTA |
| N-1 | Kidney | 1% SDS |
| N-2 | Kidney | " |
| N-3 | Liver | " |
| N-4 | Liver | " |
| N-5 | Lung | " |
| N-6 | Lung | " |

**Table 4.1 – Batch Tissue Decellularization Experimental Summary**

**Tissue and common decellularization protocol combinations were tested and studied for suitability in semi-batch decellularization. SDS and Triton X-100™ are both used frequently in decellularization literature, but have different strengths. SDS is a strong anionic detergent, and Triton X-100™ is a weak non-ionic detergent.**

After 2 days, the cells were imaged and assigned a qualitative score based on the number of apparent cells and their apparent health. Guidelines used are shown in Figure 4.2. Epifluorescent and brightfield imaging was performed on an inverted fluorescent microscope (Axiovert 200; Carl Zeiss MicroImaging GmbH, Berlin, Germany) with a monochrome high resolution CCD camera (XCD-SX910/X710; Sony Corporation, Tokyo, Japan).

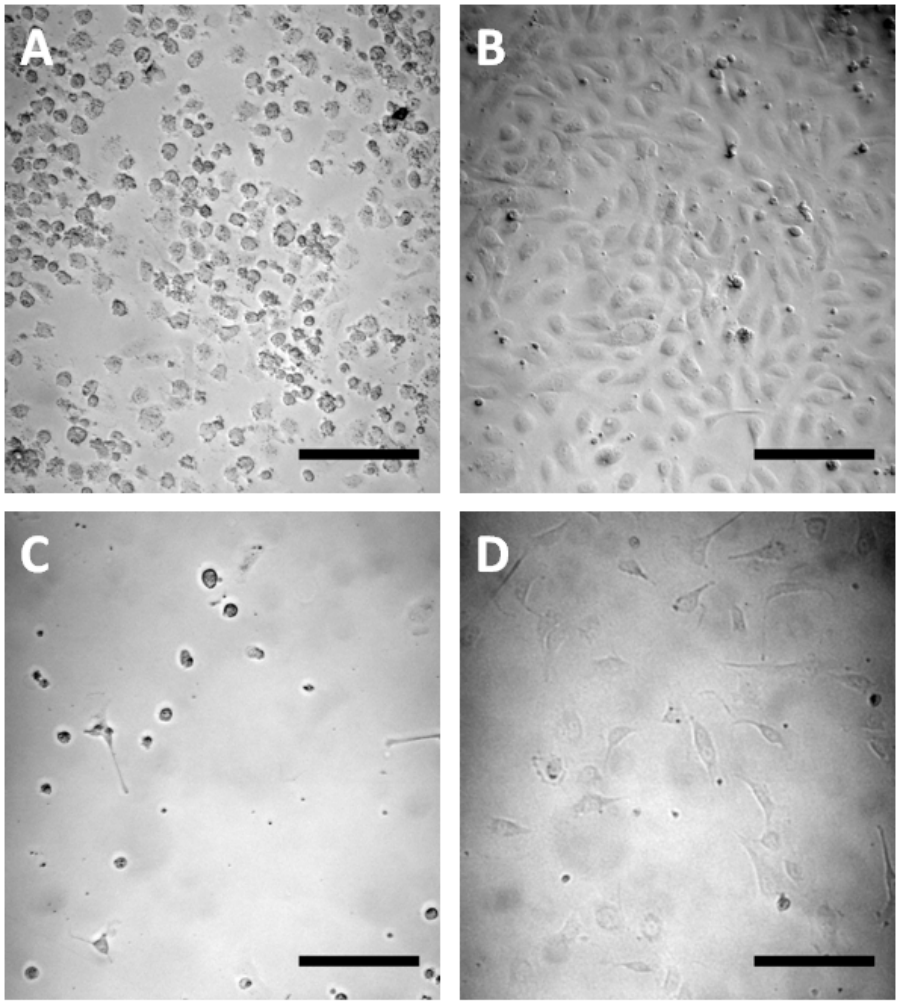


**Figure 4.2 – Cell Score Guideline Images**

**Qualitative guideline images of unhealthy phenotype with high cell number (A), healthy cell phenotype with high cell number (B), unhealthy cell phenotype with low number (C), healthy cell phenotype with low number (D). Scale bars indicate 100 µm.**

### *4.1.3 Results*

Processed tissue fragments obtained a uniform translucent appearance shown in Figure 4.3. SDS treatment tended to yield a paler ECM than milder treatments. The size of the tissue fragment was also associated with the observed completeness of decellularization, demonstrating the importance of transport limitations in the tissue. Lung was observed to more quickly achieve translucency. This may be due to lower cell density or open structure.

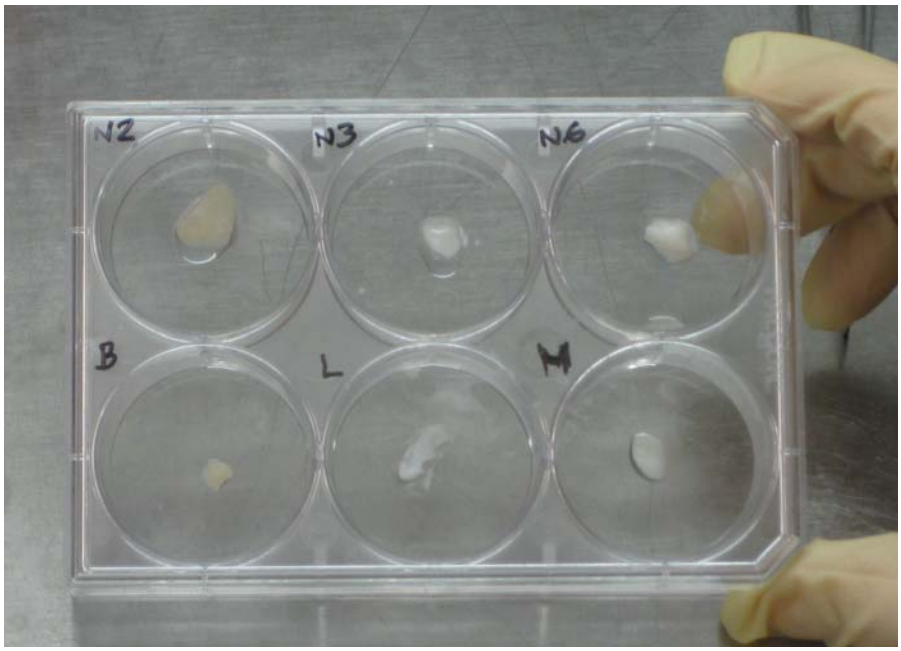


**Figure 4.3 – Semi-Batch Decellularized Tissues**

**Decellularized tissue sections (clockwise from top left) of kidney, liver, lung, ventral section of right ventricle, dorsal section of right ventricle, and right atrium. Codes correspond to the protocols outlined in Table 3.1. Increased translucency of SDS detergent treatment in the center and right well columns when compared to Triton X-100™ suggests more complete decellularization.**

Microscope imaging showed the preservation of vascular structure following decellularization as shown in Figure 4.4 after relatively harsh SDS decellularization. Strategies to address focus and depth-of-field issues were important to evaluate the complex three dimensional structures of the tissues.

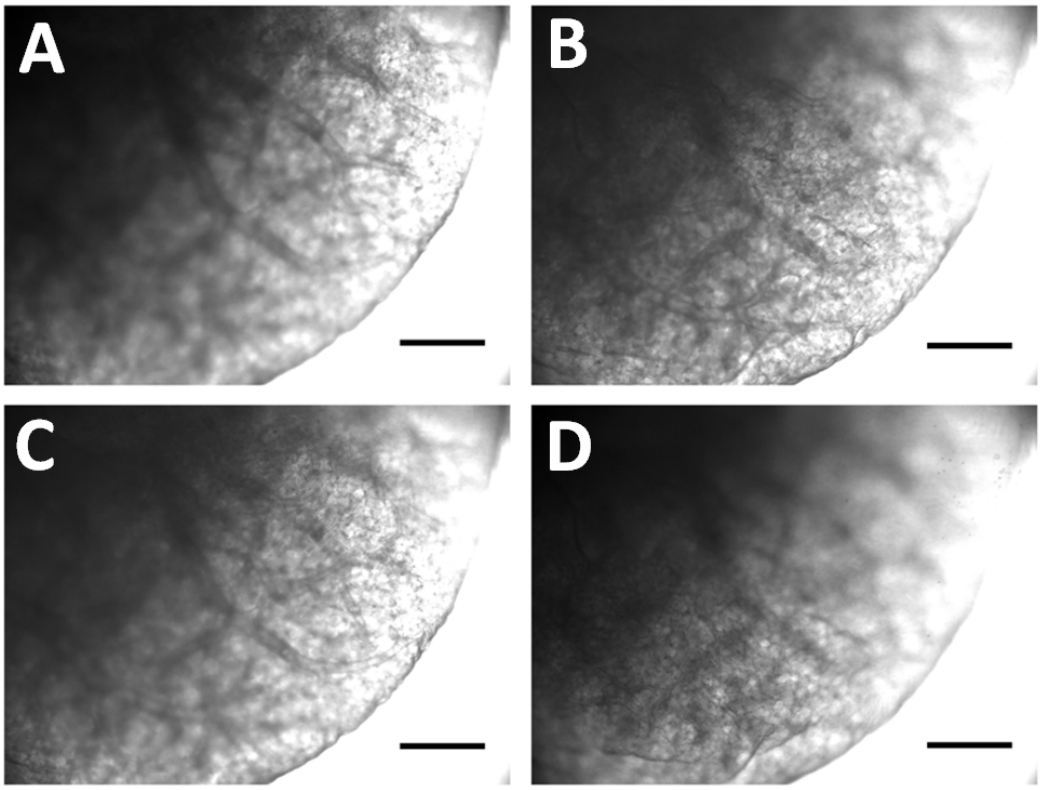


**Figure 4.4 – Capillary Structure in Decellularized Lung**

**Semi-batch SDS decellularized lung was imaged on an inverted brightfield microscope with phase contrast. Four depths of field are shown (A-D) to present the complex three dimensional structure of the tissue. Scale bars indicate 100 µm. These results show the preservation of the three dimensional vascular microstructure after harsh detergent decellularization.**

Results of the NS cytotoxicity assay are summarized in Table 4.2. One plate of four became contaminated during the NS cytotoxicity assay, and these samples were given a score of 'x'. Stronger detergents such as SDS and detergent blends with SDS tended to produce less cytotoxic material, suggesting cell debris may have a greater impact on local cytotoxicity than detergent in the short term. However, duplicate samples of SDS-treated kidney showed poor repeatability.

Imaging also suggestived of incomplete decellularization in tissues treated with semi-batch detergent treatments. DAPI staining revealed residual DNA resembling distended nuclei even in tissues treated with SDS (Figure 4.5A), which has been demonstrated to remove nuclear material in whole organ perfusion decellularization (Ott, Matthiesen et al. 2008). Tissues with associated fat, particularly kidney and heart, tended to from lipid droplets over time (Figure 4.5B) after detergent solutions were replaced with media.

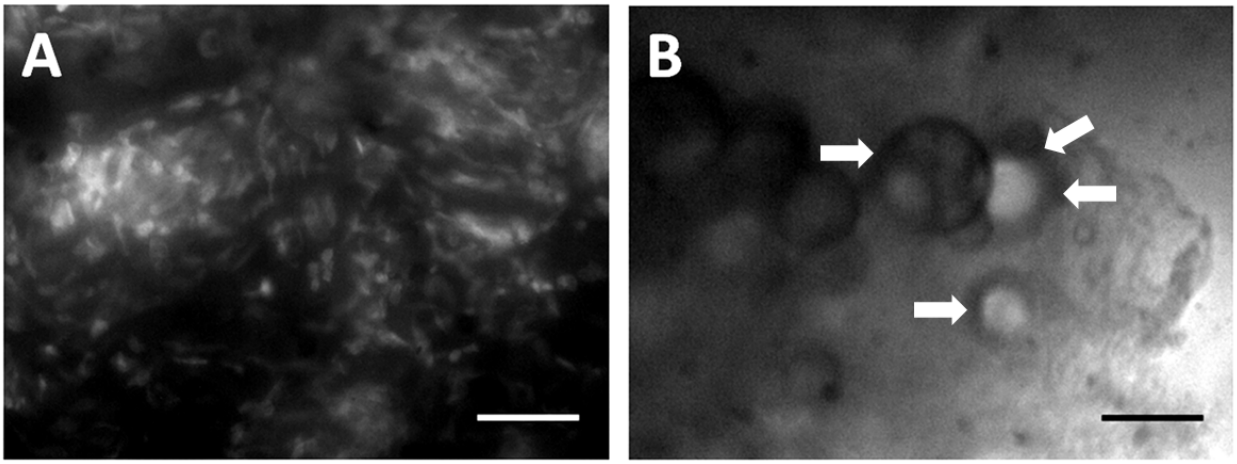


**Figure 4.5 – Indications of Incomplete Decellularization**

**DAPI staining revealed residual DNA as diffuse chromatin and distended nuclei under epifluorescent imaging (A). Brightfield images showed the formation of lipid droplets (arrows), particularly in tissues with associated fat such as kidney and heart (B). These were found develop after media changes, suggesting incomplete removal of solubilized detergent/lipid complexes. Scale bars in indicate 100 µm.**

| Sample | Tissue | Protocol Summary | Amount | Health | Score |
|---|---|---|---|---|---|
| A | Heart | Sonication, then 4% Triton | 3 | 3 | 9 |
| B | Heart | Freeze, then 4% Triton | 3 | 3 | 9 |
| C | Heart | 4% Triton | 3 | 2 | 6 |
| D | Heart | 4% Triton, 0.1% EDTA | 4 | 2 | 8 |
| E | Heart | 1% SDS, then 1%Triton | 5 | 3 | 15 |
| F | Heart | 1% SDS, 1% Triton | 6 | 4 | 24 |
| G | Heart | Freeze, Sonication, then 1% SDS, 1% Triton | 4 | 2 | 8 |
| H | Heart | 0.5% SDS | 4 | 3 | 12 |
| I-1 | Heart | 1% SDS | x | x | x |
| I-2 | Heart | 1% SDS | x | x | x |
| I-3 | Heart | 1% SDS | x | x | x |
| I-4 | Heart | 1% SDS | x | x | x |
| I-5 | Heart | 1% SDS | x | x | x |
| I-6 | Heart | 1% SDS | x | x | x |
| J | Heart | Sonication, then 1% SDS | 6 | 1 | 6 |
| K | Heart | Freeze, then 1% SDS | 4 | 1 | 4 |
| L | Heart | 1.5% SDS | 4 | 3 | 12 |
| M | Heart | 1% SDS, 0.1% EDTA | 3 | 3 | 9 |
| N-1 | Kidney | 1% SDS | 9 | 9 | 81 |
| N-2 | Kidney | " | 4 | 4 | 16 |
| N-3 | Liver | " | 3 | 4 | 12 |
| N-4 | Liver | " | 6 | 5 | 30 |
| N-5 | Lung | " | 4 | 2 | 8 |
| N-6 | Lung | " | 2 | 2 | 4 |

**Table 4.2 – Cytotoxicity Assay Results Summary**

**Decellularized tissues and the protocols tested are shown. The qualitative abundance of cells was scored between 1 and 10 using three randomly selected fields of view. A score of qualitative cell health was also assigned. The overall cytotoxicity score was the product of these two values. A score of 'x' indicates the sample was destroyed due to a contaminated plate. A higher score indicates lower cytotoxicity.**

### *4.1.4 Discussion*

The initial screening experiments demonstrated the potential of semi-batch decellularization for small tissue fragments. The preserved microstructure and partial removal of cellular material is valuable towards the production of near-native engineered materials from animal tissue.

Short term cytotoxicity assays showed reduced cytotoxicity with stronger detergents and detergent mixtures containing SDS. This suggests that the dominant cytotoxic effects observed in this experiment were due cell debris, apoptotic cell signaling molecules, or partially solubilized membrane-containing detergent, which are more likely to be removed by stronger detergents.

Although it may be desirable to produce decellularized tissues without cannulating and decellularizing an entire organ, the transport challenges of removing perfusion must be considered during protocol development. When large tissues were dissected to produce smaller samples before further processing, a gradient was observed with increasing translucency to the exterior of the tissue. Greater control over the size distribution of tissue fragments will be useful to produce repeatably decellularized materials and develop protocols that completely decellularize tissue without overly damaging the most easily-decellularized regions.

Transport issues may be particularly important for DNA removal due to its large and highly charged structures. In the protocols tested, residual distended nuclei and chromatin were

observed coating the ECM following DAPI staining, demonstrating the need for nuclease treatment for complete decellularization.

Additional residual material included droplet-forming lipids in the tissue. This is believed to be the result of detergent treatment and incomplete removal of detergent-lipid complexes. This is supported by the exaggerated formation in fattier materials such as the kidney and emphasizes the importance of upstream processing and tissue preparation. Complete removal of fatty tissues or undesired transport-limiting structures such as the renal capsule may be as important to consistent processing as tissue geometry. Unfortunately, this re-emphasis on upstream handling and surgery diminishes some of the principle advantages of this approach, such as ease of scale-up and simplified tissue preparation. The utility of this experiment lies mostly in revealing the broad processes of decellularization under varied conditions while minimizing the need to collect animal tissue.

## 4.2 Cell Seeding

### *4.2.1 Introduction*

The ECM materials being developed must support cell attachment, growth, and proliferation for effective cell therapy. Although the cytotoxicity assay presented in Section 3.1 gives an indirect measure of the quality of the extracellular matrix in biological terms, robust cell seeding and imaging protocols are ultimately required to evaluate and improve decellularized materials.

### *4.2.2 Decellularized and Seeded Slices*

Tissue slices were investigated to create a consistent geometry. Regular thickness and distance to the free solution is desirable to facilitate consistent decellularization processes, and to facilitate uniform imaging between samples. In addition, tissue slices were investigated to create an even surface for cell seeding and entrapment.

Tissues from a Sprague Dawley Rat prepared as described in 3.1.2 were mounted in a microtome (Leica Mikrosysteme GmbH, Vienna, Austria) with stainless steel razor blades (Feather Safety Razor Co. Ltd., Osaka, Japan). However, the thickness of the tissues produced was inconsistent. Firm tissues such as kidney were resistant to the blade and deformed readily. Frozen tissues could be sliced to as thin as 0.5 mm, however only a small amount of material could be produced before thawing resulted in irregular or wasted materials. Maintaining tissue temperature without using a cryomicrotome also proved impractical, and over-chilled samples were prone to cracking and splintering.

An alternative method to support the tissue and control even slicing was the use of a tissue slicer matrix shown in Figure 4.6. The tissue slicer facilitated the production of samples at 0.5 or 1.0 mm thickness, with more consistency and in greater amount that with the microtome.

Heart, Kidney, and Liver tissues were isolated as described previously and sliced to a thickness of 1.0 mm in a coronal slicer matrix. Two candidate protocols were tested in the cell seeding and cytotoxicity experiments. The first comprised 4% (v/v) Triton X-100™ with 0.1% (w/v) EDTA,

and the second comprised 1% (v/v) Triton X-100™ and 0.5% (w/v) sodium deoxycholate. These detergents were selected for being well-supported in literature (Samouillan, Lamure et al. 2000; Spina, Ortolani et al. 2003). Longer protocols, thinner tissue sections, and addition of benzonase treatment were adopted to remove cell debris shown in Section 3.1. Both protocols used two-day semi-batch detergent decellularization with agitation at 4°C, and liquid changes every 2 hours and overnight. This was followed by incubation with 25 U/mL Benzonase™ nuclease (EMD Chemicals Ltd., Gibbstown, NJ) in a buffer containing 50 mM Tris-HCl pH 8, 20 mM NaCl, and 2 mM $MgCl_2$. Decellularization solutions and nuclease buffer also contained antibiotic antimycotic solution (Sigma-Aldrich Canada Ltd., Oakville, ON, Canada) with 10,000 U/mL penicillin G, 10 mg/mL streptomycin sulfate and 25 μg/ml amphotericin B.

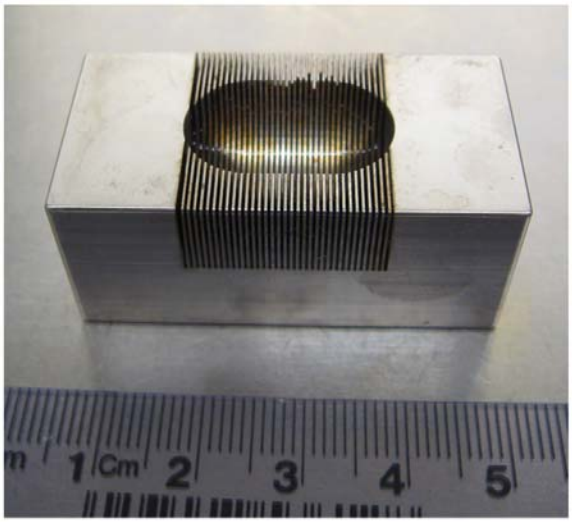


**Figure 4.6 – 0.5mm Coronal Rat Heart Tissue Slicer Matrix (Zivic Instruments™)**

**The tissue slicer matrix supports the tissue during cutting to reduce warping and produce more consistent results. Coronal matrices cut the tissue perpendicular to the long axis of heart. Razor blades are slid with downward pressure into the matrix. Slices are then collected from between the blades. 1 mm slices were found to be more repeatable than 0.5 mm slices.**

Tissues were rinsed twice in DMEM for 1 hr each, then rinsed for 1 hr in endothelial cell medium comprising MCDB-131 (Invitrogen Canada Inc., Burlington, ON, Canada) supplemented with an endothelial growth medium-2 Sinqlequot™ (Lonza, Walkersville, MD), 2 mM L-Glutamine, and 10% (v/v) fetal bovine serum (Invitrogen Canada Inc., Burlington, ON, Canada). Slicing and decellularization was found to maintain the tissue microstructure as shown in Figure 4.7.

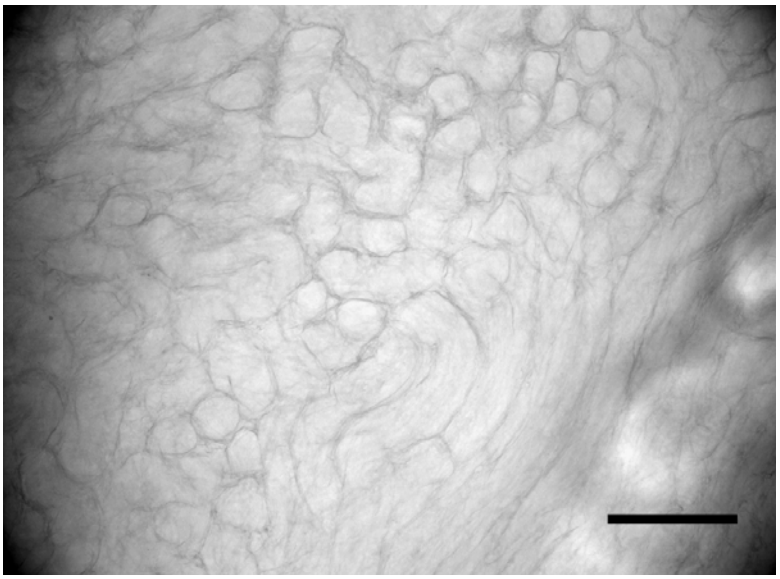

**Figure 4.7 – Microstructure of Decellularized Kidney Slide**

**The cross-section of the renal cortex is shown following mechanical processing and decellularization. The microstructure of the renal tubules are preserved, similar to the lung vasculature shown in Chapter 2. The scale bar indicates 100 µm.**

The surface of each tissue slice was overlaid with $1x10^4$ human umbilical vein endothelial cells (HUVECs) that had been cultured in the endothelial cell medium on tissue-treated 75 $cm^2$ polystyrene flasks (BD, Mississauga, ON, Canada) coated with gelatin from bovine skin, type B (Sigma-Aldrich Canada Ltd., Oakville, ON, Canada). 200 µL of endothelial cell suspension was gently applied to each tissue slice before incubation and in six-well plates in a total volume of 2 mL for 2 hours. Additional media was then gently added to each well.

After two days of culture, the wells were imaged to assess the degree of cell attachment and survival. In wells with tissue decellularized with 4% (w/v) Triton X-100™ and 0.1% (w/v) EDTA, cell phenotype was observed to be healthier and with greater attachment further from the tissue, suggesting potential cytotoxicity of the matrix. The effect was observed to a lesser degree in the tissues treated with 1% (v/v) Triton X-100™ and 0.5% (w/v) sodium deoxycholate. The quantity of cells at the bottom of the wells was also suggestive of poor attachment particularly for heart and liver tissue.

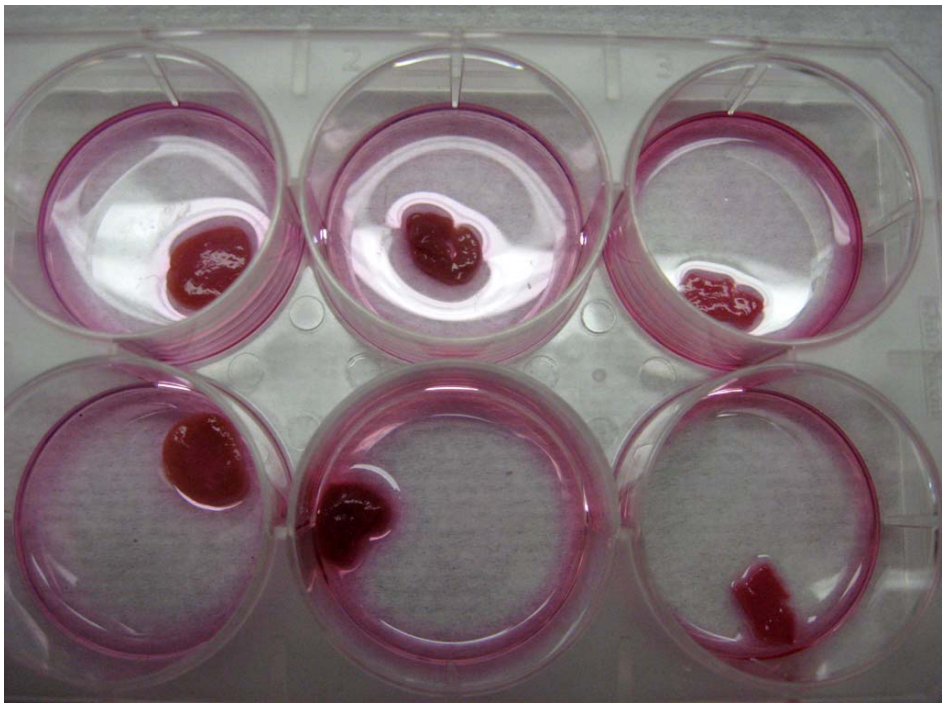

**Figure 4.8 – Cultured Tissue Slices**

**1 mm tissue sections prepared in the slicer matrix were overlaid with $1x10^4$ HUVECs and cultured for two days in a six-well plate. The sections were reversed and imaged for cell proliferation and health. The left wells contain kidney tissue, the middle wells contain heart tissue, and the right well contain liver tissue.**

Samples were incubated with 1 μM CFDA-SE for 1 hour at 37°C to image metabolically active cells in the tissue. Kidney tissue was found to present the most viable adherent cells (Figure 4.9). The porous structure of the cross-sectioned tissue may have contributed to improved cell entrapment, and may also have facilitated transport for more complete decellularization and reduced cytotoxicity.

CFDA-SE is converted by cytoplasmic enzymes to 6-carboxyfluorescein succinimidyl ester, which fluoresces and binds to free amine groups. The high level of background signal may have been caused by binding of the fluorophore to the proteins of the matrix itself after being secreted by labeled cells. This is supported by the observed increase in background signal over time. Enzyme activity in the matrix may also have contributed to fluorophore conversion.

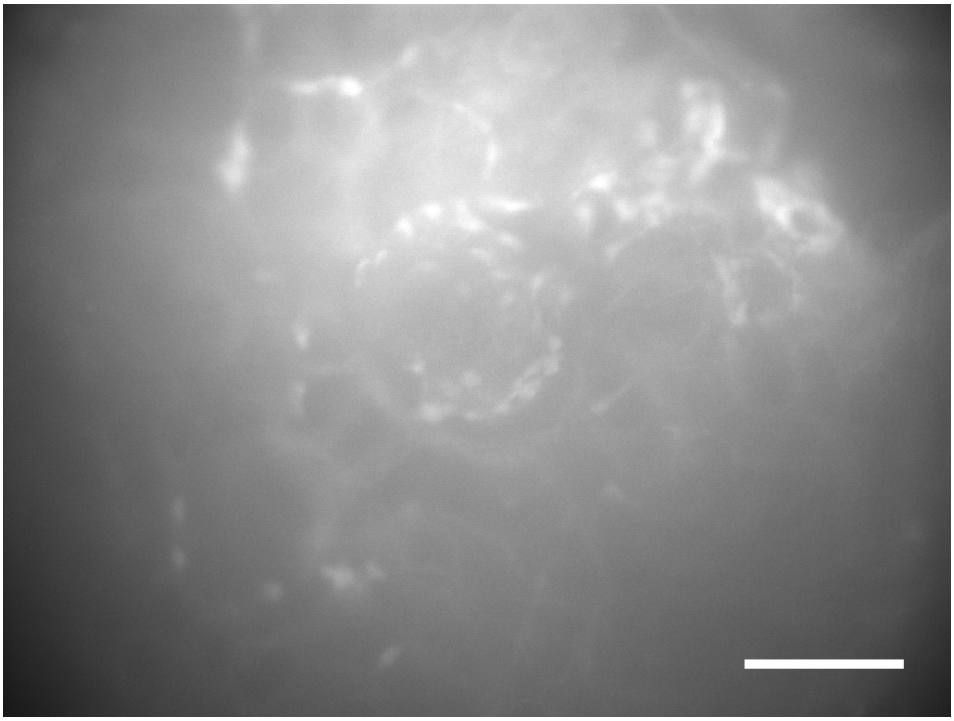

**Figure 4.9 – CFDA-SE Stained Cultured Kidney Slice**

**A 1 mm section of kidney prepared in a tissue slicer matrix and cultured with HUVECs for two days. The sample was incubated with 1 µM CFDA-SE for 1 hour, rinsed, and mounted on a glass slide. Elongated morphology suggests good cell attachment, and fluorescence indicates metabolic activity. Background fluorescence may be caused by fluorophore secretion and binding to the protein matrix. Scale indicates 100 µm.**

### *4.2.3 Gelatin-Coated ECM*

A kidney isolated from a Sprague Dawley rat was cannulated with PEEK tubing in the renal vein and stored at -80°C was thawed after 1 mo and mounted on the perfusion decellularization apparatus described in Chapter 2. The kidney was decellularized with 1% SDS in PBS with antibiotic antimycotic at 2 mL / min for 24 hr. The tissue was then disinfected by flushing with an aqueous solution of 0.1% (v/v) peracetic acid and 4% (v/v) ethanol (Rosario, Reilly et al. 2008; Liu, Bharadwaj et al. 2009) and stored in PBS at 4°C. Perfusion decellularization and sterilization were selected to produce the most completely decellularized and uniform ECM available when testing the effect of matrix coatings, with stored material used to reduce the amount of animal sacrifice.

The decellularized and disinfected kidney was then cut into 1mm thick sections (n = 6) using the tissue slicer matrix as described above. The tissue samples were rinsed twice with DMEM for 1 hr, then once with the endothelial cell media described above. Kidney sections were placed in a six well plate, and half of the samples were coated with a solution of 1 mg/mL gelatin from bovine skin, type B, with excess gelatin removed by aspiration. Endothelial cell medium was then added to each well and allowed to equilibrate in an incubator for 1 hr.

Mouse blood outgrowth endothelial cells (mBOECs) were cultured in endothelial cell medium on gelatin-coated plates, trypsinized, and seeded at $2x10^5$ cells per tissue sample. After 24 hr of culture the samples were transferred to a new well plate with fresh medium. After six additional days of culture, kidney slices were labeled with 1 μM CFDA-SE, incubated for 1 hr, turned over

to image the seeded surface and imaged (Figure 4.10). The gelatin-coated tissue appears to have improved cell attachment and morphology. However, depth-of-field and focus problems interfered with quantification. Additionally, background fluorescence obscured the majority of cells.

This experiment suggests that ECM coatings can improve seeding efficiency and viability in sectioned tissue decellularization. However, improved mounting and imaging approaches are required.

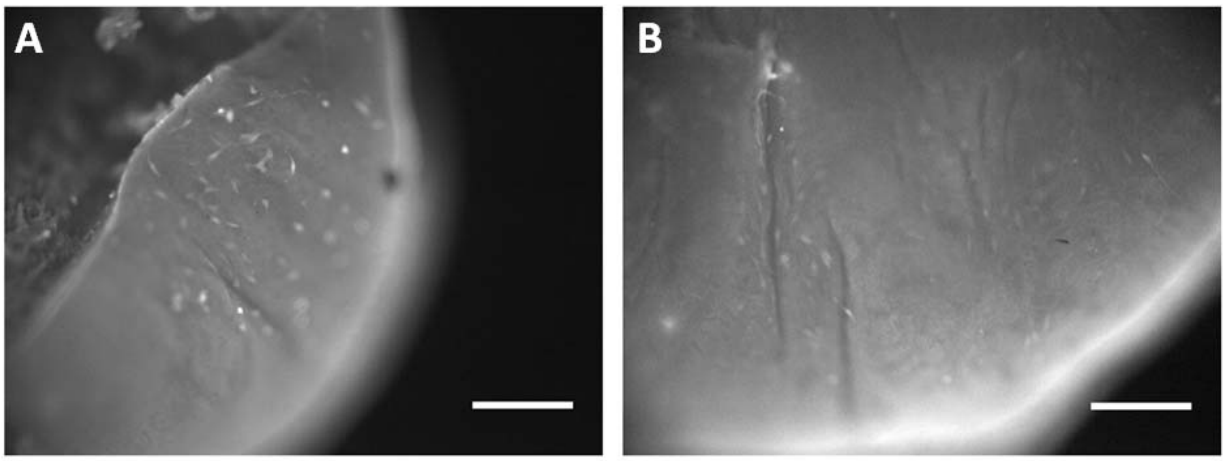


**Figure 4.10 – Gelatin-Coated Seeded Tissue Sections**

**Gelatin-coated kidney ECM (A) appears to have improved cell attachment and morphology over non-coated kidney ECM (B). Limited focus and background fluorescence reduce the quality of imaging data. Scale bars indicate 100 µm.**

## 4.3 ECM-Derived Coatings and Gels

### *4.3.1 Introduction*

Derivatives of decellularized matrices were also investigated for cell culture. In particular, gels and coatings were developed to facilitate imaging of cells during cytotoxicity bioassays. This work was aimed towards providing quantitative *in vitro* evaluation of decellularization protocols from a biocompatibility perspective.

Homogenous materials have additional advantages of improved replication for given decellularized tissue sample. Imaging several well plates coated with an identical material was anticipated to be much more consistent than imaging different regions of a complex three-dimensional tissue. The amount of material required for a two-dimensional culture was anticipated to be less than culturing complete decellularized tissues. This would increase throughput and reduce tissue requirements for decellularization process optimization.

ECM coatings and gels are also an active area of research for therapeutic applications, in addition to roles as cell culture tool and for cell-matrix studies (Lin, Chan et al. 2004; Stern, Myers et al. 2009; Zhang, He et al. 2009). These experiments also facilitated the investigation of alternative disinfection and sterilization techniques.

### *4.3.2 Acetic Acid Extraction*

The kidney of a Sprague Dawley rat was removed, cannulated, stored at -80°C for 6 wk, and decellularized with 1% SDS in PBS with antibiotic antimycotic at 2 mL / min for 24 hr. The fatty tissue and renal capsule were removed with a scalpel before the tissue was placed into a tissue press and passed twice through a 0.5 mm screen (Figure 4.11). Fibrous material in the screen was then discarded. The resulting slurry was placed in PBS with antibiotic antimycotic, agitated, allowed to settle and the supernatant was discarded. The decellularized kidney slurry was then homogenized with a pulsed sonication tip of a W-225 ultrasonic processor (Heat Systems Ultrasonic, Inc.) at 40% power for 5 min. The resulting suspension was centrifuged at 855 RCF for 10 min and the supernatant was discarded (Figure 4.12).

**Figure 4.11 – Tissue Press**

**A tissue press was used to mechanically process soft tissues into slurry following trimming of excess fat and connective tissue. Fibrous material was removed from the 0.5 mm screen and the slurry was collected in PBS with antibiotic/antimycotic.**

A solution of 0.4% (v/v) acetic acid was added to the solids and agitated until partially dissolved. Half of the resulting suspension was then passed through a 40 μm filter. The solution was used to coat 16 wells of a 24 well plate, with quadruplicate conditions each of filtered, unfiltered, 2x diluted, and undiluted solution at 250 μL material per well. The plate was exposed to UV sterilization for 30 minutes and remaining solution was aspirated. The wells were then rinsed 5 times in sterile PBS.

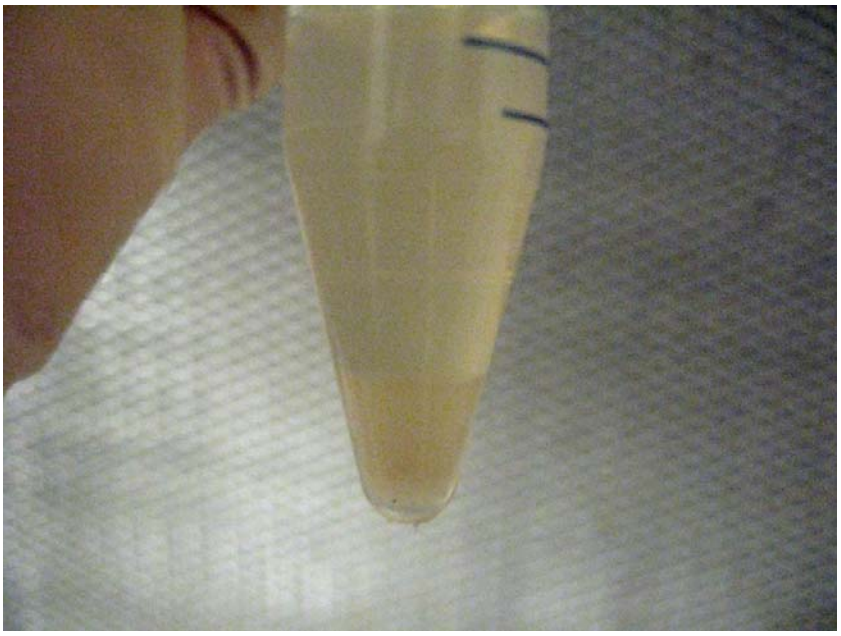

**Figure 4.12 – Sonicated and Centrifuged ECM Suspension**

**Decellularized ECM slurry was treated in a pulsed ultrasonic processor in PBS with antibiotic antimycotic and centrifuged at 855 RCF for 10 min in a centrifuge tube. The settled material had a uniform appearance. ECM debris in the supernatant was discarded.**

Canine blood outgrowth endothelial cells (cBOECs) were cultured in endothelial cell medium on gelatin-coated plates and trypsinized as described previously. Each well was then seeded with $1x10^5$ cells with gelatin-coated plastic as a control (Figure 4.13). After 5 days of culture on the adsorbed ECM coating (Figure 4.14), the cells elongated and formed capillary-like networks similar to those observed following endothelial cell culture on Matrigel™ (Kubota, Kleinman et al. 1988), a commercially available basement membrane-derived gel (BD, Mississauga, ON, Canada). This suggests that the coating retained important matrix components such as collagen, laminin, and growth factors. However, it is unknown how closely the coating reflects the original decellularized tissue slurry.

After 6 days of the culture, the adsorbed coating formed a floccular precipitate, similar to that described when ECM components are mixed in solution at physiological ratios and conditions (Kleinman, McGarvey et al. 1983; Woodley, Rao et al. 1983). A more stable surface is required for long-term cytotoxicity imaging studies. This might be achieved by additional collagen cross-linking, blending the coating with stabilizers, using ultracentrifugation and lyophilization to purify more readily soluble components (Stern, Myers et al. 2009; Zhang, He et al. 2009), or preparing a more stable gel using the protocols used to make Matrigel™.

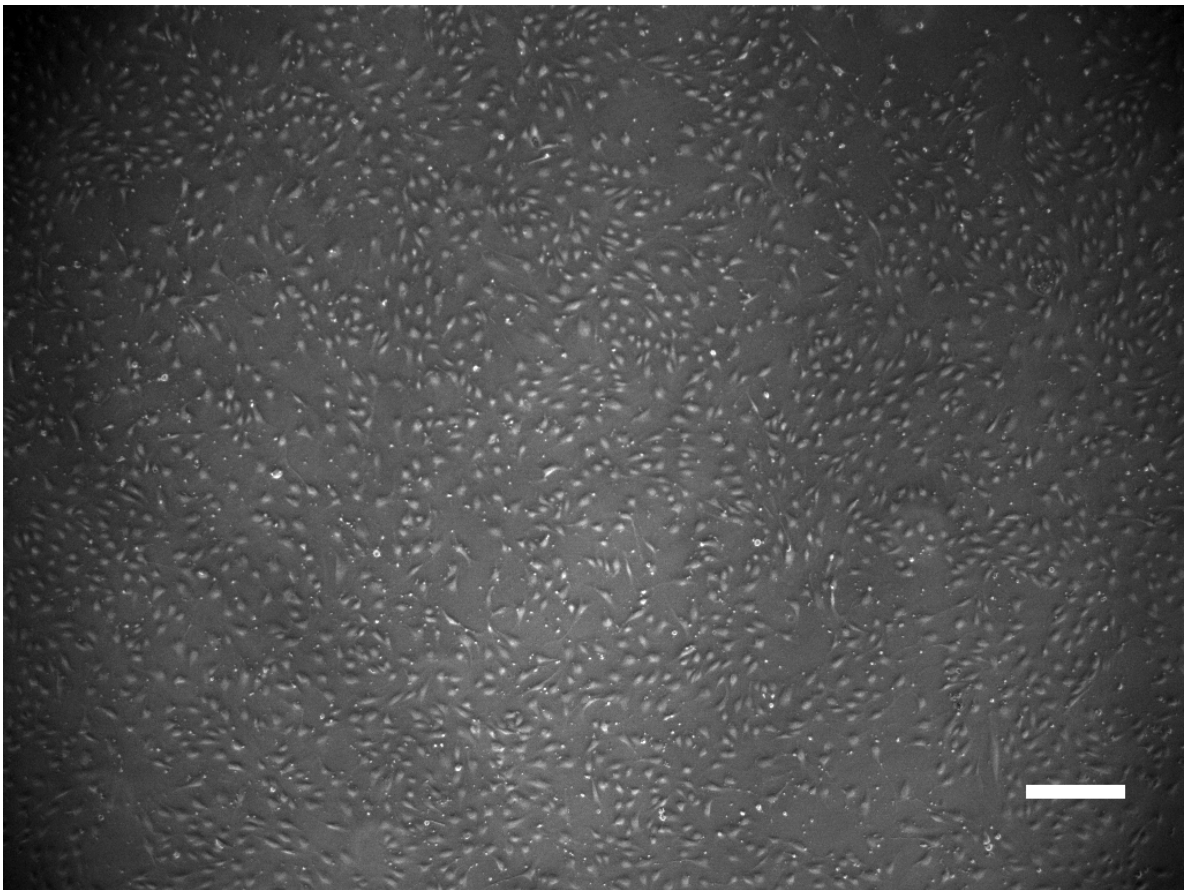

**Figure 4.13 – cBOECs on a Gelatin-Coated Surface at 5 days**

**$1x10^5$ cBOECs were cultured on a $25cm^2$ tissue-treated polystyrene T-flask with a gelatin coating for 5 days. These cells have an attached and slightly elongated morphology. Scale bar indicates 200 µm.**

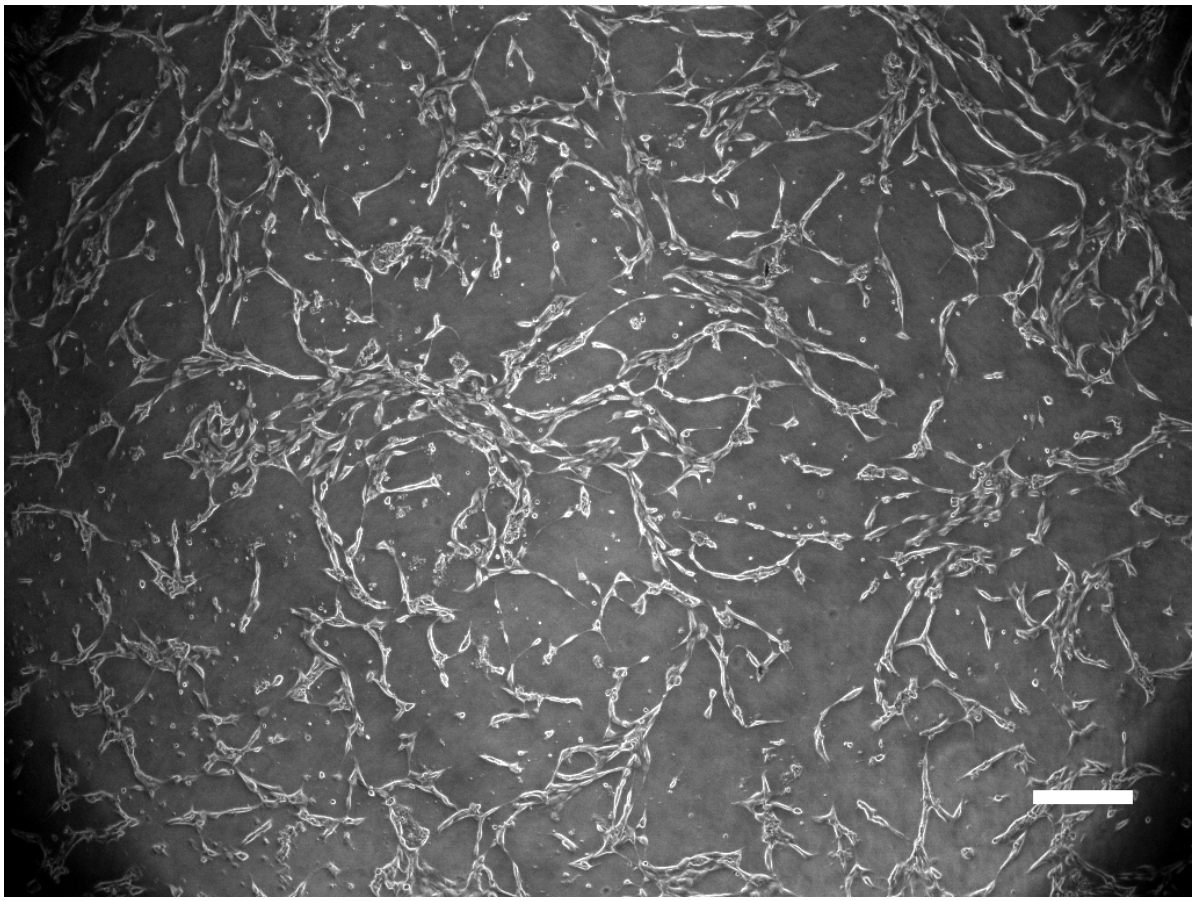

**Figure 4.14 – cBOECs on an ECM-Adsorbed Surface at 5 days**

**$1x10^5$ cBOECs were cultured on a $25cm^2$ tissue-treated polystyrene with an adsorbed ECM coating prepared from an acetic acid extraction of sonicated ECM. Cells appeared highly elongated and formed capillary-like networks. Scale indicates 200 µm.**

### *4.3.3 ECM-Derived Gels*

Perfusion decellularized kidney slurry was prepared as described above with SDS vascular perfusion followed by tissue pressing. The material was then rinsed with PBS containing antibiotic antimycotic solution, sonicated, and centrifuged as described. The solids were resuspended in 2M urea and agitated at 4°C for 3 days. The solution was centrifuged and 2 mL of supernatant was then dialyzed in 250 mL PBS with 5% (v/v) chloroform to sterilize the solution in 6000-8000 MWC dialysis tubing (Kleinman, McGarvey et al. 1986). Dialysis was performed on ice in a fume hood with 3 buffer changes. The buffer was then replaced with DMEM with 3 additional buffer changes. The solution was then brought to 0.02N acetic acid using a stock solution of 0.35N acid.

The solution was combined with rat tail collagen to produce stocks of 0%, 10%, and 50% (v/v) ECM extract in collagen. A neutralizing solution was prepared with 100mM HEPES adjusted to pH 7.3 in 2x PBS (Wozniak and Keely 2005). cBOECs were cultured as described above, trypsinized, resuspended, and combined with chilled equal parts of the collagen solutions and neutralizing solution to a final concentration of $1x10^5$ cells per mL. Solutions were mixed with chilled pipettes in a biological safety cabinet, and 5 μL volumes were cast in glass imaging chambers treated with aminopropyl trimethoxysilane (APTS). The discs were allowed to cast for 30 min in an incubator at 37°C, and the imaging chambers were then filled with media.

After 10 days of culture, the discs were stained with DAPI and imaged (Figure 4.15) under brightfield and fluorescent imaging. Figure 4.16 presents the same samples under higher magnification to resolve individual nuclei. Areas largely absent of cells in Figure 4.15 B,D, and

F, appear to correspond to areas of thin gel deposition, pointing to incomplete mixing of materials or uneven flow during casting. These may be caused by premature solidification and contribute to the technical difficulties of producing large amounts small gel carriers. However gel production facilitated the use of chloroform dialysis to ensure sterility, presenting an advantage over other materials produced in this chapter.

The rat tail collagen gel presented the most regular appearance in both the gel morphology and the distribution of cells. The 50% ECM gel has a more granular appearance than the other samples, suggesting a different organization structure which may be related to the formation of physiological supramolecular complexes of matrix components (Kleinman, McGarvey et al. 1983).

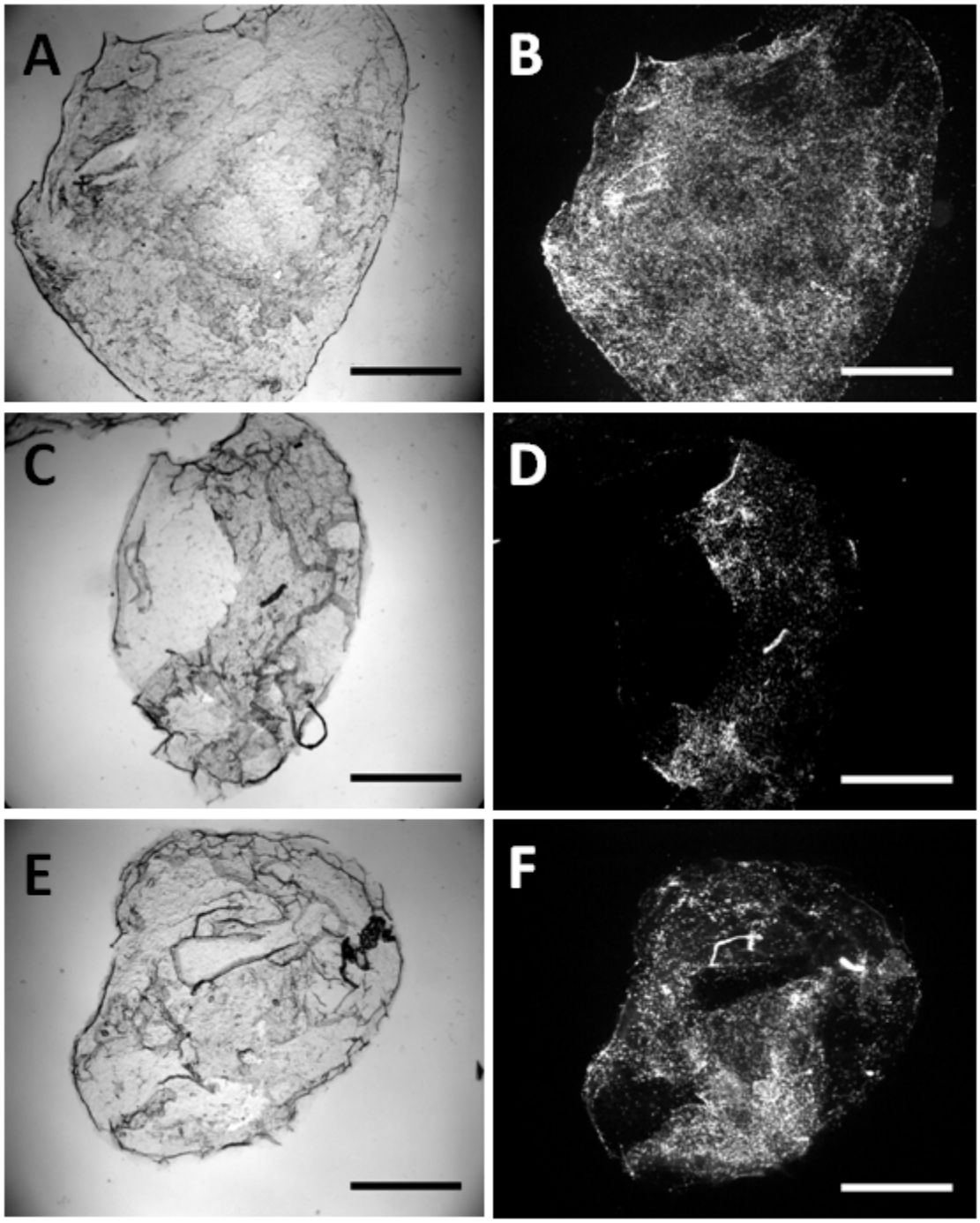


**Figure 4.15 – Cultured ECM/Collagen Discs Overview**

**ECM gel was prepared from a 2M urea extract of ultrasonicated decellularized ECM, and then dialyzed against buffer and basal medium. Brightfield (left column) and fluorescent DAPI images (right column) are shown for mixtures of ECM and collagen gel with 0% (A,B), 10% (C,D), and 50% (E,F) ECM gel content. Gels were cast at $1x10^5$ cells per mL and cultured for 10 days. Scale bars indicate 200 µm.**

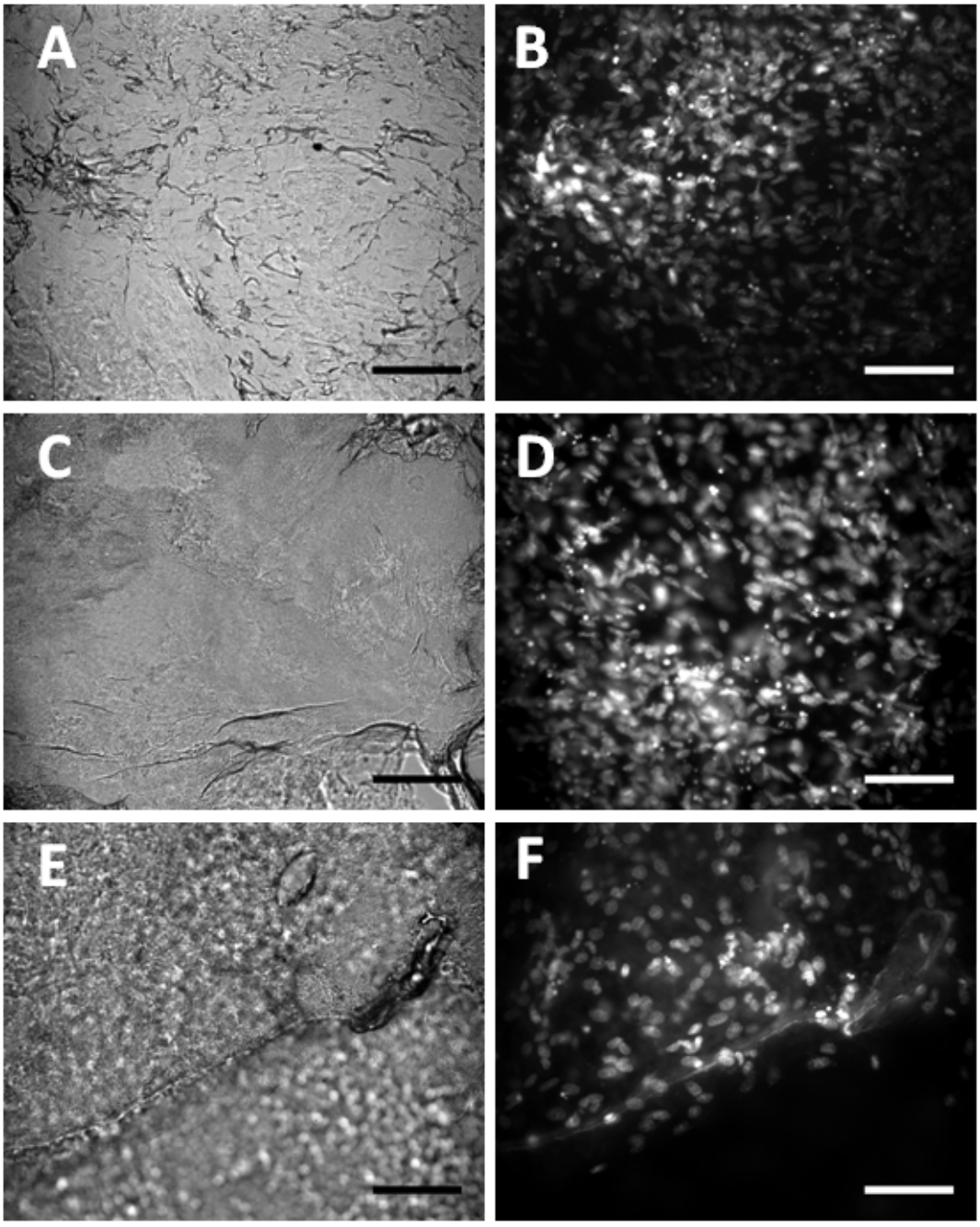


**Figure 4.16 – Cultured ECM/Collagen Discs 20x Magnification**

**The gel discs from Figure 4.16 imaged at a higher magnification. Individual nuclei can be observed, showing high confluence. Cell densities appear higher at lower ECM concentrations suggesting residual cytotoxicity from ECM gel processing. Large regions without cells may have resulted from incomplete mixing of the cell suspension and gel before casting. Scale bars indicate 50 µm.**

## 4.4 Discussion

In this chapter, decellularization of tissue sections was investigated as an alternative to whole-organ perfusion. Developing techniques to decellularize using washes and eliminating cannulation was aimed to increase throughput, scalability, and allow the production of a wider variety of materials for diverse applications.

Decellularization of tissue sections without whole-organ perfusion may have clinical potential in addition to experimental utility. Applications may include decellularization of damaged tissues and the production of tissue patches or other surgical materials. It is conceivable that the decellularization of diffuse tissues, partial tissues, or tissue sections will be more clinically relevant than the decellularization of whole organs, which may require whole-organ tissue engineering or replacement.

Cytotoxicity assays using both sensitive and robust cell lines were used to evaluate combinations of tissue and decellularization protocols. Stronger detergents and detergent blends may have produced less cytotoxic material, suggesting incomplete decellularization in the protocols tested. However, more repeatable bioassays are required. Imaging also indicated incomplete semi-batch decellularization. DAPI staining showed residual nuclei and chromatin, and lipid droplets were observed to form in the ECM.

Approaches were tested to produce more uniform tissue sections, achieve more complete decellularization, and develop robust seeding protocols. Other materials including coatings and

gels were tested. Coatings were found to induce morphological changes associated with capillary formation, implying bioactivity of the ECM and its derivatives.

Residual cytotoxicity from incomplete decellularization or reconditioning may be caused by transport limitations, particularly in the absence of vascular perfusion. Reducing the size of the ECM fragments was observed to facilitate decellularization during the production of gels and coatings. Using progressively smaller ECM also increases the surface area for cell attachment, reduces material use, and provides alternatives for handling and culture. This will be further discussed in Chapter 4.

# Chapter 5 – Micronized ECM Carriers

## 5.1 Crushed Matrix Carriers

### *5.1.1 Introduction*

The heavily processed decellularized matrix described in Chapter 3 was also investigated as a product, in addition to its previously discussed role as an intermediate to study large decellularized tissues. Potential applications of micronized decellularized material include wound modulation (Pietramaggiori, Scherer et al. 2008), surgical filler (Sclafani, Romo et al. 2000), and for soft tissue engineering (Yoo and Lim 2009). The focus of this work is the development of micronized ECM towards the support of gene-modified cell therapy by promoting survival of transplanted adherent cells *in vivo*.

Micronized matrix as a final product also has production advantages over tissue section and whole organ tissue engineering. Increased surface area facilitates decellularization mass transport processes, provides more area for seeding, and simplifies mounting and imaging. The increased surface area also facilitates higher density culture and reduces animal tissue use.

### *5.1.2 Materials and Methods*

Canine blood outgrowth endothelial cells (cBOECs) were a generous gift from Dr. David Lillicrap, Queen's University. Cells were cultured in MCDB-131 (Invitrogen Canada Inc.,

Burlington, ON, Canada) supplemented with an Endothelial Growth Medium-2 Sinqlequot™ kit (Lonza, Walkersville, MD), 2 mM L-Glutamine, and 10% (v/v) fetal bovine serum (Invitrogen Canada Inc., Burlington, ON, Canada) . Cells were cultured in tissue-treated 75 $cm^2$ polystyrene flasks (BD, Mississauga, ON, Canada) coated with rat tail collagen, type I (BD, Mississauga, ON, Canada) in a controlled atmosphere at 37°C and 5% $CO_2$. Cells were passaged at 90% confluency with 2.5 g/L trypsin with 0.38 g/L EDTA (Invitrogen Canada Inc., Burlington, ON, Canada) every 3-4 days.

All animal-related procedures were approved by the University of Waterloo Animal Care Committee. Adult Sprague Dawley rats were group housed 4 per cage at constant air temperature (20-21°C) and humidity (approx. 50%) in a 12:12-hr reverse light:dark cycle facility. Rats had free access to water and standard 22/5 Rodent Diet (W) lab chow (Harlan, Indianapolis IN). On the day of the experiment, body mass was recorded and rats were anesthetized with sodium pentobarbital injection (60 mg/kg intraperitoneally; Vetoquinol N-A, Lavaltrie, QC, Canada). Tissues were removed, and placed in chilled PBS with 100 μg/mL ampicillin and 50 μg/mL kanamycin.

A Sprague Dawley kidney was harvested and cannulated with PEEK tubing in the renal vein, and perfusion decellularized using the apparatus described in Chapter 2 with 1% Triton X-100™, 0.5% sodium deoxycholate, with 100 U/mL penicillin and 100 μg/mL streptomycin in PBS at 2 mL / min for 24 hr. The decellularized kidney was then stored for 2 months at -80°C in PBS. The tissue was thawed and passed through a tissue press as described in Chapter 3, rinsed with PBS with antibiotic antimycotic solution (Sigma-Aldrich Canada Ltd., Oakville, ON, Canada)

with 10,000 U/mL penicillin G, 10 mg/mL streptomycin sulfate and 25 μg/mL amphotericin B, and disinfected with 0.1% (v/v) peracetic acid and 4% (v/v) ethanol in deionized water for 3 min. The ECM was then rinsed with sterile PBS, equilibrated with DMEM for 2 days, and equilibrated with cBOEC medium described above for 1 day. The ECM was seeded with $2x10^6$ cBOECs with 3.5 mL of medium in a 10 mL falcon tube. The tube was allowed to equilibrate with a loosened cap in an incubator overnight, before being transferred to a six well plate for culture. To image metabolically active cells, carrier samples were incubated for 10 minutes with DMEM containing 1 μM CFDA-SE. Samples were then rinsed with PBS in a microcentrifuge tube and transferred to a glass slide as shown in Figure 5.1.

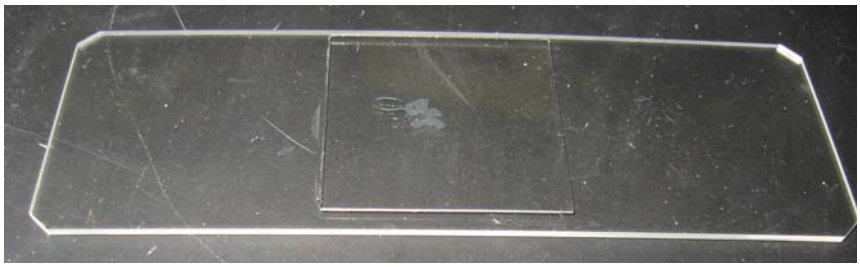

**Figure 5.1 – Mounted Tissue Carrier Sample**

**The production of small ECM carriers facilitated wet mounting. Flattened carriers reduced depth of field issues and also created a narrower column of excited tissue during fluorescent imaging, resulting in decreased background fluorescence.**

In a second protocol, an uncannulated kidney stored at -80°C in PBS without detergent treatment was tested. The tissue was thawed, removed of fatty tissue and the renal capsule, passed twice through a tissue press with fibrous tissue discarded. The material was rinsed in PBS with antibiotic antimycotic solution then ground in a mortar and pestle to further reduce carrier size.

The material was then transferred to a centrifuge tube and agitated in a decellularization solution of 1% Triton X-100™, 0.5% sodium deoxycholate, with 100 U/mL penicillin and 100 µg/mL streptomycin in PBS at 4°C, with liquid changes every 24 hr for 8 days. The material was then rinsed in nuclease buffer comprising 50 mM Tris-HCl pH 8, 20 mM NaCl, and 2 mM $MgCl_2$ for 24 hr, before incubation with 6.25 U/mL Benzonase™ nuclease (EMD Chemicals Ltd., Gibbstown, NJ) in fresh buffer for 24 hr. The carriers were rinsed in sterile PBS with antibiotic antimycotic and disinfected with 0.1% (v/v) peracetic acid and 4% (v/v) ethanol in deionized water for 3 min. The disinfected carriers were rinsed with sterile PBS, equilibrated with DMEM for 2 days, then equilibrated with cBOEC medium for 1 day. The decellularized carriers were seeded with $1x10^6$ cBOECs in 3.5 mL of medium, incubated overnight in a 5% $CO_2$ controlled atmosphere at 37°C before being transferred to imaging chambers and cultured (Figure 5.2).

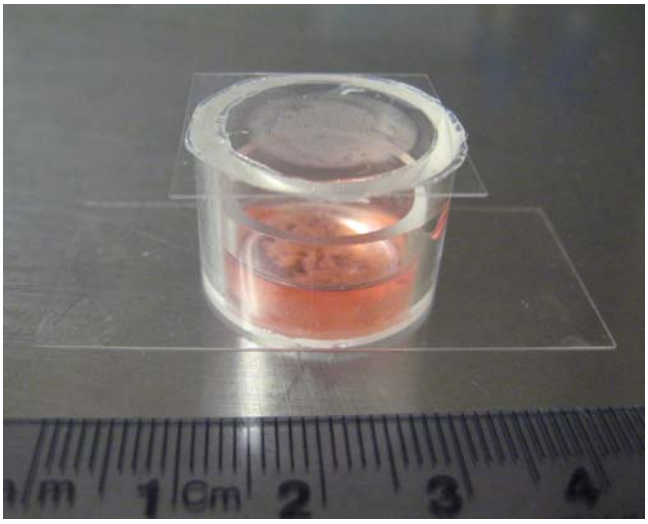


**Figure 5.2 – Crushed Matrix Carriers in Medium**

**Coated imaging chambers made from coverslips allowed culture and *in situ* imaging of cells, including long-term time course imaging. Small culture volumes reduced tissue use.**

Cultured tissue samples from the second protocol were incubated with 2 μg/mL Hoescht 33342 (ABD Bioquest, Sunnyvale, CA) for 30 min in a microcentrifuge tube. The carriers were rinsed 3 times with media, then once with PBS. The sample was fixed in 4% paraformaldehyde for 15 min, permeabilized in 0.5% (v/v) Triton-X100™ solution for 20 min, blocked with 5% BSA for 20 min, then rinsed 3 times in PBS for 5 min each, stained with AlexaFluor® 546 phalloidin (Invitrogen Canada Inc., Burlington, ON, Canada), washed 3 times for 5 min each in PBS, and placed on a coverslip. Epifluorescent imaging was performed on an inverted fluorescent microscope (Axiovert 200; Carl Zeiss MicroImaging GmbH, Berlin, Germany) with a monochrome high resolution CCD camera (XCD-SX910/X710; Sony Corporation, Tokyo, Japan), followed by sequential fluorescent imaging on a confocal microscope (FV1000; Olympus Canada Inc., Markham, ON, Canada).

### *5.1.3 Results*

Small matrix carriers were found to simplify imaging by facilitating wet mounting. This reduced the depth-of-field and focus issues that had made larger tissue carriers difficult to image without dissection, and sub-sampling. This improved imaging facilitated viability staining, as shown in Figure 5.3, pictured after 12 days of culture.

Brightfield images in the left column highlight the complex structure and texture of the extracellular matrix. This structure prevents brightfield imaging of cells with the exception of some cells on the outer edges of the tissues such as in Figure 4.3A. Although mounting reduces the problems of imaging in three dimensional cultured tissues, CFDA-SE staining remained

difficult to image due to high background signal. Fluorophore may be secreted by the cells and bind to matrix proteins. Proteases secreted by the cells may also activate the fluorophore prior to binding. Image processing comprised Background subtraction with a 50 pixel rolling ball algorithm in the ImageJ software package (National Institutes of Health, Bethesda, MD). The low number of imaged cells suggests poor attachment and growth; however, many of these cells present a healthy elongated phenotype and not a rounded necrotic or apoptotic structure.

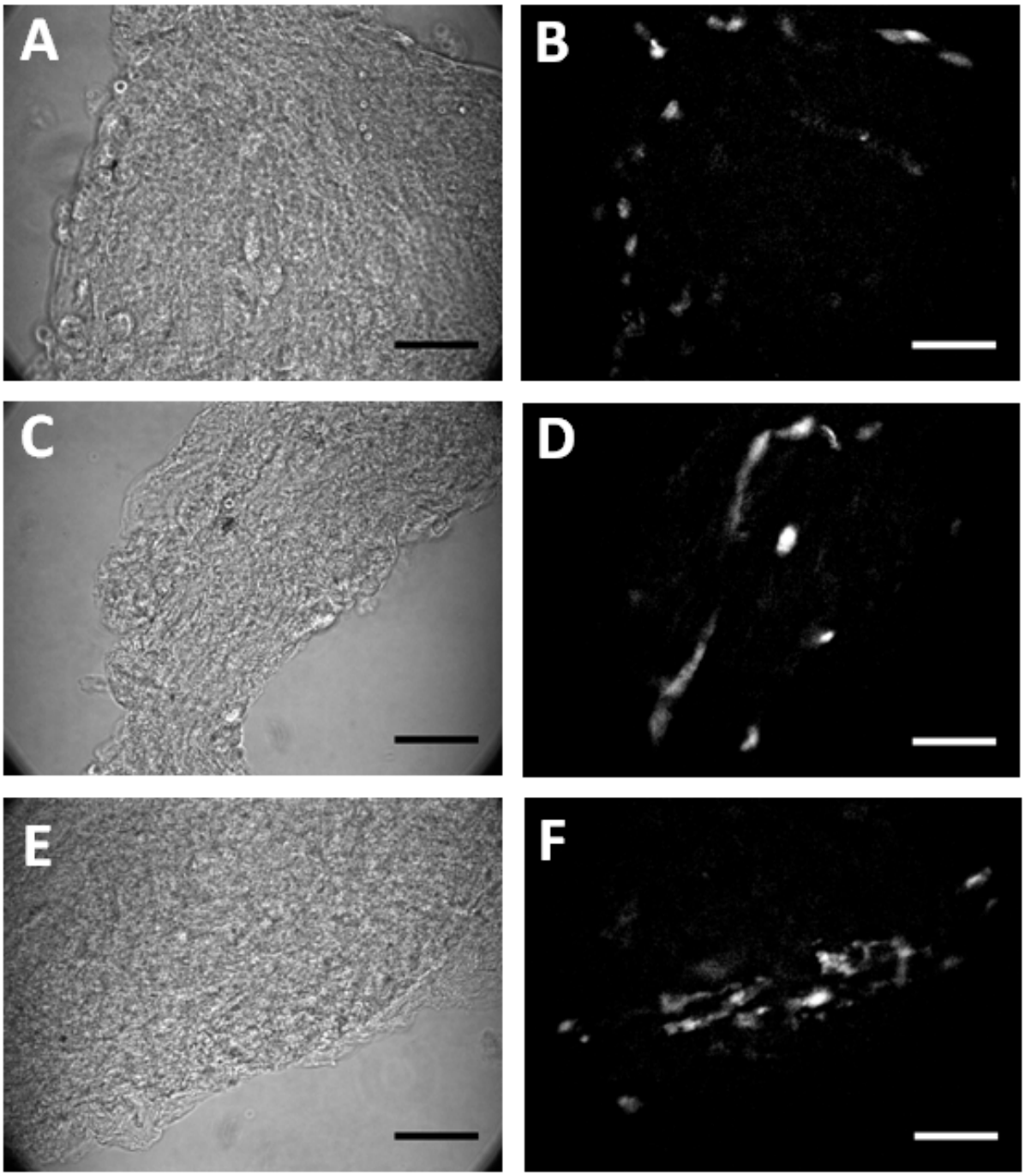


**Figure 5.3 – Mounted Carriers with Viability Staining**

**Crushed kidney tissue was detergent decellularized, seeded with $1x10^6$ cBOECs, and cultured for 12 days. Wet mounted tissue pieces facilitated brightfield (left column) and epifluorescent (right column) imaging of the samples. Incubation with 1 µM CFDA-SE revealed metabolically active cells with attached morphology. Image processing of the fluorescent images allowed for background subtraction (right column), however weaker cell signals may also be removed. Scale bars indicate 50 µm.**

In the subsequent experiment, decellularization was performed after mechanical processing. Rather than using these small tissue pieces to study the properties of larger decellularized materials, this experiment was in context of crushed carriers as a separate product. The increase in surface area and reduction of ECM thickness facilitates improved mass transfer, and wash times were increased to reflect indications of residual cytotoxic material from semi-batch decellularization described in Chapter 2. After 12 days of cBOEC culture, nuclear staining and cytoskeletal staining was performed to identify attached cells (Figure 5.4) and indicate cell attachment, health, phenotype, and the formation of larger structures on the extracellular matrix substrate (Kubota, Kleinman et al. 1988).

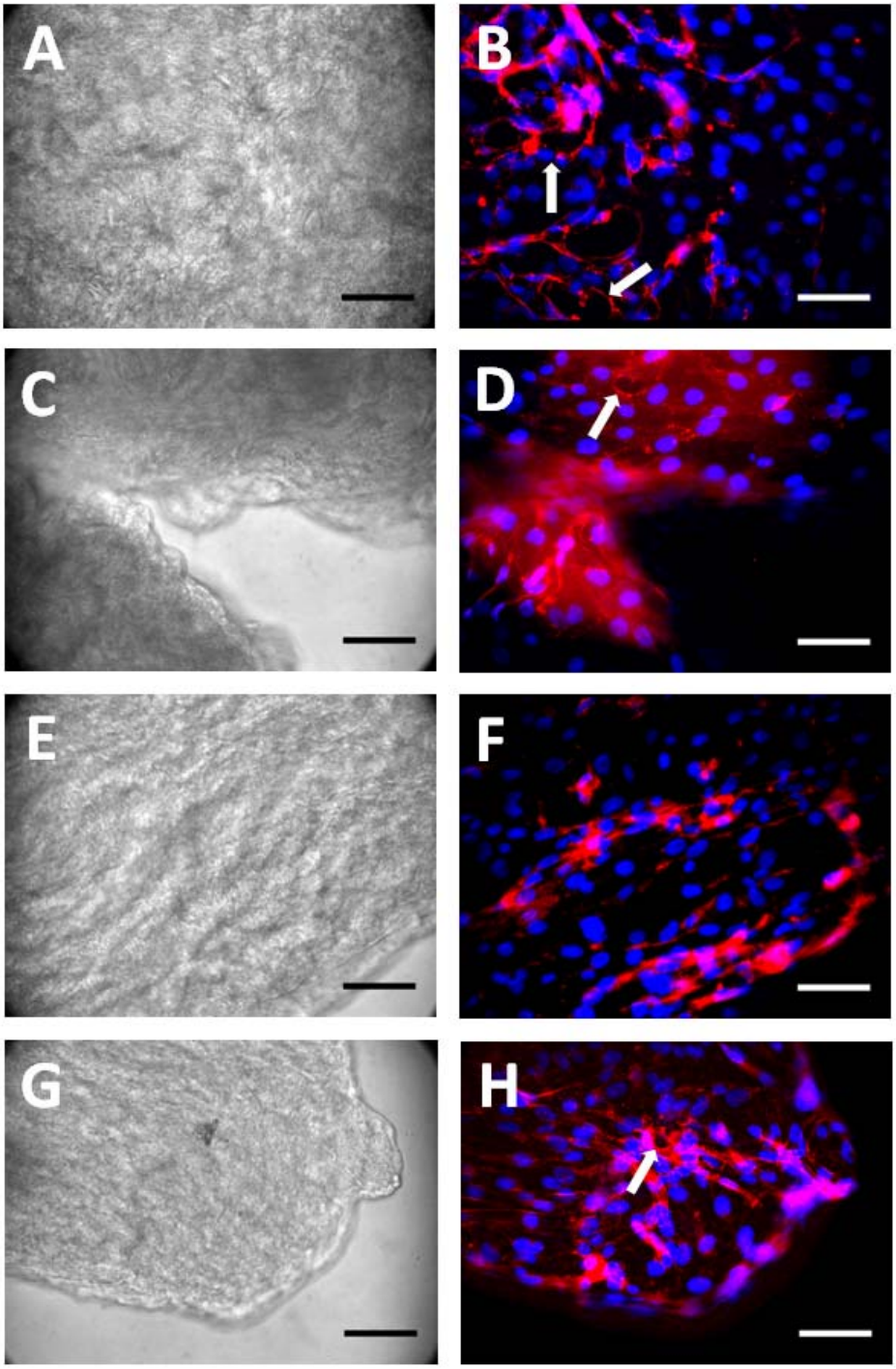


**Figure 5.4 – Mounted Carriers with Nuclear and Cytoskeletal Staining**

**Brightfield imaging did not indicate widespread cell attachment (left column), however nuclear staining (blue) showed areas of dense cell coverage (right column). Cytoskeletal staining (red) showed cell spreading in all areas. In well stained regions (D) a continuous layer of endothelial cells is visible. Cells were also observed to form closed-loops resembling capillary-like structures (arrows). Scale bars indicate 50 µm.**

## 5.2 Sonicated Tissue Carriers

### *5.2.1 Introduction*

The advantages of mechanically processed fresh tissue in decellularized tissue engineering applications can be increased further by reducing the size of tissue fragments closer in size to commercially available microcarriers. Smaller tissue carriers increase surface area for mass transport processing steps, seeding, and reduced tissue use. Microcarrier-sized tissue fragments simplify tissue culture strategies by providing established microcarrier seeding and culture protocols as a basis for process development. By facilitating spinner culture, micronized ECM also facilitates scale-up and three dimensional cultures and may help provide therapeutically significant cell numbers.

### *5.2.2 Materials and Methods*

Wistar rats were housed as described previously for Sprague-Dawley rats and were sacrificed by carbon dioxide asphyxiation for an unrelated project. Hearts, lungs, livers, and kidneys were collected to reduce animal sacrifice and waste. Tissues were stored in PBS with antibiotic antimycotic and frozen at -80°C for up to 4 months before use.

Tissues were mechanically pressed as described above, with trimming of fatty and connective tissues, and fibrous material discarded from the press. Slurries were rinsed three times in PBS

and samples were sonicated and taken for histological analysis. The remaining slurries were then decellularized with washes of 1% Triton X-100™, 0.5% sodium deoxycholate, changed twice a day for 5 days, and rinsed nuclease buffer. Samples were taken again for histological investigation, and the remaining material was incubated with 25 U/mL of benzonase at 37°C. These materials were then rinsed three more times with PBS. All solutions contained 1x antibiotic antimycotic. The slurry was disinfected with peracetic acid as described previously. The tissue was then sonicated with the tip of a W-225 ultrasonic processor (Heat Systems Ultrasonic, Inc., Farmingdale, NY) pulsed at 40% power for 2 min. The solids were then allowed to settle for 4 hours, and rinsed in sterile PBS.

Samples of settled ECM solids were sonicated without nuclease treatment, and pipetted on to positively charged glass slides (Superfrost™; Fisher Scientific Company; Ottawa, ON, Canada), and desiccated for two days to ensure adherence of the decellularized matrix to the slides. The slides were then loaded into a rack and rehydrated for 2 min in deionized water. The slides were then transferred to a working solution of hematoxylin for 5 min to stain nuclei and other basophilic structures, rinsed under running tap water for 5 min, transferred to a working solution of eosin for 5 min to stain collagen and cytoplasm, rinsed with running tap water for 2 min, and mounted with aqueous mounting medium under a coverslip.

3 mL of micronized heart carriers were conditioned in fetal bovine serum, allowed to settle for 4 hours, rinsed twice in complete endothelial cell medium, settled and seeded with 1 mL of medium containing $1x10^6$ cBOECs. Seeded carriers were incubated for 4 hr with gentle agitation every hour. The seeded carriers and unattached cells were loaded into a small spinner

flask at 120 rpm with 80 mL of medium and incubated. Samples from the spinner culture were stained, fixed, and wet mounted.

### *5.2.3 Results*

Sonicated carriers have the advantage of reduced size. Individual fragments can be brought to sizes comparable to conventional microcarriers on the order of 100 μm (Yang, Rossi et al. 2007). This allows the adaption of common microcarrier culture techniques and scalable high-density culture. The decreased size also creates more surface area for cell seeding per gram of decellularized tissue, reducing the matrix required for a given target cell load and decreasing the need for fresh tissue. However, sonication was observed to reduce of portion matrix fragments to debris of insufficient size to support multiple cells. This material is not recovered during washes with mild centrifugation, while ultracentrifugation produces pellets that are impractical to dissociate by trituration. The resulting loss of ECM to debris, and uneven reduction of size between tissue fragments must be addressed to efficiently produce uniform carriers.

Sonication also produces fibrous materials when used with some tissues (Figure 5.5), particularly liver and lung, which were observed to form aggregates during handling and rinsing. Additionally, fibrous carriers may result in warping during culture and send undesirable signals to the cells via mechanotransduction (Ma, Liu et al. 2008). Finally, excessive sonication may denature matrix proteins (Krishnamurthy, Lumpkin et al. 2000), reducing their activity.

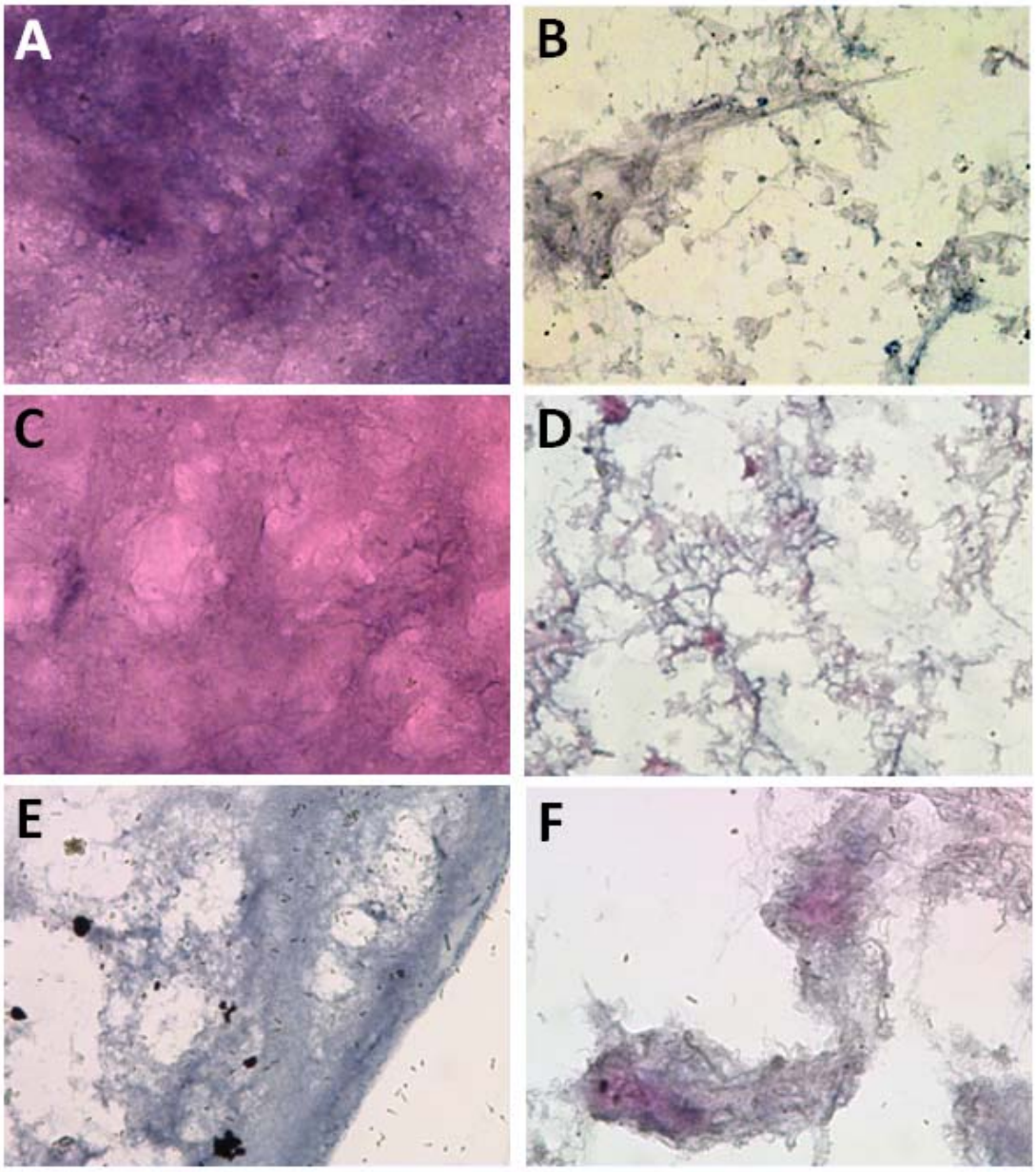


**Figure 5.5 – H&E Staining of Decellularized Tissues**

**Hematoxylin and eosin stains of sonicated tissue before (left column) and after (right column) detergent decellularization. Kidney, Liver, and Lung are shown in the top, middle and bottom rows, respectively. In H&E staining, nucleic acids stain blue, revealing diffuse chromatin in the sonicated tissues. This is reduced during detergent decellularization, however condensed nuclei remain entangled in the matrix as observed in Chapter 3. Pink stains indicate alkaline eosinophilic stuctures, such as proteins. These persist in the thick regions of tissue (D,F) after decellularization, and may correspond to undesired residual cellular components or valuable matrix components that have not been stripped. The fibrous ultrastructure of sonicated the tissues is also revealed.**

Unlike other tissues tested, particularly liver and lung, sonicated cardiac tissue forms rounded carriers desirable for handling and spinner culture. Samples of heart microcarriers from a spinner flask were sampled after 1 week of culture, fixed, permeabilized, stained and mounted (Figure 5.6). Near-confluent cell coverage on the ECM carriers, demonstrates effective cell seeding, and may indicate proliferation in spinner culture.

Samples of heart microcarriers in media removed from spinner culture were also loaded in APTS-treated gelatin-coated glass imaging chambers after 1 week of culture. Chambers were positioned on an inverted fluorescent microscope (Axiovert 200; Carl Zeiss MicroImaging GmbH, Berlin, Germany) with a monochrome high resolution CCD camera (XCD-SX910/X710; Sony Corporation, Tokyo, Japan), with controlled temperature and atmosphere. Time-course images of carriers were constructed using a custom robotic stage and image processing software (Figure 5.7). Although some cell movement was observed in the brightfield movies, no cell egress was observed. Additionally, dead cells and debris were observed to settle from the solution, with only several viable cells observed on the gelatin surface. The slow settling time of the debris suggests simple media changes may be sufficient for debris removal in long-term spinner cultures. The carrier itself was observed to drift over time which may have prevented cell egress to the chamber surface.

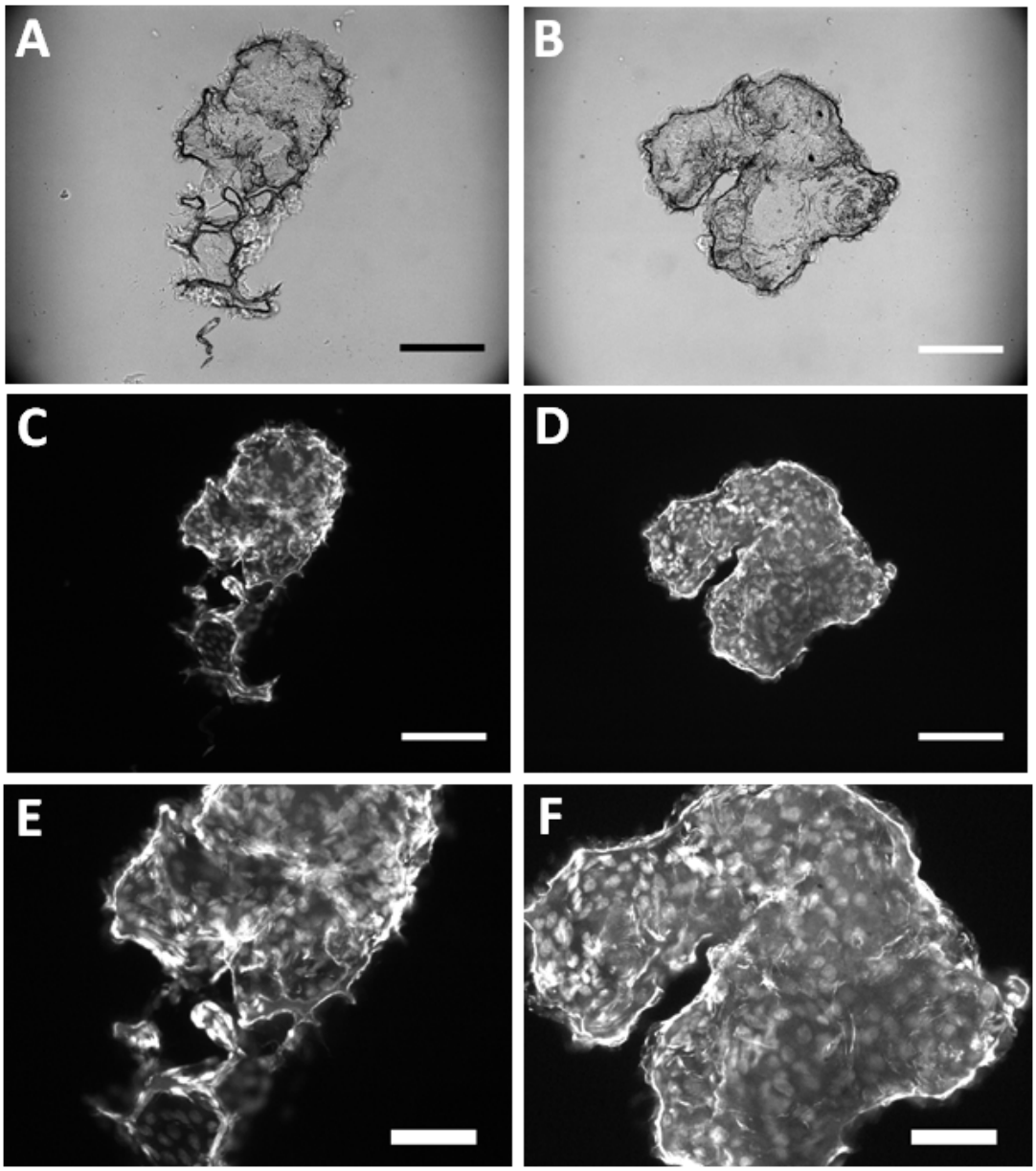


**Figure 5.6 – Cultured Sonicated Heart Carrier Staining**

**Samples of heart microcarriers from a spinner flask were sampled after 1 week of culture, fixed, permeabilized, stained and wet mounted. Sonication may have damaged collagen fibrils on the edge of the carriers, resulting in the frayed edge morphology shown in the brightfield images (A,B; 100 µm scale) after paraformaldehyde fixing. These edges were also observed to broadly autofluoresce as shown in the ultraviolet channel (C-F; 100 µm scale), obscuring cytoskeletal staining (results not shown). Nuclear staining indicated a near-confluent layer of endothelial cells, indicating effective cell seeding and low cytotoxicity (E,F; 50 µm scale).**

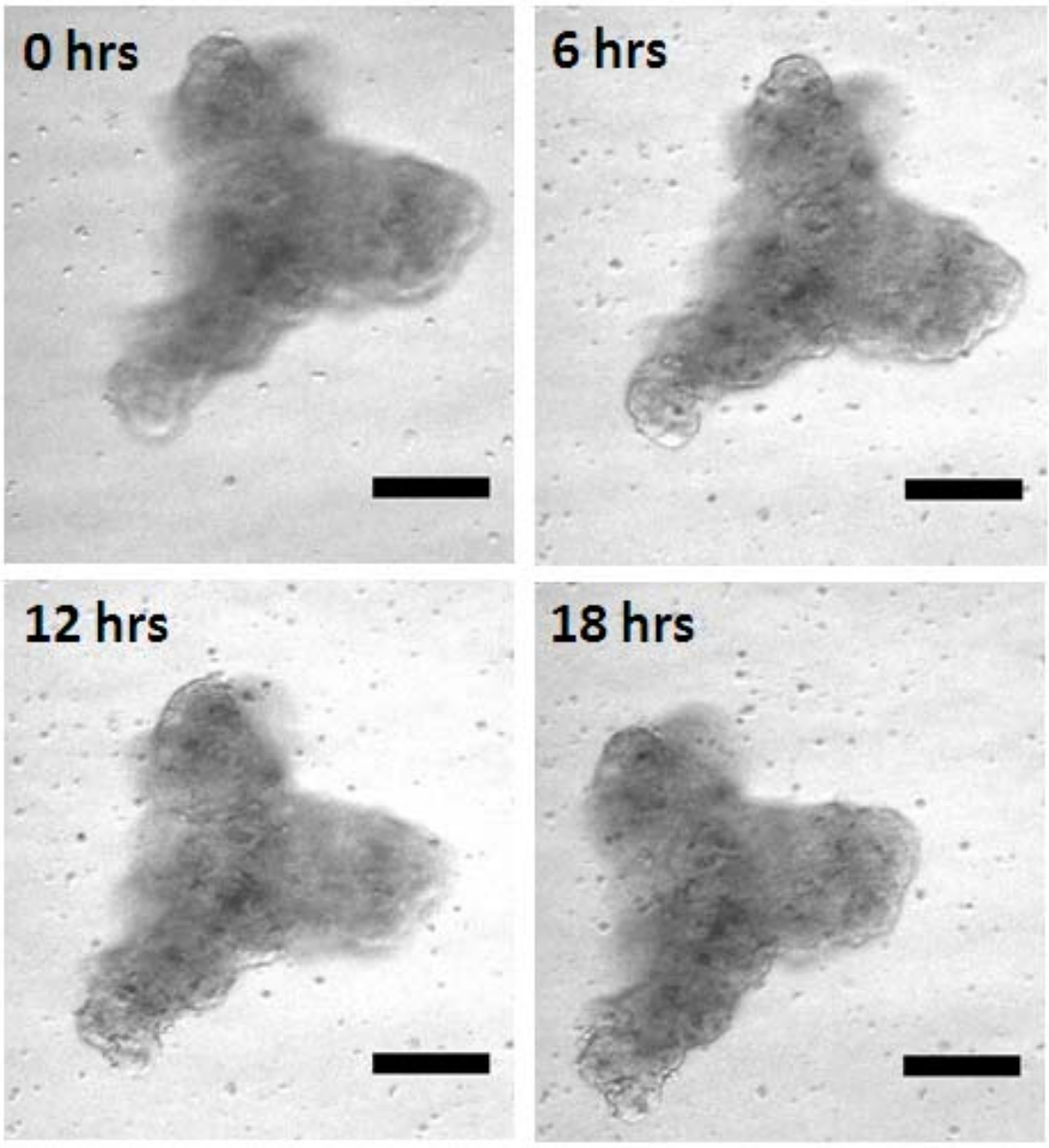


**Figure 5.7 – Cultured Sonicated Heart Carrier Timecourse Imaging**

**Sonicated heart ECM microcarriers were seeded with $1x10^6$ cBOECs in 1 mL of medium, and cultured for 1 week in a spinner flask at 120 rpm. Samples were loaded in gelatin-coated imaging chambers and imaged at controlled temperature and atmosphere for 24 hrs. Timecourse images revealed limited cell movement and no cell egress. Over time, dead cells and debris were observed to settle from the solution. Media changes may be required to remove debris from the system. Motion of the microcarrier may have prevented cell bridging and egress. Scale bars indicate 200 µm.**

Samples of carriers cultured for 9 days were rinsed in sterile PBS and cast in rat tail collagen, type I (BD, Mississauga, ON, Canada) combined with a neutralizing solution of 100mM HEPES adjusted to pH 7.3 in 2x PBS (Wozniak and Keely 2005), and handled with chilled pipettes and solutions. The gels were cast in glass imaging chambers, allowed to set in a 37°C incubator for 30 min, and overlaid with fresh media. Time course images were prepared on an inverted microscope with controlled temperature and atmosphere (Figure 5.8). Cell division and egress into surrounding collagen were observed throughout the timecourse images.

At 72 hours following gel casting, carriers were imaged at lower magnification to resolve depth-of-field and study the cell egress pattern (Figure 5.9). The images showed nearly all of the particles to carry viable dividing cells following extended spinner culture. These results and the divisions observed on the carrier during timecourse imaging support the study of ECM microcarriers for high-density culture in addition to cell delivery.

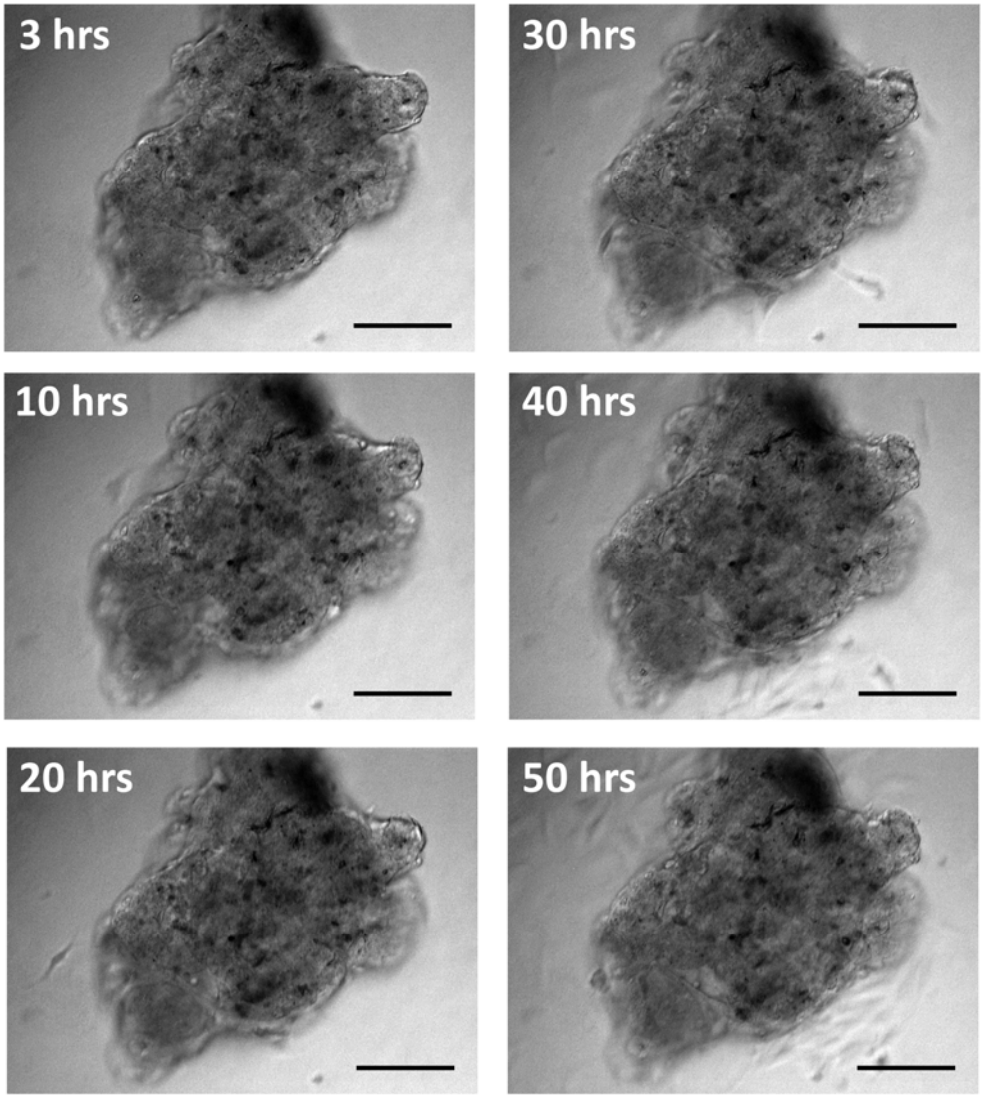


**Figure 5.8 – Cultured Sonicated Heart Carrier, Collagen Cast, Timecourse Imaging**

**Sonicated heart ECM microcarriers were seeded with $1x10^6$ cBOECs in 1 mL of medium, and cultured for 9 days in a spinner flask at 120 rpm. Samples were rinsed in sterile PBS and cast in type I rat tail collagen with a neutralizing solution in glass imaging chambers. Solutions and materials were chilled to 4°C. Imaging chamber gels were allowed to set at 37°C under controlled atmosphere for 30 min before adding fresh media. High-resolutions time course imaging revealed cell movement and cell division on the ECM surface. Egress into the surrounding collagen with proliferation was also observed. Scale bars indicate 100 µm.**

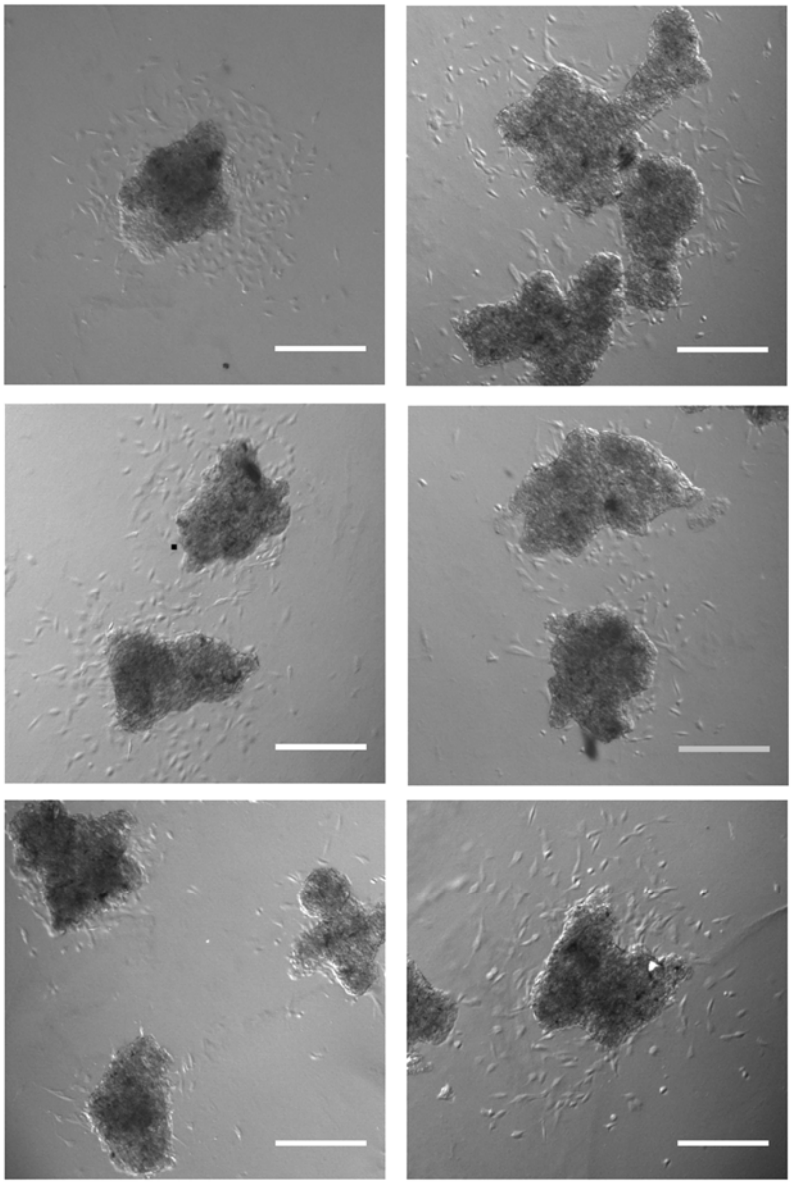

**Figure 5.9 – Cultured Sonicated Heart Carrier, Collagen Cast, 72 Hour Cell Egress**

**Sonicated heart ECM microcarriers were seeded with cBOECs, and cultured for 9 days in a spinner flask. Samples were rinsed in sterile PBS and cast in type I rat tail collagen with in glass imaging chambers. Gels were allowed to set at 37°C under controlled atmosphere for 30 min before adding fresh media. After 72 hours of 3D gel culture most particles had released dividing cells, demonstrating the ability of spinner cultured ECM microcarriers to support proliferative cells for delivery. Scale bars indicate 200 µm.**

## 5.3 Cryopulverized Tissue Carriers

### *5.3.1 Introduction*

Mechanical processing of fresh collagen induces shear that can separate collagen fibers (Gilbert, Stolz et al. 2005). This may be reflected in the frayed morphology observed in sonicated tissue carriers. Snap freezing and tissue cracking was investigated to break collagen fibrils more evenly. This was anticipated to prevent the fibrous morphology observed in some tissues and reduce microcarrier entanglement and aggregation during handling and culture.

Pulverization by tissue cracking was also anticipated to reduce the formation of matrix debris lost in the supernatant following sonication, by mechanically favoring the destruction of larger particles. This would result in more uniform carriers and reduce wasted ECM.

### *5.3.2 Materials and Methods*

Tissues from Wistar rats stored as described previously were thawed, removed of fatty tissue, cut into sections of approximately 0.5 mL volume, and were placed in microcentrifuge tubes on ice. The tubes were then snap frozen in liquid nitrogen and stored at -80°C until needed. A stainless steel mortar and pestle type cryopulverizer was custom-machined (Figure 5.10) to process large amounts of tissue. The pulverizer was carefully submerged in liquid nitrogen in a polystyrene foam container with heavy gloves. Snap frozen tissues were loaded into the pulverizer and the

piston was struck with a heavy hammer approximately 5 – 10 times until the tissue formed a fine powder. This was then emptied into a centrifuge tube with PBS, allowed to settle and washed three times with fresh PBS.

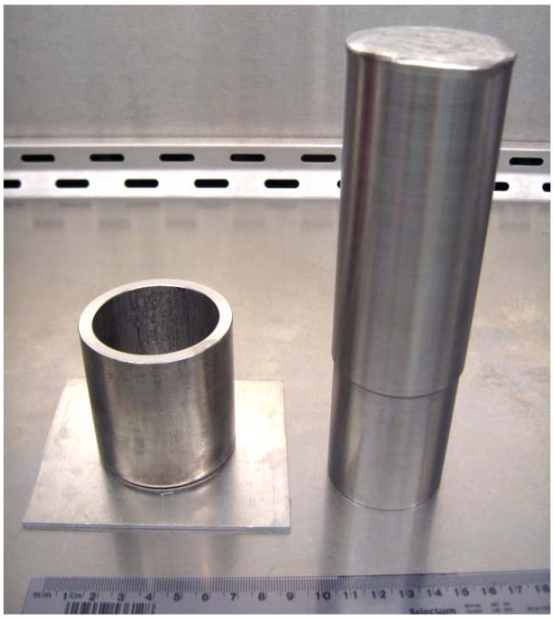

**Figure 5.10 – Custom High Capacity Cryopulverizer**

**A high capacity cryopulverizer was milled from stainless steel. The mortar and piston surfaces were cooled and the mortar was semi-submerged in liquid nitrogen in a polystyrene foam container. Small tissue pieces were loaded into microcentrifuge tubes, and submerged in liquid nitrogen until frozen. Tissues were loaded in the mortar, and the piston was struck several times with a hammer. The mortar was then removed from the liquid nitrogen with locking pliers, and micronized ECM was collected.**

The micronized tissue was rinsed in a decellularization solution of 1% Triton X-100™ (Sigma-Aldrich Canada Ltd., Oakville, ON, Canada) and 0.5% sodium deoxycholate (Bioshop Canada, Inc., Burling, ON, Canada) changed twice per day for 7 days, rinsed with nuclease buffer, then incubated with 6.25 U/mL units of Benzonase™ (Sigma-Aldrich Canada Ltd., Oakville, ON, Canada) in buffer for 24hr. The tissue was then rinsed 3 times with PBS. All solutions contained 1x antibiotic antimycotic solution (Sigma-Aldrich Canada Ltd., Oakville, ON, Canada) and kept at 4°C. Carriers were disinfected with 0.1% (v/v) peracetic acid (Sigma-Aldrich Canada Ltd., Oakville, ON, Canada) and 4% ethanol for 5 min, rinsed 3 times with sterile PBS, aliquoted in centrifuge tubes and stored at -80°C for up to 1 month (Figure 5.10). Microcarrier aliquots were then thawed at 4°C to reduce the bubble nucleation in the matrix and improve settling. Microcarriers were conditioned in fetal bovine serum (Invitrogen Canada Inc., Burlington, ON, Canada) for 2 days, and rinsed with endothelial cell medium.

Trypsinized endothelial cells were added to microcarriers in medium, gently agitated every hour and allowed to settle in an incubator with a loosened cap. Samples of the supernatant were taken to determine the proportion of unattached cells. In one experiment, CFDA-SE labeled cells were used to study cell entrapment and seeding. Seeded carriers were then loaded into glass imaging chambers, or into a spinner flask and cultured in an incubator at 37°C and 5% $CO_2$. To test cell seeding kinetics, $3.5x10^5$ cells in 1 mL of media were seeded on 0.5 mL settled volume of lung carrier, with supernatant gently triturated and sampled hourly.

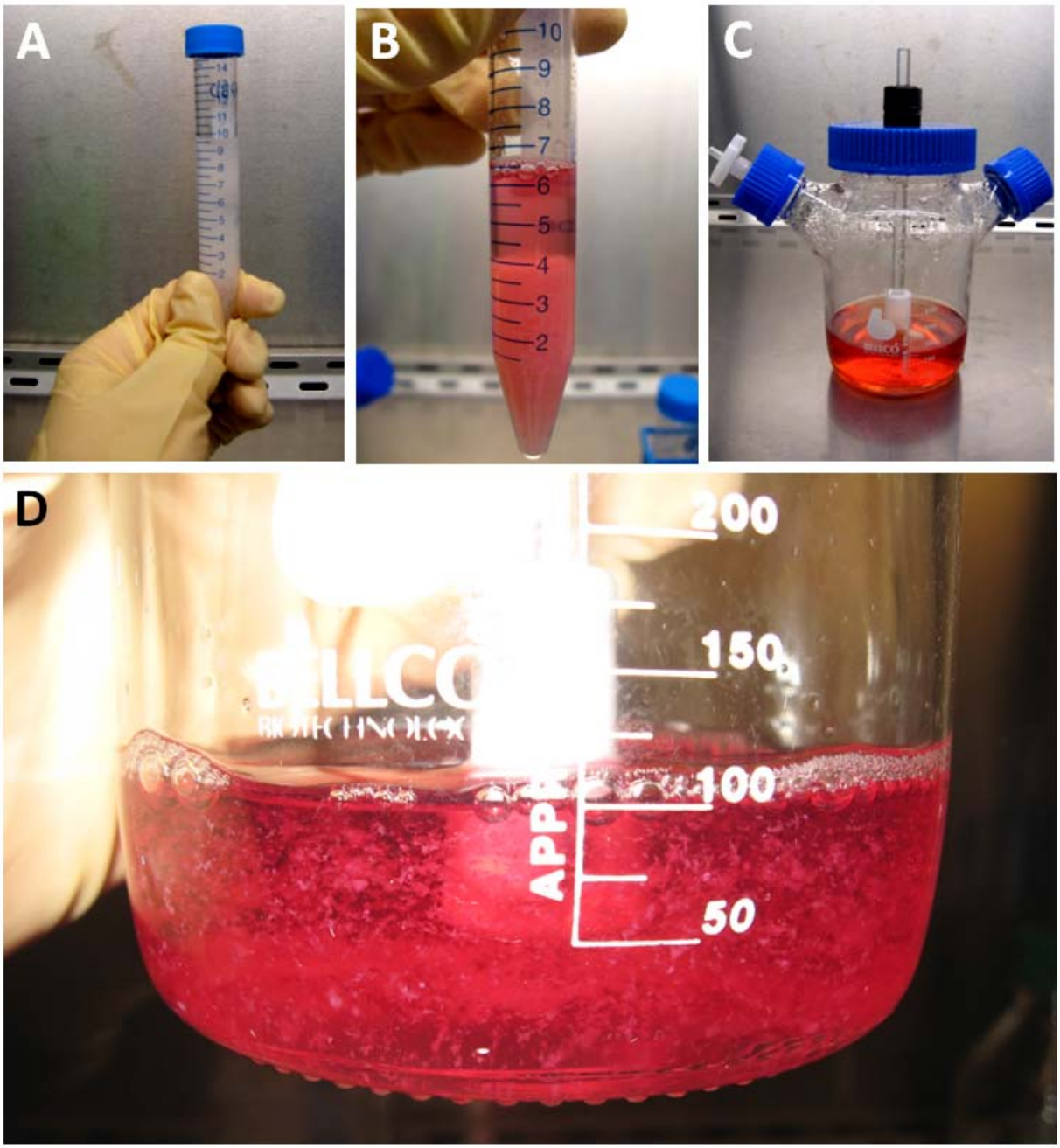


**Figure 5.11 – Cryopulverized Lung Carrier Spinner Culture**

**Aliquots of micronized ECM were aliquoted in PBS and stored at -80°C (A). After thawing, ECM samples were reconditioned with FBS and complete medium washes. Cells were then added to tissue microcarriers and allowed to attach in a centrifuge tube with a loosen cap in a controlled 5% $CO_2$ atmosphere at 37°C (B), with gentle agitation every hour. Once seeded, the tissue microcarriers were loaded in a spinner flask (C, D). Microcarriers shown here are based on lung tissue.**

### *5.3.3 Results*

The cell seeding kinetics test showed indicated 16% entrapment at 1 hour, and 94% cell entrapment at 2 hours. These cells were not found in the gently triturated sampled supernatant, and were considered bound to the matrix or otherwise associated with the carriers during 20 minutes of settling time. Microcarriers seeded with CFDA-SE labeled cells after 4 hr seeding are shown in Figure 5.12. The small size of these carriers and brightly labeled cells facilitate imaging without flattening the three dimensional structure by mounting under a glass slide. The roughness of the tissue may contribute to cell entrapment. Loading was also observed to be more even than the cell attachment observed in larger crushed carriers seeded without agitation.

Sonicated heart carriers were also observed to support cell survival after 10 days of culture as demonstrated by cell egress in Figure 5.13. Sampled carriers were loaded on a glass imaging chamber coated with type I rat tail collagen, and imaged after 16 hours.

Reduced carrier size observed when compared to other carrier production approaches increases attachment area and facilitates mass transport during decellularization, disinfection, and reconditioning processes. Egress was also observed without gel casting and this may be caused by using a collagen coating rather than the gelatin coatings used previously. Alternatively, the smaller carrier size may also require fewer cells to anchor the microcarrier during bridging, facilitating egress.

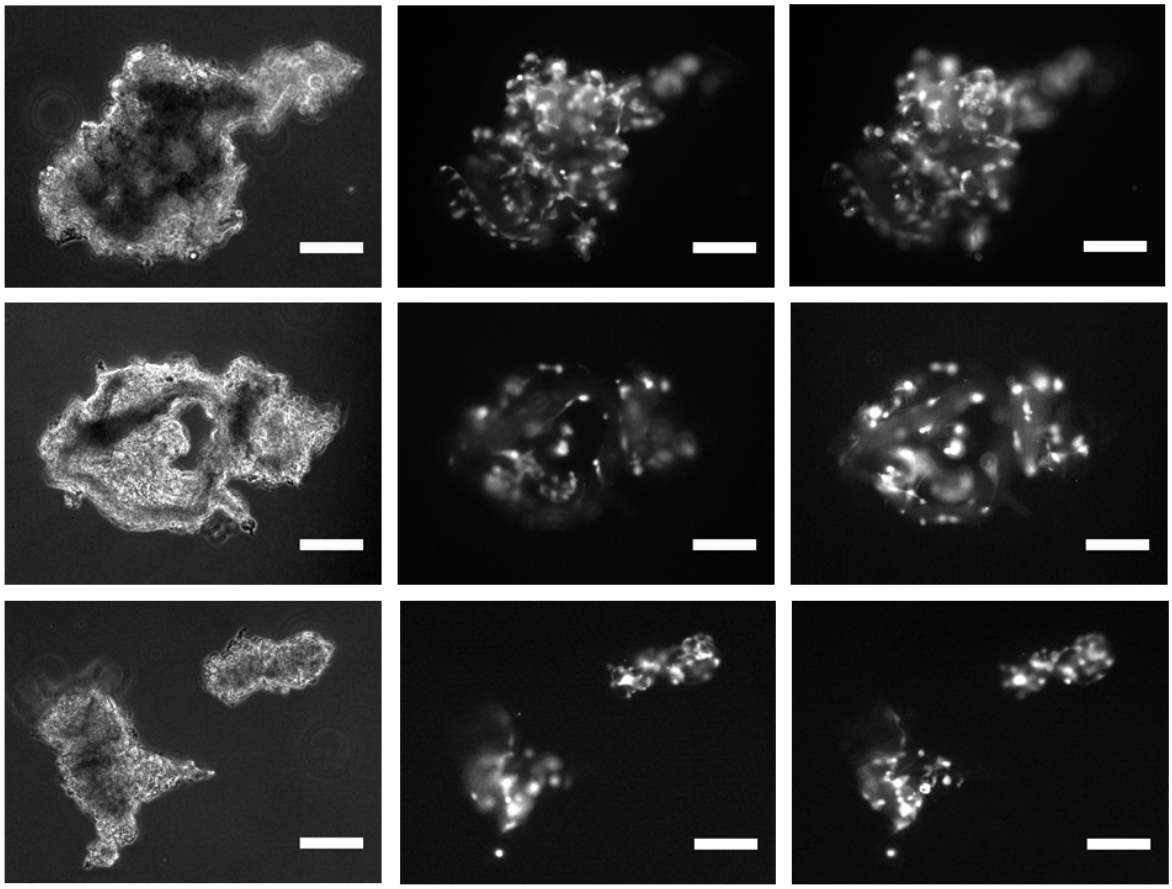

**Figure 5.12 – Lung Carriers at 4 hr Seeding**

**Microcarriers are shown seeded with CFDA-SE labeled cells after 4 hr seeding. Brightfield images are shown in the left column, with corresponding epifluorescent images at two depths-of-field in the middle and right columns. The complex surface of the microcarriers may facilitate cell entrapment and improve cell seeding efficiency. Even cell attachment is observed. Microcarrier size facilitates wet mounting. Scale bars indicate 100 µm.**

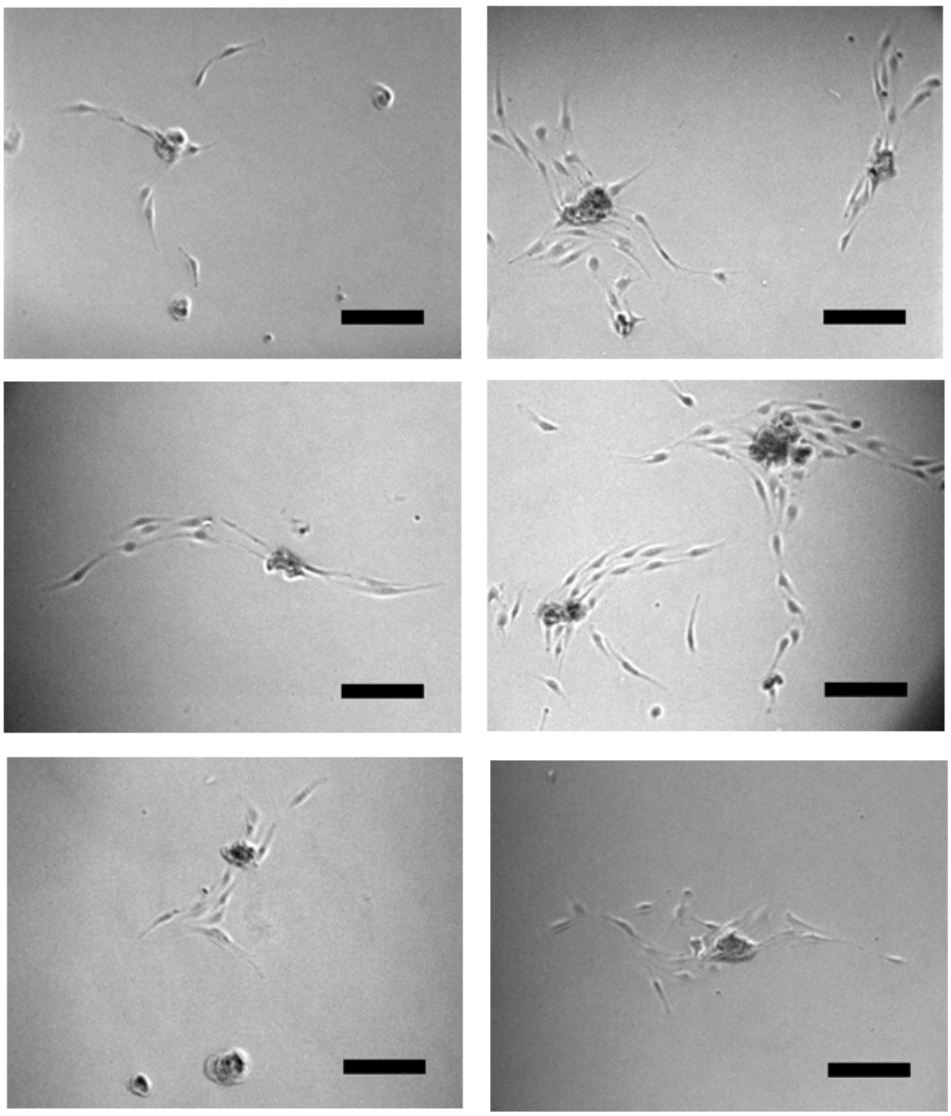

**Figure 5.13 – Heart Microcarrier 16 hr Egress**

**Sonicated heart ECM microcarriers were cultured for 10 days. Sampled carriers were loaded on a glass imaging chamber coated with type I rat tail collagen, and imaged after 16 hours. Egress was observed without gel casting and may be facilitated by the collagen coating or the decreased microcarrier size relative to cell bridge strength. Streams of cells show high cell density on carriers and maintenance of proliferative potential on ECM in multiple imaged regions. Scale bars indicate 50 µm.**

## 5.4 Co-culture Survival Assay

### *5.4.1 Introduction*

A primary goal of this work is to develop a carrier to facilitate cell survival in gene-modified BOEC transplanted for the treatment of hemophilia (Matsui, Shibata et al. 2007). This can only be directly tested with animal experiments including survival surgery. However, it is desirable to develop an assay that simulates the *in vivo* environment, particularly with respect to death of transplanted BOECs (Matsui, Shibata et al. 2007; Milbauer, Enenstein et al. 2009), to minimize animal use. This will facilitate meaningful testing of the carriers developed in the protocols above, and their role in cell survival.

A confluent layer of HeLa cells was selected to produce a competitive culture environment as an intermediate step towards animal experiments. HeLa cells divide rapidly to quickly cover exposed culture surface. This was designed to recapitulate the assumed absence of acellular surface at the transplant site of the host animal. Additionally, the metabolic activity of the HeLa cells was desired to further challenge transplanted cells with and without carrier. Imaging of viable cells was desirable to directly study cell survival, attachment, health, and proliferation.

Preliminary studies of CFDA-SE labeling of cBOECs showed loss of signal intensity during culture. In Figure 5.14, CFDA-SE labeled cells were loaded into a collagen-coated glass imaging chamber as described above. After 3 days, the fluorescent cell signal became nearly unidentifiable at low magnifications. These imaging issues were resolved by the availability of gene-modified GFP-expressing mBOECs.

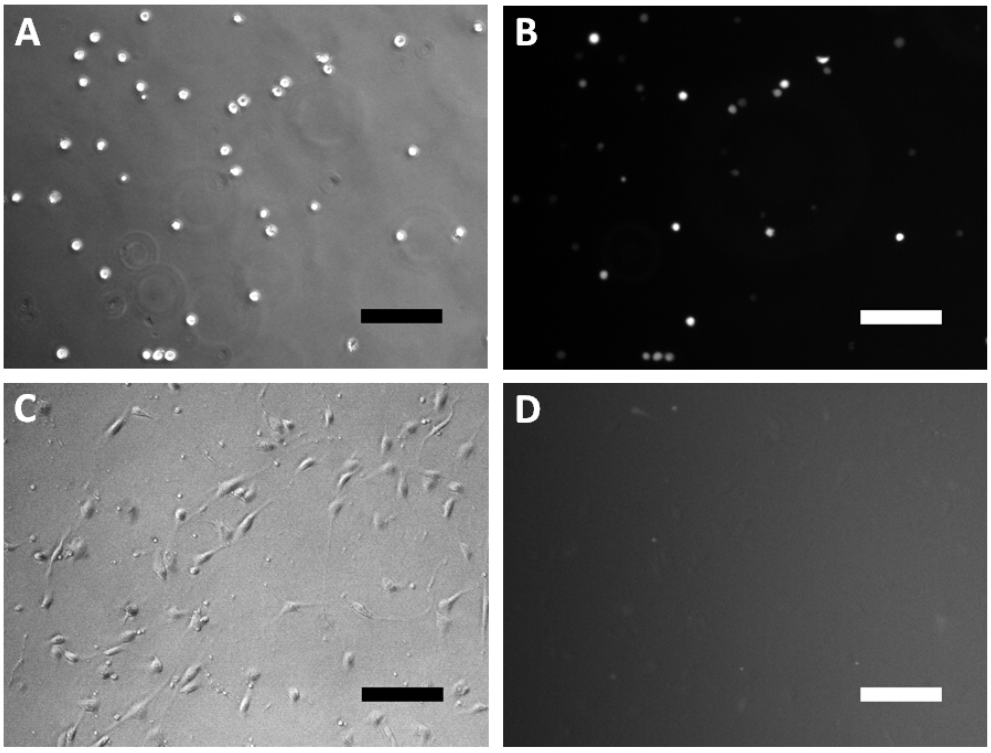


**Figure 5.14 – Loss of Fluorescent Signal in CFDA-SE labeled cBOECs**

**CFDA-SE labeled cells were loaded into collagen-coated glass imaging chamber. Chambers were imaged in brightfield (left) and fluorescent channels (right), at 0 hr (top) and 3 days (bottom). After 3 days, fluorescent cell signal became nearly unidentifiable at low magnifications (D). Low magnification is desired to image the three dimensional structure of the carriers *in situ* while minimizing depth-of-field issues. Additionally, background fluorescence in the media increased due to release of the fluorophore from the BOECs. This may then bind and concentrate protein carriers, further complicating the study of carriers in a survival assay. Scale bar indicates 100 µm.**

### *5.4.2 Materials and Methods*

APTS-treated glass imaging chambers were loaded with $4x10^5$ HeLa cells, or left empty as controls (Figure 5.14). After 2 days, the HeLa cells formed a confluent layer. Media was replaced with the endothelial medium described above. $1x10^5$ GFP-expressing mBOECs were seeded in each well or loaded onto 25 μL of settled cryopulverized kidney carriers prepared as described above. After 2 hr of seeding, the carriers were transferred to the glass chambers and imaged as described above. Every 2 days, half of the medium was removed from the chambers and replaced with fresh medium.

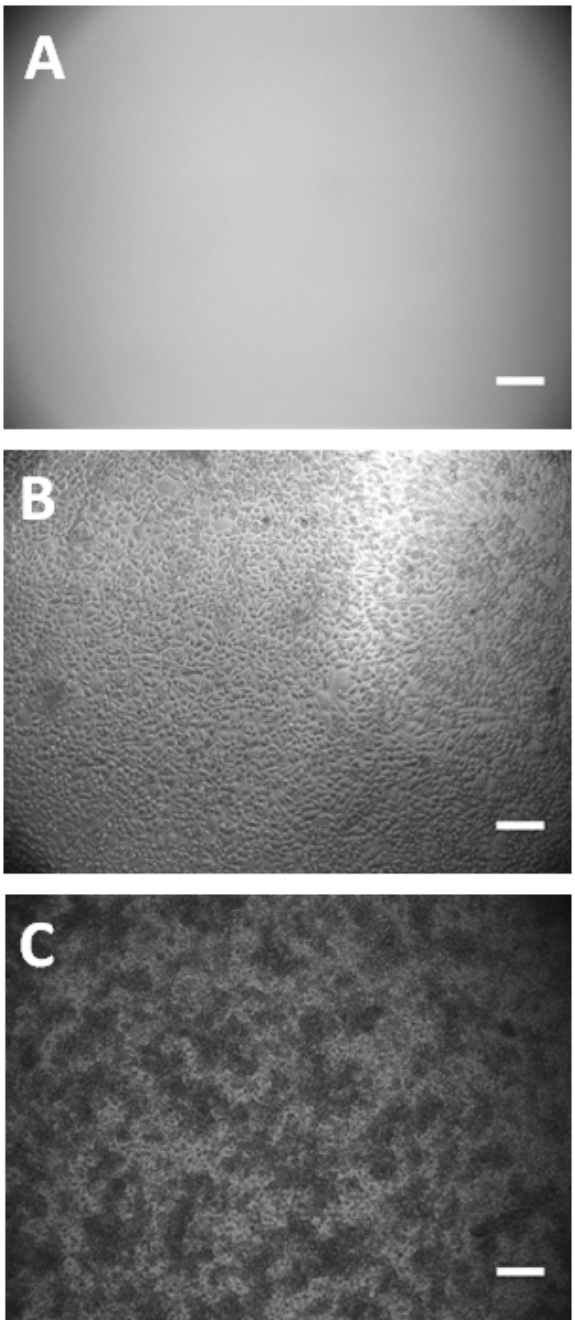


**Figure 5.15 – Experimental HeLa Layers**

**Imaging chambers were loaded with $4x10^5$ HeLa cells, or left empty as controls (A). A confluent layer of HeLa cells was formed after 2 days (B). $1x10^5$ GFP-expressing mBOECs were seeded in each well or loaded onto 25 µL settled volume of cryopulverized kidney for 2 hr prior to imaging. Half media changes and imaging were performed every 2 days. Overgrowth of HeLa cells at 16 days is shown (C). Scale bar indicates 100 µm.**

### *5.4.3 Results*

Seeded mBOECs were found to adhere and adopt a spread morphology within 24 hours, proliferating and becoming confluent within a week as shown Figure 5.16. Seeded carriers showed good attachment and egress onto the surface of the imaging chamber.

While BOECs were able to attach in the presence of the HeLa cells at 24 hr, they exhibited an elongated phenotype. This may indicate that individual cells found small areas between HeLa cells on which to attach, but these are irregular and widely spaced. By 9 days, GFP cell debris and widespread cell death is apparent. This may be caused by the movement and division of the pre-existing cell layer, further disrupting proper attachment and resulting in programmed cell death (Frisch and Ruoslahti 1997). By 16 days, only small debris remained.

Seeded tissue carriers cultured on the HeLa layer were found to maintain attachment as long as 16 days. However, imaging was obscured by the increasingly thick HeLa cell layer. The HeLa layer caused reduced proliferation in the first days of culture, and prevented significant BOEC egress. By 1 week the HeLa layer began to cause cell death.

These results suggest that ECM microcarriers can promote transplant cell survival in a confluent and competitive environment by providing a stable attachment surface. Growth factors in the matrix deposited during FBS conditioning may also have contributed to cell survival, suggesting an additional role of the carrier as a drug delivery vehicle to promote transplant cell survival in tissue engineering.

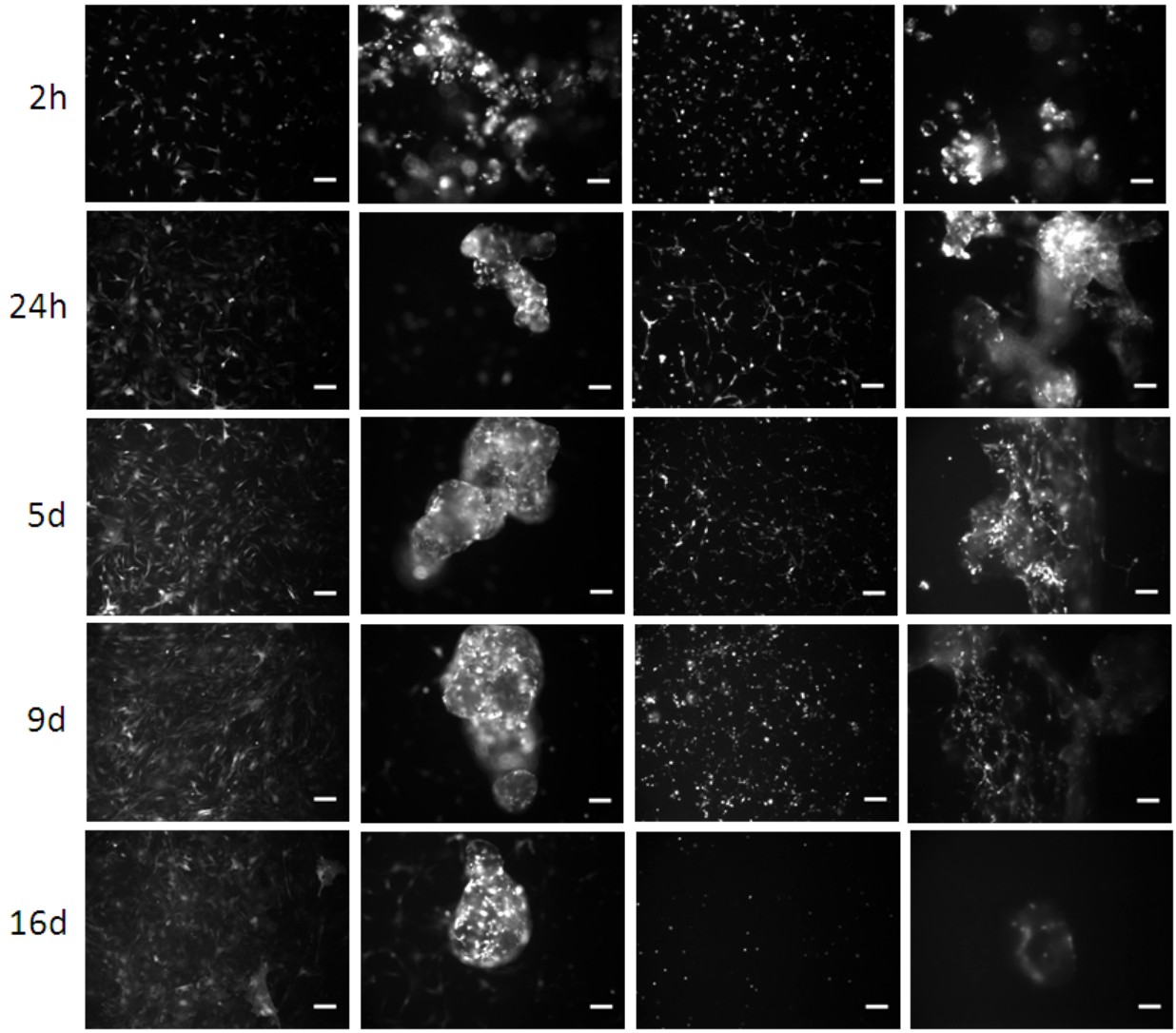


**Figure 5.16 – GFP mBOECs on HeLa Layer with and without Micronized Tissue Carriers**

**GFP mBOECs are shown in the left column. These cells attached with spread morphology within 24 hours before becoming confluent. Seeded carriers shown in the second column exhibited good attachment and egress of proliferative cells. In the third column, BOECs seeded on the HeLa layer attached at 24 hr, but exhibited a distorted phenotype. By 9 days, GFP cell debris and widespread cell death is apparent. By 16 days, only small debris remained. In the forth column, seeded tissue carriers on the HeLa layer are shown to maintain attachment as long as 16 days. However, imaging was increasingly obscured by the thick HeLa cell layer shown in (C). The HeLa layer caused reduced proliferation in the first days of culture, and prevented significant BOEC egress. By 1 week the HeLa layer began to cause cell death. Scale bars indicate 100 µm.**

## 5.5 Discussion

Methods were developed to produce and evaluate micronized ECM. This work was focused toward developing a carrier to support gene-modified adherent cell therapy by providing a biological surface for attachment and support for implanted cells.

Tissue micronization had additional production advantages by resulting in a more homogeneous material prior to decellularization, facilitating process optimization, simplifying handling, and allowing the adaptation of established microcarrier protocols. Increased surface area and reduced tissue thickness also facilitate decellularization transport processes and provide more attachment sites for seeded cells. Improved transport may also reduce hypoxia in microcarriers following implant.

A tissue press was used first to produce small ECM fragments in Section 4.1. These were studied for culture and decellularization. For the second generation carriers, ultrasonication was applied to reduce the size of the fragments in Section 4.2. These smaller fragments further facilitated imaging, handling, and seeding, and were cultured in spinner flasks. However, this approach destroys a portion of the ECM by shredding to debris, and tends to produce fibrous carriers from liver and lung.

In the third generation of microcarriers, we employed snap-freezing and cryopulverization of tissue pieces. This approach was anticipated to reduce the formation of debris by preferentially applying force to larger particles, reducing waste and improving uniformity. Tissues were cracked by snap freezing and crushing prior to decellularization, further increasing surface area

and reducing bulk transport distances during decellularization. Resulting microcarriers behaved more closely to commercial microcarriers, further facilitating scalable, high-density spinner culture.

Imaging assays were primarily used to evaluate seeding efficiency, cell survival, and proliferation. Viability stains demonstrated cell metabolic activity, and cytoskeletal staining showed cell morphology on the ECM surface. Time course imaging showed cell migration and proliferation on the carriers. Collagen gel casting and coating egress assays demonstrated retention of proliferative and migratory cells during long-term spinner culture.

An *in vitro* assay was developed to produce a competitive environment and test the ability of the ECM microcarriers to support implanted cells. GFP-expressing BOECs were overlaid on confluent layers of HeLa cells with and without microcarrier support. The experiment ended after 16 days, when the HeLa layer had overgrown and interfered with imaging. Cells on the microcarrier demonstrated an attached morphology for the duration of the experiment. Cells without microcarrier support were able to attach, however this attachment appeared stretched and distorted. Widespread cell death was observed within days for those without carriers, and at the end of the experiment only fluorescent debris remained. The debris was timecourse imaged to confirm Brownian motion. The results suggest that short term engraftment of implanted cells is possible, but ultimately unstable and agrees with reports of high losses of BOECs within days of injection (Milbauer, Enenstein et al. 2009). These results also demonstrate that ECM microcarriers can support cell survival, however, *in vivo* experiments are ultimately needed to test therapeutic potential.

# Chapter 6 – Conclusions and Recommendations

## 6.1 Tissue Decellularization

Whole-organ perfusion decellularization was investigated from a process engineering and mass transport perspective. An emphasis was placed on process staging and production "stops". Perfusion decellularization employs the transport advantages of the native vasculature, which was preserved during decellularization with harsh detergents. The microvasculature reduces the distance between material in the tissue mass and the detergent solution. However, in the absence of systematic heparinization, variations of 6 to 24 hrs were observed in decellularizing hearts. This variation may be caused by microclots and resulting poor microcirculation. Since systematic heparinization is may not be possible for human tissue and excessive detergent treatment may be undesirable, decellularization protocols may require process analysis to determine completeness of decellularization. However, many decellularization protocols simply prescribe durations of detergent treatment.

Studying the flow properties of the decellularizing heart showed a reduction in volume and mixing over time. Additionally, muculent effluent was observed at late decellularization. This suggests muculent material accumulation in the vasculature such as chromatin or mucins that act as a barrier to transport in late decellularization. Whole-organ perfusion decellularization protocols with alternating DNAse incubation and detergent perfusion may be valuable to ensure completeness in decellularization.

Tissue piece decellularization showed poor mass transport efficiency in the absence of vascular perfusion. This was improved by reducing tissue size and the development cryopulverized ECM microcarriers from diverse source tissues. Cryostorage of tissues and microcarrier aliquots was used throughout, with storage considered an essential step for commercial or therapeutic applications.

## 6.2 Extracellular Matrix to Support BOEC Delivery

BOECs were found to adopt an elongated phenotype when cultured on ECM and ECM derived gels, in contract to the cobblestone morphology observed when cultured on tissue-culture treated plastic or gelatin-coated surfaces. The formation of capillary-like structures was also observed on both ECM and ECM gels. Cells cultured on ECM remained proliferative and divisions were observed on the ECM surface during time-course imaging. Extensive cell egress was observed following loading of BOEC tissue constructs onto gelatin, collagen, or tissue-treated plastic surfaces. SDS and Tri-Col approaches are well-supported in literature and both produced carriers capable of supporting BOECs in spinner culture and releasing proliferative cells following seeding and imaging.

No single tissue emerged as ideal for all ECM derivatives. Heart tissue produced carriers with desirable rounded morphology following sonication, while kidney produced small jagged fragments, and lung and liver produced filamentous material. However, cryopulverization increased recovery and produced materials with rounded morphology for all tissues. Liver tissue

was used primarily due to availability, but produced the smallest volume of ECM of the materials tested. Lung was found to produce the greatest volume of ECM per volume of raw tissue, and was studied extensively. For cryopulverized BOEC carriers kidney and lung may be the most appropriate candidates due to their abundance of endothelial structures, however all tissue microcarriers tested supported cell attachment, culture, and egress.

## 6.3 Cell Survival Assays

Initial testing of decellularized materials included a semi-quantitative evaluation of cytotoxicity by culturing cells in the presence of decellularized tissue. This indirect testing strategy was chosen for being unaffected by imaging challenges in large tissues. Subsequently, seeded tissue microcarriers were cast in collagen or overlaid onto tissue-treated surface. Cell egress was studied, and migration and division was observed with time-course imaging. Viability and cytoskeletal staining was used with cultured whole organ samples and carriers to investigate survival and morphology.

Following the results of these experiments, cryopulverized decellularized tissue microcarriers were selected as a candidate platform for BOEC delivery. Microcarriers have the advantages of being scalable in spinner culture, providing high surface area for attachment, and can be injected subcutaneously. Although cells were shown to be proliferative and form capillary-like structures on ECM carriers, it is unknown if the constructs can improve FVIII levels *in vivo* over cells alone.

To determine if the ECM carriers improve BOEC survival in a competitive environment, seeded carriers and cells alone were cultured on a confluent layer of HeLa cells. Cells alone were shown to attach with a highly elongated morphology with widespread death within 9 days of culture. The carrier was found to promote cell survival until 16 days when HeLa overgrowth interfered with imaging. The results of this assay demonstrate that ECM microcarriers can promote cell survival in co-culture with robust cells, and contribute to the selection of cryopulverized ECM microcarriers as the candidate platform for animal studies.

## 6.4 Future Work

The focus of the work presented here was to develop an ECM-based tissue engineering approach to support *ex vivo* gene-modified cell therapy. Although a promising candidate has been developed, additional characterization is required. Important considerations include improved process understanding of decellularizing particles through chemical digestion and analysis, as well as histology over time. Growth curves and kinetics of cells on the microcarriers, as well as cell FVIII productivity in culture also may provide indications of microcarrier quality. However, it remains unknown if ECM microcarriers can effectively support BOECs *in vivo*.

Lung and kidney microcarriers have been selected for an animal study to determine effectiveness and differences between the two materials. If the microcarriers demonstrate effectiveness in cell survival and functional clotting assays, characterization will be critical to material and process optimization.

## References


"Detergents properties and applications." Retrieved June 9th, 2009, from http://www.sigmaaldrich.com/etc/medialib/docs/Sigma/Instructions/detergent_selection_table.Par.0001.File.tmp/detergent_selection_table.pdf.

Aivaliotis, M., P. Samolis, et al. (2003). "Molecular size determination of a membrane protein in surfactants by light scattering." Biochim Biophys Acta **1615**(1-2): 69-76.

Akhyari, P., H. Kamiya, et al. (2008). "Myocardial tissue engineering: the extracellular matrix." Eur J Cardiothorac Surg **34**(2): 229-41.

Badylak, S. F., D. Taylor, et al. "Whole-Organ Tissue Engineering: Decellularization and Recellularization of Three-Dimensional Matrix Scaffolds." Annu Rev Biomed Eng.

Beattie, A. J., T. W. Gilbert, et al. (2009). "Chemoattraction of progenitor cells by remodeling extracellular matrix scaffolds." Tissue Eng Part A **15**(5): 1119-25.

Blanch, H. W. and D. S. Clark (1996). Biochemical engineering. New York, M. Dekker.

Brown, B., K. Lindberg, et al. (2006). "The basement membrane component of biologic scaffolds derived from extracellular matrix." Tissue Eng **12**(3): 519-26.

Cebotari, S., I. Tudorache, et al. "Detergent decellularization of heart valves for tissue engineering: toxicological effects of residual detergents on human endothelial cells." Artif Organs **34**(3): 206-10.

Chisti, Y. (2000). "Animal-cell damage in sparged bioreactors." Trends Biotechnol **18**(10): 420-32.

Demetriou, A. A., A. Reisner, et al. (1988). "Transplantation of microcarrier-attached hepatocytes into 90% partially hepatectomized rats." Hepatology **8**(5): 1006-9.

Engler, A. J., S. Sen, et al. (2006). "Matrix elasticity directs stem cell lineage specification." Cell **126**(4): 677-89.

Feldman, B. M., M. Pai, et al. (2006). "Tailored prophylaxis in severe hemophilia A: interim results from the first 5 years of the Canadian Hemophilia Primary Prophylaxis Study." J Thromb Haemost **4**(6): 1228-36.

Fogler, H. S. (2006). Elements of chemical reaction engineering. Upper Saddle River, NJ, Prentice Hall PTR.

Frisch, S. M. and E. Ruoslahti (1997). "Integrins and anoikis." Curr Opin Cell Biol **9**(5): 701-6.

Frisch, S. M. and R. A. Screaton (2001). "Anoikis mechanisms." Curr Opin Cell Biol **13**(5): 555-62.

Gani, S. A., D. K. Chattoraj, et al. (1999). "Solubilization and binding of DNA-CTAB complex with SDS in aqueous media." Indian J Biochem Biophys **36**(4): 233-9.

Gilbert, T. W., T. L. Sellaro, et al. (2006). "Decellularization of tissues and organs." Biomaterials **27**(19): 3675-83.

Gilbert, T. W., D. B. Stolz, et al. (2005). "Production and characterization of ECM powder: implications for tissue engineering applications." Biomaterials **26**(12): 1431-5.

Gratzer, P. F., R. D. Harrison, et al. (2006). "Matrix alteration and not residual sodium dodecyl sulfate cytotoxicity affects the cellular repopulation of a decellularized matrix." Tissue Eng **12**(10): 2975-83.

Grefrath, S. P. and J. A. Reynolds (1974). "The molecular weight of the major glycoprotein from the human erythrocyte membrane." Proc Natl Acad Sci U S A **71**(10): 3913-6.

Griffin, W. (1949). "Classification of surface active agents by HLB." J So Cosmet Chem(1): 311-326.

Handa-Corrigan, A. and A. N. Emery (1989). "Effect of gas-liquid interfaces on the growth of suspended mammalian cells: mechanisms of cell damage by bubbles." Enzyme Microb. Technol. **11**(4): 230-35.

Haydon, D. A. and J. Taylor (1963). "The stability and properties of bimolecular lipid leaflets in aqueous solutions." J Theor Biol **4**(3): 281-96.

Helenius, A. and K. Simons (1975). "Solubilization of membranes by detergents." Biochim Biophys Acta **415**(1): 29-79.

Hudson, T. W., S. Y. Liu, et al. (2004). "Engineering an improved acellular nerve graft via optimized chemical processing." Tissue Eng **10**(9-10): 1346-58.

Hynes, R. O. (2009). "The extracellular matrix: not just pretty fibrils." Science **326**(5957): 1216-9.

Katz, M. A., T. Barrette, et al. (1992). "Hydraulic conductivity of basement membrane with computed values for fiber radius and void volume ratio." Am J Physiol **263**(5 Pt 2): H1417-21.

Keller, S., A. Tsamaloukas, et al. (2005). "A quantitative model describing the selective solubilization of membrane domains." J Am Chem Soc **127**(32): 11469-76.

Kemp, P. (2006). "History of regenerative medicine: looking backwards to move forwards." Regen Med **1**(5): 653-69.

Ketchedjian, A., A. L. Jones, et al. (2005). "Recellularization of decellularized allograft scaffolds in ovine great vessel reconstructions." Ann Thorac Surg **79**(3): 888-96; discussion 896.

Kleinman, H. K., M. L. McGarvey, et al. (1983). "Formation of a supramolecular complex is involved in the reconstitution of basement membrane components." Biochemistry **22**(21): 4969-74.

Kleinman, H. K., M. L. McGarvey, et al. (1986). "Basement membrane complexes with biological activity." Biochemistry **25**(2): 312-8.

Krishnamurthy, R., J. A. Lumpkin, et al. (2000). "Inactivation of lysozyme by sonication under conditions relevant to microencapsulation." Int J Pharm **205**(1-2): 23-34.

Kubota, Y., H. K. Kleinman, et al. (1988). "Role of laminin and basement membrane in the morphological differentiation of human endothelial cells into capillary-like structures." J Cell Biol **107**(4): 1589-98.

Levenspiel, O. (1999). Chemical reaction engineering. New York, Wiley.

Levick, J. R. (1987). "Flow through interstitium and other fibrous matrices." Q J Exp Physiol **72**(4): 409-37.

Lin, P., W. C. Chan, et al. (2004). "Assessing porcine liver-derived biomatrix for hepatic tissue engineering." Tissue Eng **10**(7-8): 1046-53.

Lin, Y., L. Chang, et al. (2002). "Use of blood outgrowth endothelial cells for gene therapy for hemophilia A." Blood **99**(2): 457-62.

Lin, Y., D. J. Weisdorf, et al. (2000). "Origins of circulating endothelial cells and endothelial outgrowth from blood." J Clin Invest **105**(1): 71-7.

Liu, Y., S. Bharadwaj, et al. (2009). "Optimization of a natural collagen scaffold to aid cell-matrix penetration for urologic tissue engineering." Biomaterials **30**(23-24): 3865-73.

Lopez, O., M. Cocera, et al. (1999). "Solubilization of liposomes by sodium dodecyl sulfate: new mechanism based on the direct formation of mixed micelles." Arch Biochem Biophys **367**(2): 153-60.

Lopez, O., A. de la Maza, et al. (1998). "Direct formation of mixed micelles in the solubilization of phospholipid liposomes by Triton X-100." FEBS Lett **426**(3): 314-8.

Ma, Z., Z. Liu, et al. (2008). "Mechanotransduction and anoikis: death and the homeless cell." Cell Cycle **7**(16): 2462-5.

Matsui, H., M. Shibata, et al. (2007). "Ex vivo gene therapy for hemophilia A that enhances safe delivery and sustained in vivo factor VIII expression from lentivirally engineered endothelial progenitors." Stem Cells **25**(10): 2660-9.

Meezan, E., J. T. Hjelle, et al. (1975). "A simple, versatile, nondisruptive method for the isolation of morphologically and chemicaly pure basement membranes from several tissues." Life Sci **17**(11): 1721-32.

Mertsching, H., T. Walles, et al. (2005). "Engineering of a vascularized scaffold for artificial tissue and organ generation." Biomaterials **26**(33): 6610-7.

Milbauer, L. C., J. A. Enenstein, et al. (2009). "Blood outgrowth endothelial cell migration and trapping in vivo: a window into gene therapy." Transl Res **153**(4): 179-89.

Miyazawa, Ogawa, et al. (1984). "The physico-chemical properties and protein denaturation potential of surfactant mixtures." Int J Cosmetic Sci **6**(1): 33-46.

Montoya, C. V. and P. S. McFetridge (2009). "Preparation of ex vivo-based biomaterials using convective flow decellularization." Tissue Eng Part C Methods **15**(2): 191-200.

Murphy, S. L. and K. A. High (2008). "Gene therapy for haemophilia." Br J Haematol **140**(5): 479-87.

Nauman, E. B. (2004). Residence Time Distributions. Handbook of industrial mixing: science and practice. E. L. Paul, V. A. Atiemo-Obeng and S. M. Kresta. Hoboken, N.J., Wiley-Interscience**:** 1-17.

Netti, P. A., D. A. Berk, et al. (2000). "Role of extracellular matrix assembly in interstitial transport in solid tumors." Cancer Res **60**(9): 2497-503.

Ossipow, V., U. K. Laemmli, et al. (1993). "A simple method to renature DNA-binding proteins separated by SDS-polyacrylamide gel electrophoresis." Nucleic Acids Res **21**(25): 6040-1.

Ott, H. C., B. Clippinger, et al. (2010). "Regeneration and orthotopic transplantation of a bioartificial lung." Nat Med **16**(8): 927-33.

Ott, H. C., T. S. Matthiesen, et al. (2008). "Perfusion-decellularized matrix: using nature's platform to engineer a bioartificial heart." Nat Med **14**(2): 213-21.

Otzen, D. E. (2002). "Protein unfolding in detergents: effect of micelle structure, ionic strength, pH, and temperature." Biophys J **83**(4): 2219-30.

Pietramaggiori, G., S. S. Scherer, et al. (2008). "Healing modulation induced by freeze-dried platelet-rich plasma and micronized allogenic dermis in a diabetic wound model." Wound Repair Regen **16**(2): 218-25.

Remlinger, N. T., C. A. Czajka, et al. "Hydrated xenogeneic decellularized tracheal matrix as a scaffold for tracheal reconstruction." Biomaterials **31**(13): 3520-6.

Reynolds, J. A. and C. Tanford (1970). "The gross conformation of protein-sodium dodecyl sulfate complexes." J Biol Chem **245**(19): 5161-5.

Roberts, M. S., J. D. Donaldson, et al. (1988). "Models of hepatic elimination: comparison of stochastic models to describe residence time distributions and to predict the influence of drug distribution, enzyme heterogeneity, and systemic recycling on hepatic elimination." J Pharmacokinet Biopharm **16**(1): 41-83.

Rosario, D. J., G. C. Reilly, et al. (2008). "Decellularization and sterilization of porcine urinary bladder matrix for tissue engineering in the lower urinary tract." Regen Med **3**(2): 145-56.

Rosenberg, I. M. (2004). Protein Analysis and Purification. Benchtop Techniques. Boston, Birkhäuser.

Samouillan, V., A. Lamure, et al. (2000). "Characterisation of elastin and collagen in aortic bioprostheses." Med Biol Eng Comput **38**(2): 226-31.

Saporta, S., C. Borlongan, et al. (1997). "Microcarrier enhanced survival of human and rat fetal ventral mesencephalon cells implanted in the rat striatum." Cell Transplant **6**(6): 579-84.

Schubert, R. and K. H. Schmidt (1988). "Structural changes in vesicle membranes and mixed micelles of various lipid compositions after binding of different bile salts." Biochemistry **27**(24): 8787-94.

Sclafani, A. P., T. Romo, 3rd, et al. (2000). "Evaluation of acellular dermal graft in sheet (AlloDerm) and injectable (micronized AlloDerm) forms for soft tissue augmentation. Clinical observations and histological analysis." Arch Facial Plast Surg **2**(2): 130-6.

Spina, M., F. Ortolani, et al. (2003). "Isolation of intact aortic valve scaffolds for heart-valve bioprostheses: extracellular matrix structure, prevention from calcification, and cell repopulation features." J Biomed Mater Res A **67**(4): 1338-50.

Stefonek-Puccinelli, T. J. and K. S. Masters (2008). "Co-immobilization of gradient-patterned growth factors for directed cell migration." Ann Biomed Eng **36**(12): 2121-33.

Stern, M. M., R. L. Myers, et al. (2009). "The influence of extracellular matrix derived from skeletal muscle tissue on the proliferation and differentiation of myogenic progenitor cells ex vivo." Biomaterials **30**(12): 2393-9.

Uygun, B. E., A. Soto-Gutierrez, et al. (2009). "Organ reengineering through development of a transplantable recellularized liver graft using decellularized liver matrix." Nat Med.

Walter, A., P. K. Vinson, et al. (1991). "Intermediate structures in the cholate-phosphatidylcholine vesicle-micelle transition." Biophys J **60**(6): 1315-1325.

Woodley, D. T., C. N. Rao, et al. (1983). "Interactions of basement membrane components." Biochim Biophys Acta **761**(3): 278-83.

Woods, T. and P. F. Gratzer (2005). "Effectiveness of three extraction techniques in the development of a decellularized bone-anterior cruciate ligament-bone graft." Biomaterials **26**(35): 7339-49.

Wozniak, M. A. and P. J. Keely (2005). "Use of three-dimensional collagen gels to study mechanotransduction in T47D breast epithelial cells." Biol Proced Online **7**: 144-61.

Xu, J., D. Rodriguez, et al. (2001). "Proteolytic exposure of a cryptic site within collagen type IV is required for angiogenesis and tumor growth in vivo." J Cell Biol **154**(5): 1069-79.

Yang, Y., F. M. Rossi, et al. (2007). "Ex vivo expansion of rat bone marrow mesenchymal stromal cells on microcarrier beads in spin culture." Biomaterials **28**(20): 3110-20.

Yoo, G. and J. S. Lim (2009). "Tissue engineering of injectable soft tissue filler: using adipose stem cells and micronized acellular dermal matrix." J Korean Med Sci **24**(1): 104-9.

Yu, J., D. A. Fischman, et al. (1973). "Selective solubilization of proteins and phospholipids from red blood cell membranes by nonionic detergents." J Supramol Struct **1**(3): 233-48.

Zhang, X., Z. Deng, et al. (2009). "Expansion and delivery of human fibroblasts on micronized acellular dermal matrix for skin regeneration." Biomaterials **30**(14): 2666-74.

Zhang, Y., Y. He, et al. (2009). "Tissue-specific extracellular matrix coatings for the promotion of cell proliferation and maintenance of cell phenotype." Biomaterials **30**(23-24): 4021-8.